THE ROLE OF NPC2 IN CHOLESTEROL TRANSPORT AND THE ENDOCYTIC SYSTEM IN NEUROBLASTOMA CELLS

by

Aaron Woblistin

Submitted in partial fulfilment of the requirements
for the degree of Doctor of Philosophy

at

Dalhousie University
Halifax, Nova Scotia
March 2022

TABLE OF CONTENTS

LIST OF TABLES

LIST OF FIGURES

ABSTRACT

Niemann-Pick type C (NPC) disease is an autosomal recessive, neurodegenerative disorder caused by mutations in either Niemann-Pick Type C1 (NPC1) or NPC2. NPC disease is a lysosomal lipid-storage disease characterized by accumulation of unesterified cholesterol in late endosomes/lysosomes (LE/L). NPC2, located to the LE/L lumen, binds cholesterol and hands it off to NPC1 in the LE/L perimeter membrane to be presented to the plasma membrane and the ER. Mature neurons do not synthesize cholesterol efficiently and rely on uptake for their cholesterol needs, thereby highlighting the importance of this cholesterol transport pathway. In human fibroblasts, depletion of either NPC1 or NPC2 leads to sequestration of cholesterol in LE/L. Here, I show that only NPC1, but not NPC2 depletion led to LE/L cholesterol accumulation in a human neuroblastoma cell line (SH-SY5Y), contrary to results in fibroblasts using the same RNA interference system. NPC2-depleted cells still showed impaired transport of endocytosed cholesterol to the ER, similarly to NPC1-depleted cells. Cellular cholesterol levels were lower in NPC2-depleted cells compared to control or NPC1-depleted cells. Cholesterol secretion was markedly reduced in NPC1- and NPC2-depleted SH-SY5Y cells, with NPC2-deficient cells showing a more severe reduction. This reduction was accompanied by a decreased capacity for lysosomal exocytosis in both NPC1- and NPC2-depleted compared to control SH-SY5Y cells. The most striking abnormalities were seen in the endocytic system of NPC2-depleted SH-SY5Y cells, where early and late endosomes were reduced in number but similar in size compared to control cells. In contrast, NPC1-depleted SH-SY5Y cells maintained the number of vesicles but showed a significant increase in their size. This effect of NPC2 depletion on the endocytic system was rescued by simultaneous expression of wildtype NPC2 but also of NPC2 variants that are unable to bind NPC1, are sterol binding-deficient, or glycosylation- and cellular retention-deficient. These results suggest a role of NPC2 in addition to cholesterol transport out of LE/L, which is not dependent on the ability of NPC2 to bind cholesterol or interact with NPC1, potentially regulating endosome homeostasis. These findings highlight the importance of NPC2 outside the dogmatic role as merely the cholesterol transport partner of NPC1.

LIST OF ABBREVIATIONS USED

3'UTR – 3' Untranslated Region

ACTB – Actin Beta

BCA – Bicinchoninic acid

BSA – Bovine serum albumin

CE – Cholesteryl ester

D4H – Domain 4 higher affinity

DMEM – Dulbecco's Modified Eagle Medium

DMSO – Dimethyl sulfoxide

DNA – Deoxyribonucleic acid

ER – Endoplasmic reticulum

FA – Fatty acid

FBS – Fetal bovine serum

HMGCR – HMGCR 3-hydroxy-3-methylglutaryl-CoA reductase

IF – Immunofluorescence

IgG – Immunoglobulin G

ILV – Intralumenal vesicles

LDL – Low density lipoprotein

LDLR – Low density lipoprotein receptor

LE/L – Late endosome/lysosome

LPDS – Lipoprotein deficient serum

MEM – Minimum essential media

NAG – N-Acetylglucosaminidase

NPC1 – Niemann-Pick type C1

NPC2 – Niemann-Pick type C2

PAGE – Polyacrylamide gel electrophoresis

PBS – Phosphate-Buffered Saline

PFA – Paraformaldehyde

PM – Plasma membrane

RNA – Ribonucleic Acid

ROI – Region of interest

RT – Reverse transcription

SDS – Sodium dodecyl sulfate

SOAT1 – Sterol O-acyltransferase 1

TAG – Triacylglycerol

TLC – Thin layer chromatography

UBC - Polyubiquitin C gene promotor

WGA – Wheat Germ Agglutinin

ACKNOWLEDGEMENTS

First and foremost, I would like to thank my supervisor, Dr. Barbara Karten. Her guidance and support throughout the project was imperative to its completion. She was able to lead me through my thesis with unwavering nerves, even with all the complications that came along with it, while still helping me with everything regarding my scientific work in and around the lab. She welcomed me in her lab with open arms, although I am from Austria, and supported me from the get-go starting my life in Canada. My transition working in a new country would not have been so smooth without her. Barbara is one of the kindest persons I know, always putting her students first and genuinely wanting them to succeed. I always saw her as the role model of a professor and hope she is proud of what we were able to achieve in my time in her lab. I will never forget the skills I was able to learn from her, as a researcher but also as a person. Our lab get-togethers were always fun, as were the countless games of Viking Chess (Kubb) and will stay as very fond memories of Canada.

I would also like to extend my thanks to all the members of the Karten and Too lab and Krueger lab, that helped me through my work. Especially Lynn Thomas, whose knowledge and expertise in the lab was vital to the success of a lot of my experiments. She was always supportive and shared the valuable experience she collected in 30+ years working in research. It was also always a blast to chat with her, about the current Hockey league and everything Canadian and I very much appreciate her sense of humor. Furthermore, I would like to thank and remember my dear friend and colleague Luke Hattie, who sadly and unexpectedly passed away after completion of a great Masters project. The world lost a great researcher and kind and loving person that day and I will always fondly remember the fun we had in and out of the lab, with great Friday night foosball nights. My thanks extend to all the present and past members of the Karten lab, which all contributed in some way to the successful completion of my thesis: Victoria Palmgren, Lindsay Cormier, Shawna Dexter, Madhav Makkena, Turner Kinal, Kareem

Abdelgabar, Julia Verboom and our new PhD student taking over the torch, Stanley Ibeh. I also have to thank my committee members, whose insight and guidance helped the project out immensely, Dr. Catherine Too, Dr. Neale Ridgway, and Dr. Thomas Pulinilkunnil.

My experience in Canada wouldn't have been the same without all the awesome people I met along the way. From my first room mate and now one of my best friends Alexa Wilson, to the people I met at the legendary Tupper Mixer, Michal Scur, Patrick Slaine, Dane Sands, Jeff Simmons, Sarah van der Ende, Jordan Lukacs, Ryan Holloway and all the other fabulous folks I met in my time here. This period of my life and the friends and memories I made will always be cherished.

At last, I would like to thank my wonderful fiancée Isabelle Fantina, whose love and support I appreciate every day and I couldn't have done my Ph.D. without her. Together with our cat Scully they had my back from the start and have been by my side through happy and sad times, always making things brighter in the end. I also would like to extend my thanks to my family at home, Claudia and Rainer Woblistin and my sisters Iris and Michaela, who always supported me throughout my academic career, always believed in me, and allowed me to pursue my dreams in Austria and in Canada.

1. CHAPTER 1 INTRODUCTION

1.1. Cholesterol:

Cholesterol is a small amphiphilic steroid, part of the broader class of lipids, and an essential part of all mammalian membranes (1). Cholesterol distribution across different membrane in the cell is very uneven. While the PM contains between 60-80 % of cellular cholesterol, the endoplasmic reticulum only contains around 10 % and the mitochondria, being one of the most cholesterol poor organelles, has only around 2 % (2). Cholesterol plays an important part in the regulation of membrane fluidity and curvature as well as being instrumental in membrane organisation and nanodomains (3–5). Furthermore, different pools of cholesterol in the plasma membrane can act to convey signals between proteins by modulating their activity according to accessibility of cholesterol (6). Besides its importance in membranes, cholesterol is also the sole precursor for the initial step of steroid hormone synthesis, which takes place in the mitochondria, namely the conversion to pregnenolone by cytochrome P450 cholesterol side chain cleavage enzyme (CYP11A1). Pregnenolone is then converted into a variety of hormones in the endoplasmic reticulum (ER), regulating development and metabolism (7,8). Additionally, cholesterol is also an essential precursor of bile acids, important for cholesterol secretion out of the organism (9).

1.1.1. Cholesterol biosynthesis:

Cellular cholesterol content is tightly regulated, given its vital role in many cellular functions. There are two main sources of cholesterol for the cell, de-novo synthesis of cholesterol from acetyl coenzyme A (acetyl-CoA) or uptake through lipoprotein particles (10). Biosynthesis of cholesterol starts in the cytoplasm at the ER membrane with acetyl-CoA. The first rate-limiting step is the conversion of 3-hydroxy-3-methylglutaryl coenzyme A (HMG-CoA) by HMG-CoA reductase (HMGCR) to mevalonate. However, most other steps are then carried out in the ER directly, due to the increasing hydrophobicity, to a total of ~30 steps to cholesterol (10,11). Regulation of biosynthesis is achieved through phosphorylation and sterol-mediated negative feedback degradation of HMGCR, as well as on the transcriptional level through the ER-resident

protein sterol regulatory element-binding protein 2 (SREBP2) (12). SREBP2 binds to SREBP-cleavage activating protein (SCAP), and the SREBP-SCAP complex binds to the ER membrane anchored insulin-induced gene (INSIG) depending on cholesterol levels (13,14). During sterol depletion, the SREBP-SCAP complex is released from INSIG, causing a change in SCAP morphology that allows for binding of coatomer II (COPII), which transports the SCAP-SREBP complex to the Golgi where SREBP2 is cleaved by proteases S1P and S2P, releasing its N-terminal domain. This domain translocates into the nucleus, where it acts as a transcription factor for sterol response elements (SRE)-containing promoters, up-regulating SREBP2 and most cholesterol biosynthesis genes transcription, including HMGCR as well as low-density-lipoprotein-receptors (LDLR) responsible for cholesterol uptake (15). During sterol repletion, insulin-induced gene (INSIG) binds to SCAP, inhibiting the morphological change that allows SCAP to bind COPII. This arrests the SREBP-SCAP complex in the ER, blocking the transcriptional activation (13). Besides transcriptional regulation over SREBP, HMGCR is also directly regulated by INSIG through induction of proteasomal degradation. High sterol content induces binding of INSIG to HMGCR, which leads to ubiquitination of HMGCR and extraction from the ER to be degraded by the proteasome (16). These steps combined ensure that cholesterol biosynthesis is tightly controlled and cholesterol is only produced, if levels at the ER are low.

1.1.2. Cholesterol uptake:

Cholesterol biosynthesis is an energy-demanding process. Alternatively, cells can take up cholesterol by endocytosis of cholesterol-rich low-density lipoproteins (LDL). This uptake is facilitated primarily by LDLR, which bind LDL particles, and subsequent clathrin-mediated endocytosis (17). The endocytosed LDL-LDLR complex is released in the acidic lumen of the early endosome (EE), the first step of the endocytic system (18). The LDLR is recycled back to the plasma membrane (PM) (19), while the LDL particles move through the endocytic system. Reaching the late endosome/lysosome (LE/L), cholesteryl esters (CE) in LDL are hydrolysed by lysosomal acid lipase. The unesterified cholesterol can then be bound by the lumenal Niemann-Pick disease type C2 (NPC2)

protein and presented to the transmembrane protein NPC1 for transport out of the LE/L and subsequent delivery to other cellular compartments like the ER and PM (20). The major protein facilitating cholesterol uptake, namely LDLR, is transcriptionally regulated by an SRE-containing promoter, similar to cholesterol biosynthesis genes. However, most cholesterol synthesis genes appear to have multiple cooperative SRE elements, whereas the LDLR gene only has one. Comparison of the response rate of LDLR with a single SRE containing promotor to multiple two-SRE-containing cholesterol biosynthesis genes showed that LDLR is upregulated faster initially until a certain SREBP threshold is reached and synthesis gene regulation catches up (21–23). These findings emphasize the priority of uptake over biosynthesis.

1.1.3. Cholesterol storage:

LDL-derived cholesterol reaches the ER through the NPC2-NPC1-facilitated transport as unesterified cholesterol, regulating cholesterol biosynthesis and uptake. However, excess unesterified cholesterol is cytotoxic, due to changes of cholesterol to phospholipid ratios in membranes, altering membrane fluidity, or interference with signaling proteins in membranes (24,25). To prevent cytotoxic effects, excess cholesterol is stored as cholesteryl esters, a process regulated and catalyzed by Sterol O-Acyltransferase 1 (SOAT1, formerly known as Acyl-Coenzyme A: Cholesterol Acyltransferase – ACAT1)(26,27). CEs are then stored in lipid droplets in the cytoplasm and can be hydrolysed if needed. However, this process has been suggested to only be short term buffer (28). Mammalian cells cannot fully degrade cholesterol and rely on liver cells for conversion of cholesterol into bile salts or secretion with bile for removal from the organism (24,29). Cells can efflux cholesterol by members of the ATP-binding cassette (ABC) transporters superfamily, most notably ABCA1 and ABCG1. These transporters shuttle cholesterol across the PM to extracellular high density lipoprotein (HDL), which can transport cholesterol back to the liver (30,31).

1.2. Niemann-Pick disease type C

Niemann-Pick disease (NPD) is a neurological lysosomal lipid storage. The disease can manifest many different symptoms including ataxia, cataplexy, seizures, and dysphagia, as some of the more common ones (32). NPD was originally classified into the 4 subgroups, type A-D, by Crocker et al. in 1961 (33). However, type D was later combined with type C, as the disease-causing genes were identified to be the same (34). Types A and B are primarily characterized by sphingomyelin accumulation, caused by mutations of sphingomyelin phosphodiesterase 1 (35). Type C primarily accumulates cholesterol, but not exclusively (36). Niemann-Pick disease type C (NPC) is an autosomal recessive neurodegenerative disorder with loss of neurons and demyelination in the brain, most notably the loss of Purkinje cells in the cerebellum, and widespread neurological deterioration (37–39). The gold standard for clinical diagnosis of NPC disease used to be biopsy and cultivation of patient skin fibroblasts, followed by staining of cellular cholesterol to identify accumulation. After identification of the genetic alterations, sequencing became the screening method of choice (40). The genes involved in NPC disease were identified by the end of the 20th century and named NPC1 and NPC2 (41,42). In 95 % of all NPC cases, mutations in *NPC1* can be identified as the cause, whereas only 5 % of cases are attributed to *NPC2* mutations (43). Both proteins are localized to the endo-lysosomal system and important for cholesterol transport out of the LE/L. Dysfunction of either can lead to accumulation of cholesterol in the LE/L and cause NPC. Although the lysosomal cholesterol accumulation is one of the hallmarks of NPC disease, it is still not entirely clear how disruption of cholesterol transport causes neurodegeneration (36).

1.2.1. Niemann-Pick type C1

NPC1 is a ubiquitously expressed, 1278 amino acids long protein that localizes to the LE/L perimeter membrane. NPC1 mediates the transport of LDL-derived cholesterol across the perimeter membrane to be further transported to the rest of the cell, including the ER and PM (44). The protein consists of 13 transmembrane domains anchoring it in the lysosomal membrane (45). The transmembrane domains 3-7

furthermore contain a sterol-sensing domain (SSD), similar to that of SCAP or HMGCR, that can bind cholesterol (41,46,47). The C-terminal domain of NPC1 contains a dileucine motif, which is responsible and critical for directing it to the perimeter membrane, acting as a lysosomal targeting sequence (48). The ~230 residue N-terminal domain (NTD) and lumenal loop 2 and 3 make up the majority of the protein in the lysosomal lumen, and are important for the interaction with NPC2 (20,49). The NTD is a flexible domain, and structural work by Li et al. proposed that this flexibility could transfer cholesterol to the SSD (50). Although the NTD seems to accept cholesterol from NPC2, crystal structure analysis revealed that the lumenal loop 2 is responsible for the binding of NPC2 (51). Although a lot of work has been done recently on the matter, the exact mechanisms of how NPC1 transports cholesterol across the lysosomal membrane are not yet fully clear. Mutations in NPC1 are the main cause for NPC disease, leading to sequestration of cholesterol in the lysosome. However, NPC1 also has been shown to be required for Ebola virus cytoplasm entry and recently been implicated in SARS-CoV-2 virus entry, making it the topic of intense study (52–54).

1.2.2. Niemann-Pick type C2

NPC2 is a small soluble protein located in the endosomal lumen, but can also be found in secretory fluids (55). It is 151 amino acids long and N-glycosylated at two sites. NPC2 has a hydrophobic core capable of binding unesterified cholesterol with its hydroxyl group facing outwards, opposite to the orientation in the binding pocket of the NPC1 N-terminal domain (51). After LDL uptake and CE hydrolysis, NPC2 mobilises cholesterol from the lysosomal lumen and transports it to the perimeter membrane. It can then bind to lumenal loop 2 of NPC1 to transfer cholesterol to its NTD in what is called the “hydrophobic hand-off” transfer model (20,51). Early in-vitro studies of vesicular cholesterol transfer found that the presence of NPC2 increases the cholesterol binding activity of NPC1 by 15-fold in liposomes (56). Work in the lab of Judith Storch revealed that the lysobisphosphatidic acid (LBPA) enriched at endosomal intralumenal vesicles (ILV) plays an important role for cholesterol binding with NPC2 (57,58). They found that LBPA binds to NPC2 and drastically enhances its cholesterol transfer rates, and that

enrichment of LBPA was sufficient to reduce cholesterol storage in NPC1-deficient fibroblasts, in an NPC2-dependent manner (58,59). This work suggested that LBPA enrichment enhances LE and lysosome fusion, thereby providing NPC2 a path to deliver cholesterol into the perimeter membrane, circumventing the glycocalyx of lysosomes (59). In contrast to NPC1, NPC2 does not contain a lysosomal targeting motive. NPC2 is glycosylated after synthesis and is directed to the lysosomal lumen by transport along the secretory pathway before direction into the endocytic pathway by the Mannose 6-phosphate/insulin-like growth factor 2 receptor (M6P/IGF2R) (60). Willenborg et al. found that depletion of IGF2R, as well as NPC2 glycosylation deficient mutants, induce cholesterol accumulation similar to NPC2 depletion, highlighting that IGF2R sorting to the lysosomal pathway is critical for NPC2 function (60). Besides interaction with NPC1, studies showed that NPC2 is also able to interact with Lysosomal Associated Membrane Protein 2 (LAMP2) and deliver cholesterol to it and suggested that this process can form a considerable pool of cholesterol at the perimeter membrane for further transport (61). Additionally, previous work in the Karten lab has shown that NPC2 is crucial for STARD3-mediated cholesterol transport to mitochondria, especially in NPC1-deficient cells (62). Mutations of NPC2 lead to NPC disease in a similar manner as NPC1, however, only 5 % of all cases are caused by NPC2 defects.

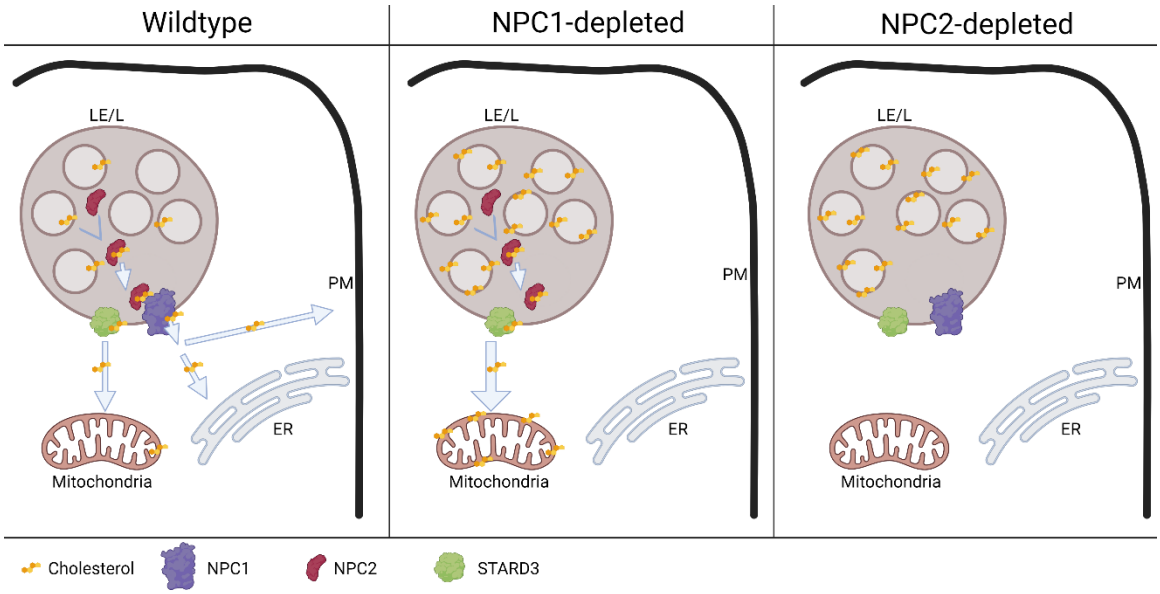

Figure 1.1: Overview of LE/L cholesterol efflux in wildtype an NPC-disease cells. In wildtype cells NPC2 binds cholesterol in the LE/L lumen and transports it to the perimeter membrane. NPC1 binds NPC2 and transports the cholesterol over the perimeter membrane to be transported to the rest of the cell, such as the PM or the ER. STARD3 can also take the cholesterol from the perimeter membrane and transport it to the mitochondria. In NPC1-depleted cells cholesterol accumulates in the LE/L, as the "hand-off" from NPC2 can not take place. This surplus of cholesterol induces increased transport to mitochondria by STARD3. In NPC2-depleted cells cholesterol accumulates as NPC1- and STARD3-mediated transport as dependent on NPC2. Image generated with BioRender.com.

1.3. The endocytic system

Endocytic uptake is one of the main sources of cholesterol for the cell. The endocytic system is a complex network spread over the whole cell, responsible for uptake, transport, secretion, as well as degradation, of vesicular cargo. A master regulator for the homeostasis of the endo-lysosomal system is the transcription factor EB (TFEB). TFEB activity is regulated by its phosphorylation state, with multiple phosphorylation sites that can either arrest it in the cytosol or initiate translocation to the nucleus where it then activates autophagic and lysosomal genes (63).

1.3.1. Endocytic uptake and recycling

Endocytosis is a vital function of the cell and mediates a variety of functions, from nutrient uptake to signal transduction. This process is facilitated by two main mechanisms, clathrin- dependent (CDE) and clathrin-independent endocytosis. CDE is

the most studied pathway and responsible for most receptor-mediated endocytosis, such as uptake of LDL through LDLR (17,64). Upon initiation of CDE, clathrin assembles on the PM and induces invagination of the PM including the cargo, followed by constriction of the neck and budding-off facilitated by dynamin (65–67). These endocytosed particles form an early endosome, also called the sorting endosome, from which the fate of the cargo is decided (68). Endocytosed cargo can either be sent for degradation to the lysosome, transported to the trans-Golgi network (TGN) via the retromer protein complex, or recycled (69). Recycling can be separated into 2 different processes, the fast geometry-based pathway or through the Ras-related protein Rab-11 (RAB11) positive endocytic recycling compartment (ERC), both mediated in part by Rab4 (69,70). The first separates membrane proteins, including LDLR, from the soluble cargo by formation of narrow endosomal tubules, increasing the ratio of surface protein to luminal protein base on geometrical limitations of the compartment without the need of targeting sequences (71). The second process shuttles the cargo to a separate compartment called the ERC, which can mediate recycling processes to the Golgi or PM, based on lipid composition or glycosylation (70).

1.3.2. Endosome maturation

The process of endosome maturation is the transformation of the EE into the late endosome (LE) before fusion with the lysosome to form the late endosome/lysosome (LE/L). The maturation is comprised of 3 major physiological changes: formation of intralumenal vesicles (ILVs), acidification of the medium, and centripetal movement to the perinuclear area (72). These steps serve to stop further recycling and initiate degradation of cargo.

The master regulator of this process is the “Rab switch”, an exchange of the surface markers and GTPases, Rab5 for Rab7 (73). This transition is initiated by the activation of Rab5 through the GDP/GTP exchange factor (GEF), Rabex-5, and triggers a feedback loop to activate and recruit more Rab5 (69,74). However, activation of Rab5 leads to recruitment of effectors, which in turn lead to recruitment and activation of Rab7. These effectors initiate a “cut-off switch” that leads to deactivation of Rab5 and replacement

with Rab7 (75,76). This Rab switch is crucial in regulating the exchange of endosomal fusion machinery from the early endosome Vps-C complexes CORVET (class C core vacuole/endosome tethering) to the late endosome HOPS (homotypic fusion and vacuole protein sorting) complex (77). These complexes regulate the membrane fusion specificity of the different endosomes and consist of the same 6 vacuolar protein sorting (Vps) protein core complex but differ in additional Vps proteins. CORVET binds to Rab5 and facilitates the tethering and fusion of EE with other endocytosed cargo vesicles, while HOPS binds to Rab7 and is responsible for fusion of the LE with the mature lysosome. This transition ensures that only cargo designated for degradation can fuse with the LE.

During endosome maturation, one of the most notable steps is the formation of ILVs. This process ensures access of membrane bound cargo to lumenal hydrolases and deactivates signalling receptors by depriving them of access to the cytosol. ILVs are enriched in cholesterol. According to the hand-off model, NPC2 takes up cholesterol from the ILV and transfers it to NPC1. Cholesterol is then exported by the NPC2 and NPC1 hand-off transport (78,79). The formation of ILVs is mainly driven by the endosomal sorting complexes required for transport (ESCRT) (72,80). Through a sequential multistep process, mono-ubiquitinated cargo on the cytosolic side of the endosome is clustered together and internalized by inward budding of the vesicle. The ESCRT-0, ESCRT-I and ESCRT-II complexes are responsible for the first step in this process. By interacting with ubiquitinated cargo on the surface and recruitment of the complexes from the cytosol, ESCRT complexes form clusters of cargo to be internalized. ECSRT-III then initiates formation of a filamentous structure, bending the endosomal membrane away from the cytosol. This structure is built around the ubiquitinylated cargo, forming a protrusion into the endosomal lumen, before budding off and formation of the ILV (81).

Another step during endosomal maturation is the acidification of the endosome lumen. Through this process, the internal pH changes drastically from around 6.8 down to 4.5 (82). This acidification is necessary to provide the right milieu for lysosomal hydrolases,

but also for inactivation of pathogens and cargo sorting (72). LE are protected from these hydrolases and the acidic environment by heavily glycosylated proteins like lysosome-associated membrane glycoprotein 1 (Lamp1) (83). The proton pump Vacuolar-type ATPase (V-ATPase) is the main driver for acidification of the lumen and is dependent on influx of Cl^- counter ions (84). V-ATPase activity is influenced by the cholesterol content in the membrane (85).

The last major change during maturation involves a decrease in endosomal motility and clustering in the perinuclear area of the cell. Endosomes are mobile vesicles, transported along the microtubule network by kinesins and dynein-mediated movement (86). Endosomes are transported bi-directionally, allowing for regular fusion and fission of endosomes, but start to cluster at the perinuclear during maturation, inhibiting further fission and fusion events (87–89). Centrifugal movement of endosomes is dependent on kinesins, while centripetal movement is facilitated through dynein and dependent on activated Rab7 (90). Rab7-dependent movement is in part facilitated and controlled by ORP1L and its cholesterol sensing ability (91,92). The transport to the perinuclear area is also necessary for the fusion of the LE with the mature lysosome, the terminal stage for degradation of cargo.

1.3.3. Lysosomal fusion, re-formation and exocytosis

For degradation of LE cargo, the LE fuses with the mature lysosome, which contains hydrolytic enzymes like proteases and lipases (93). This fusion is mediated by soluble N-ethylmaleimide-sensitive factor-attachment protein receptor (SNARE) complexes and depends on association of LE membrane proteins including Rab7 and the HOPS complex (94–97). These membrane proteins initiate the close association of the two compartments while the SNARE complexes on both membranes facilitate their fusion, forming the new hybrid compartment called the LE/L. Furthermore, calcium release through P2X4 ion channel from the lysosomes is also important for the correct formation of the hybrid compartment, but other channels like TRPML1 have been implicated as well (98–100). It has been shown that in NPC1-deficient cells, calcium release from lysosomes through TRPML1 is diminished, potentially due to increased

sphingomyelin storage and reduced calcium uptake (101,102). NPC1-deficiency inhibits LE/L hybrid organelle fusion, most likely associated with the depletion of LE calcium (101).

To recover lysosomal enzymes and membrane proteins after degradation of LE/L cargo, the mature lysosome is re-formed. Lysosomal re-formation is still a relatively enigmatic process, however, progress has been made recently in understanding the molecular mechanics in the context of autophagy. The recovery process starts by polymerisation of clathrin on the surface of the vesicle and outward budding of the membrane. KIF5B then initiates tubulation of the membrane along the microtubule cytoskeleton. The protolysosome is then split from the tubulation in a dynamin 2-mediated process before maturation into the lysosome (103–105). Work done in the lab of Goldman and Krise showed that although depletion of NPC2 does not affect LE/L hybrid organelle formation like NPC1 depletion, loss of functional NPC2 increases LE/L size and inhibits fission events from these organelles that would reduce their size like the lysosomal reformation (106).

Another important process of the endocytic system is lysosomal exocytosis, describing the program of fusion of lysosomes with the PM. This process can serve many functions, such as PM damage repair after injury and secretion of waste (107). Fusion of lysosomes with the PM is largely dependent on calcium release by TRPML1, which can be sensed by synaptotagmin at the PM to initiate fusion (108–110). Prior to fusion, lysosomes are transported to the cell periphery in a kinesin-dependent manner along the microtubule network. Fusion is then facilitated by SNARE complexes (111). Lysosomal exocytosis also requires small GTPases such as RAB3A and RAB10 (112). Similar to lysosomes, LE/L can also fuse with the PM. This process releases the ILVs into the extracellular milieu, forming extracellular vesicles, including the exosome subset. Exosomes are widely studied for their role in cell-cell communication and as biomarkers for certain diseases (113).

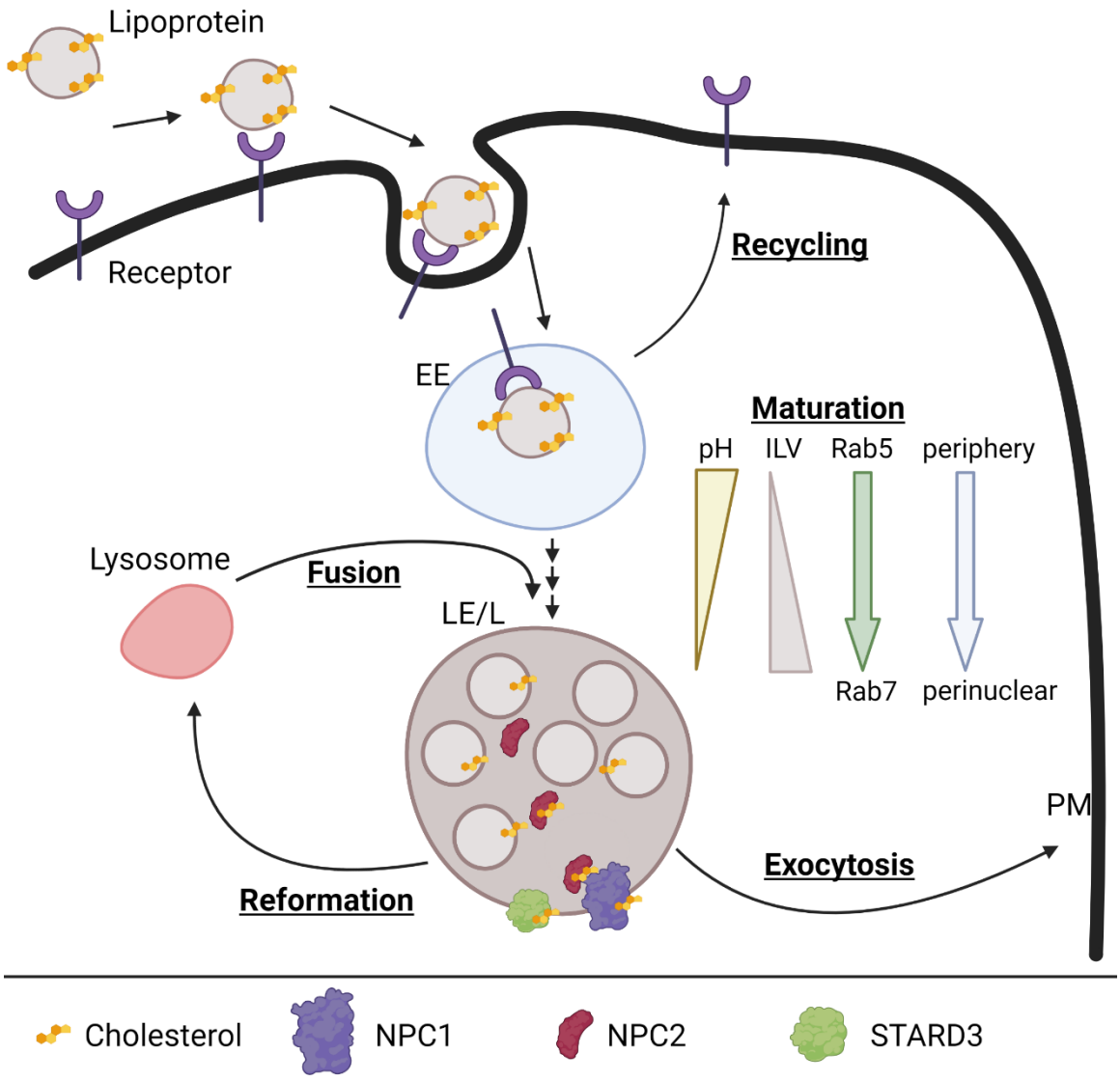

Figure 1.2: Overview of the endocytic system progression. Lipoprotein particles are bound on the cell surface by lipoprotein receptors and endocytosed together forming the EE. Receptors and other cargo can then be recycled back to the PM. EE with cargo destined for degradation enter the maturation process, reducing their lumenal pH, forming ILVs, switching from Rab5 to Rab7 surface marker, and moving towards the perinuclear area to form the LE. The LE then fuses with a mature lysosome to form the hybrid compartment LE/L. Enzymes within this hybrid compartment catalyse cargo degradation and export to the rest of the cell. LE/L can also be recruited to the PM in case of membrane damage or for secretion of cargo. The LE/L undergoes fission processes after cargo catalysis to reform the mature lysosome and prevent loss of lysosomal enzymes. Image generated with BioRender.com.

1.4. Mitochondria

1.4.1. Mitochondrial cholesterol

Mitochondria are the powerhouse of the cell. On average, more than 60 % of the total cellular ATP is produced by oxidative phosphorylation in the mitochondria (114). In addition, mitochondria play a vital role in steroid hormone and phospholipid production as well as overall cell regulation. Mitochondrial cholesterol is low compared to other organelles, with the ER showing 5-fold higher levels and the PM showing even 40-fold higher levels in yeast (2). However, these low cholesterol levels can act as a tool to regulate mitochondrial steroid and oxysterol synthesis by regulation of mitochondrial cholesterol import rather than enzyme activity (115). The first step in steroidogenesis is the formation of pregnenolone at the inner mitochondrial membrane (IMM) by cytochrome P450 (CYP11A1). Cholesterol can be imported to mitochondria along a plethora of pathways, however, the best known one is the import over steroidogenic acute regulatory protein (StAR), later renamed START domain-containing protein 1 (STARD1) (115,116). STARD1 facilitates the transport of cholesterol from the OMM to the IMM, however, the exact mechanisms on how STARD1 facilitates cholesterol import are still elusive (117). STARD1 is targeted to mitochondria by its N-terminal domain and undergoes several proteolytic cleavage events while imported into the mitochondrial matrix in adrenal cells (118–120). While arrest of STARD1 at the OMM, but not IMM, allows for cholesterol transport, import of STARD1 seems to be important for full cholesterol transport activity in steroidogenic cells (115,121–123). Stard1 associates with the voltage-dependent anion channel (VDAC), which is also responsible for metabolite transfer between membranes (124,125). In MA10 cells, STARD1-facilitated cholesterol import into mitochondria has been associated with VDAC complexes and with mitochondria to ER contact sites (MERC) (126)

1.4.2. Mitochondria-ER contact sites

Membrane contact sites between the ER and the outer mitochondrial membrane (OMM) are called MERC and are one of the best studied inter-organelle contact sites. These contacts were originally discovered by Jean E. Vance as the location of

phospholipid synthesis between ER and mitochondria (127). To form membrane contact sites, closely apposed organelles are held together with protein tethers without fusion of the corresponding membranes. The distance between the two membranes can vary in size between 10 – 80 nm (128). This close contact of membranes allows for the exchange of various metabolites and the regulation of mitochondrial function, such as exchange of lipids, calcium release and signalling, as well as regulation of mitochondrial dynamics and cell death (129). Formation of MERC depends on protein tethers of both organelles. For example, the ER-resident protein inositol triphosphate receptor (IP3R) interacts with a mitochondrial chaperone called 75 kDa glucose-regulated protein (GRP75), mediating a connection with VDAC on the OMM. This interaction links the two organelles close together and allows for the direct uptake of calcium released from the ER into mitochondria (130,131). Calcium release to the mitochondria regulates oxidative phosphorylation and also apoptosis (131,132). MERC also regulate mitochondrial morphology by initiating fission and fusion events. Dynamin-related protein 1 (DRP1) as well as mitofusin 1 (MFN1) and MFN2 localize to the MERC, regulating mitochondrial fission and fusion, respectively (133,134). Another important aspect of MERC is lipid transport. Phosphatidylethanolamine (PE) synthesis relies on the production of phosphatidylserine (PS) in the ER, transport across the MERC, and conversion to PE at the mitochondria (127,135,136). Cholesterol and cholesterol homeostatic enzymes are enriched in MERC (137–139). Although there is no evidence for direct cholesterol transport at the MERC yet, circumstantial evidence for this transport can be found in yeast and mammalian cells by association of cholesterol binding/transport proteins in MERC and the regulation of STARD1 activity at these sites (115,140,141).

1.4.3. Endosome – mitochondria contact site

Contact sites between endosomes and mitochondria are less well known than the MERC and most data comes from models in yeast. Nevertheless, there are strong indications for these contacts to exists (115). In yeast, vacuolar to mitochondrial tethers have been identified and named vacuole and mitochondrial patches (vCLAMPs) (142). Sterol binding proteins also associate with vCLAMPs, although direct transfer of sterols has not

been shown yet (143,144). Interestingly, this contact is also regulated by the ER-mitochondria contact site in yeast to some extent, as elimination of one expands the other (144). In mammalian cells, work done by the Karten lab shows first indications for the existence of endosomal – mitochondria cholesterol transport through STARD3 (62,145). During NPC1 deficiency induced cholesterol accumulation in the lysosome, STARD3 was able to transport cholesterol to mitochondria in an NPC2-dependent fashion. Furthermore, in steroidogenic COS1 cells, overexpression of STARD3 leads to increased pregnenolone formation, indicating increased cholesterol transport to the mitochondria (146,147). STARD3 is a lysosomal perimeter membrane protein, facing the cytosolic side of the organelle, and contains a cholesterol-binding START domain with high homology to STARD1 (148). How STARD3 interacts with mitochondria is not yet known. However, recent studies show evidence of physical interaction of lysosome with mitochondria based on super-resolution and electron microscopy (147,149,150). A recent study also showed that mitochondria associate with ER – late endosome membrane contact sites, proposing the idea of 3-way interaction, similar to what is seen in yeast (151).

1.5. Conclusion

In this thesis, my goals were to elucidate the role of NPC1 and NPC2 on mitochondrial function and the endocytic system in the human neuroblastoma cell line SH-SY5Y. I found that NPC1- but not NPC2-depletion induces lysosomal cholesterol accumulation. However, NPC1-depletion had no effect on mitochondrial length distribution or ER-to-mitochondria lipid transfer at MERCs. NPC2-depleted SH-SY5Y cells show an endosome to ER cholesterol transport defect but appeared cholesterol depleted compared to NPC1-depleted cells. Additionally, NPC2-depletion led to severe reduction of endosomal vesicle density. This defect was prevented by expression of wild type NPC2 or NPC2 variants, independent of their functional domains or retention in the cell. Together these findings suggest a role of NPC2 in endocytic system regulation that does not rely on any known interactions.

2. CHAPTER 2 MATERIALS AND METHODS

2.1. Materials and cell models

2.1.1. Materials

Cell culture medium, fetal bovine serum (FBS), Nu-Serum, and other cell culture supplements were obtained from Life Technologies (Burlington, ON, Canada). Chemicals were obtained from Sigma (Oakville, ON, Canada) or Thermo Fisher Scientific (Waltham, MA, USA). Other materials were sourced as indicated in the methods.

2.1.2. Human tissue cultures

Human neuroblastoma derived cell lines SH-SY5Y (CRL-2266, ATCC) and IMR-32 (CCL-127, ATCC) were cultured in DMEM:F12 medium supplemented with 5 % FBS, 5 % Nu-Serum, GlutaMAX™ (2mM L-alanyl-L-glutamine dipeptide), 1 mM sodium pyruvate, and antibiotics (10 Units/mL Penicillin, 10 Units/mL Streptomycin). Cells were incubated in a humidified 5 % CO_2 atmosphere at 37°C and replated every 3-4 days at 1,800,000 cells per 10 cm dish.

Human embryonal kidney cell line HEK293T (CRL-3216, ATCC) and human osteosarcoma cell line U2OS (HTB-96, ATCC) were cultured in DMEM supplemented with 10 % FBS and antibiotics (10 units/mL penicillin, 10 Units/mL streptomycin). Cells were incubated in humidified 5 % CO_2 atmosphere at 37 °C and split every 3-4 days to be replated at 2,000,000 and 1,500,000 cells per 10 cm dish, respectively.

2.1.3. Rat primary neuron cultures

Hippocampal neurons from E17 embryonic rats were received from the lab of Dr. Stefan Krueger, Dept. of Physiology and Biophysics, Dalhousie University. Neurons were plated on coverslips coated with poly-L-lysine (Vivitide/Peptides International, Gardner, MA) and conditioned in MEM with 5% FBS. After 3 h, the medium was changed to serum-free Neurocell maintenance medium (Wisent) with 2% B27 supplement (Life Technologies), 250 µM GlutaMax, and Penicillin/Streptomycin.

2.2. Molecular Biology

2.2.1. Vectors and vector construction

Generation of pGIPz – microRNA vector: The original pGipz RNA interference vectors were obtained from the GIPZ lentiviral shRNAmir library developed by Open Biosystems (now Thermo Scientific, Waltham, MA, USA). To increase the knockdown efficiency, the hairpin region from the original pGipz RNAi vectors was first doubled, and then an additional hairpin based on a design described by Myburgh et al was inserted between the two original pGipz hairpins (152). Using the triple hairpin vectors, knock down efficiencies of up to 90% were achieved.

To generate a double pGipz hairpin vector, the desired hairpins were amplified in two separate PCR reactions with primers: Upstream Hairpin Forward: 5'-aaacacttgctgggattacttcttcagGTT-3', Reverse: 5'-TCTTGGATCACTAGTATCGTAGCCCTTGAATTCCGAGGCA-3'; Downstream hairpin Forward: 5'-GGCTACGATACTAGTGATCCAAGAAGGTATATTGCTGTTG-3' and Reverse: 5'-ttttgtaatccagaggttgattgttccaga-3'. These amplicons were cloned in a one-step Gibson assembly reaction using NEB HiFi cloning MasterMix (New England Biolabs) according to manufacturer's instructions into the pGipz vector digested with HpaI and MluI. This digest cuts out the hairpin region, so that it can be replaced by the two new amplified hairpins. The reverse primer of the upstream hairpin and the forward primer of the downstream hairpin overlap to enable Gibson assembly and introduce a SpeI restriction site.

A double hairpin cassette did not lead to sufficient depletion of NPC1; therefore, a third hairpin was inserted with a newer design by Myburgh et al., based on mir-16 and with longer flanking regions compared to the original pGipz hairpin design based on mir-30 (152). Hairpins were designed using the i-score algorithm described by Ichihara et al and following the steps outlined by Myburgh et al. (152,153).

To generate the full hairpin for insertion into the vector, a 90 bp synthetic oligo with the general sequence of

TGTCAGCAGTGCCTnnnnnnnnnnnnnnnnnnnnnGTGAAGCCACAGATGmmmmmmmmmm
ZmmmmmmmmmmZAAGTAAGGTTGACCATA, where “n” are targeting sequence nucleotides, “m” are antisense sequence nucleotides, and “Z” are mismatched nucleotides, was amplified with primers forward: 5’-CGGAATTCAAGGGCTACGATACTAGTGGTGATAGCAATGTCAGCAGTGCCT-3’; reverse: 5’-GCAATATACCTTCTTGGATCATCGATGTAGAGTATGGTCAACCTTACTT-3’. pGipz vectors with a double hairpin were digested with SpeI and the hairpin amplicon was inserted using a Gibson assembly reaction.

Generation of pLenti – micro RNA vector: RNAi vectors concomitantly targeting NPC2 and candidate factors in cholesterol trafficking, were generated based on the pLenti-MP2 vector (gift from Pantelis Tsoulfas, Addgene plasmid # 36097 ; http://n2t.net/addgene:36097 ; RRID:Addgene_36097). Four fragments were PCR amplified separately, namely mitomCherry (forward: 5’-tgacctccatagaagacaccgcccACCGGTgccaccATGTCCG-3’, reverse: 5’-CTCCACGTCTCCAGCCTGCTTCAGCAGGCTGAAGTTAGTAGCTCCGGATCCCTTGTACAGCTCGTCCATG-3’), puromycin resistance gene puroR (forward 5’-GCCTGCTGAAGCAGGCTGGAGACGTGGAGGAGAACCCTGGACCTATGGCCACCGAGTACAAG-3’, reverse: 5’-GTATCCGGAACACTGGCGATTCAGGCCGCTCGTACGTTAGGCACCGGGCTTGC-3’), upstream hairpin of gene of interest (forward: 5’-agcggcctgaatcgccagtgttccggatactagtGGTGATAGCAATGTCAGCAGTGCCT-3’, reverse: 5’-CCTCTAGACTGGAAGCTTACTAGTGTAGAGTATGGTCAACCTTACTT-3’), and downstream hairpin NT or NPC2 (forward: 5’-ACACTAGTAAGCTTCCAGTCTAGAGGTGATAGCAATGTCAGCAGTGCCT-3’, reverse: 5’-ATCCAGAGGTTGATTGTCGATACGCGTGTGGATTATCACCACTTTGTACAAGAAAGCTGGGTCTAGAGTAGAGTATGGTCAACCTTAC-3’). These fragments were cloned in a one-step Gibson assembly reaction using NEB HiFi cloning MasterMix Gibson assembly reaction with the pLenti-MP2 vector digested with EcoRV and SmaI. For amplification of the hairpins, the same synthetic oligonucleotides were used as templates as were used for cloning of the middle mir-16 based hairpin in triple hairpin pGipz vectors. The reverse primer for

mitomCherry amplification and the forward primer for puroR amplification encode a P2A element that allows for bicistronic expression of mitochondrial mCherry and puromycin-N-acetyltransferase (puroR).

Generation of pGIPz – micro RNA and NPC2 variant vector: Y119A and V81D were previously established in the Karten lab by Kennedy et al. (62). Wild-type NPC2 was obtained from Dr. Heiko Runz (University of Heidelberg, Heidelberg, Germany). NPC2 variants were amplified with primers forward: 5'-GAAGACACCGACTCTACTAGAGGATCTACCGGTGCCACCATGCGTTTCCTG-3': reverse: 5'CATGGGAGGTGGGAGATGAGAAACGATCTG-3'. Cleavage resistant mCHerry tag was amplified from previous mitomCherry construct with primers truncating the first 11 AA, as published by Huang et al. (154) with primers forward: 5'-CAGATCGTTTCTCATCTCCCACCTCCCATGATCATCAAGGAGTTCATG-3': reverse 5'-GGGGAGGGAGAGGGGCGGAATTTGCGGCCGCCTACTTGTACAGCTCGTC-3'. These fragments were cloned in a one-step Gibson assembly reaction with Triple hairpin vectors pGIPz miRNA vectors digested with AgeI and NotI.

Generation of FUGW – micro RNA and NPC2 variant vector: RNAi vectors targeting NPC1 and NPC2 and expressing wild-type NPC2 or NPC2 variants with point mutations Y119A, V81D and N58A (155,156,62,60,157) (corresponding to Y100, V62 and N39, respectively, in the mature NPC2 protein) were generated base on the UBC promotor containing FUGW-PercevalHR vector gifted from Gary Yellen (Addgene plasmid # 49083 ; http://n2t.net/addgene:49083 ; RRID:Addgene_49083). The plasmid was digested with EcoRI and XbaI to cut out the Perceval open reading frame. The entire cassette of mCherry ORF, IRES element, puroR ORF, and triple microRNA cassettes (shNT, shNPC1, shNPC2) was amplified from the pGIPz constructs with primers forward: 5'-GCAGGTCGACTCTAGACCACCATGCGTTTCCT-3'; reverse: 5"-CTAGCTTCGAAGAATTACGCGTCCTAGGTAATAC-3' and inserted between in the digested FUGW backbone by one step cloned in a one-step Gibson assembly reaction.

Table 1: miRNA targeting sequences

Target	Species	Sequence	Source
Non-targeting (NT)		ttactctcgcccaagcgag	Open Biosystems
NPC1	Human	tcagtagctgtaacattca	Open Biosystems V3LHS_353067
STARD3	Human	tgacaatgaggaatgcact	Open Biosystems V3LHS_359121
NPC2	Human	tgttgaagcagcagagctg	Open Biosystems V2LHS_197809
NPC1	Human, rat	tttattgcattaataaagctct	mirGE
NPC2	Human	attcaagagtaaatttccaggt	mirGE
NPC2	Rat	ttatctgacatcctcaagcatc	mirGE
ARL8	Human	agttatacattacattcatcca	mirGE
IGF2R	Human	ttaaatatgtctttcttgcagg	mirGE
ORP1L	Human	agttacatttaggtataaacct	mirGE
PSAP	Human	tttctcctttaatgatgtcca	mirGE
RAB3A/RAB3B	Human	ttgaagtcgatgcccacggtgc	mirGE
VPS41	Human	ttagtaaacataatggtgcagg	mirGE

Expression and isolation of plasmids: For amplification of plasmid DNA, vectors were transformed into electrically competent STBL4 (*Escherichia coli*, *E.coli*) by electroporation. Plasmid DNA was isolated using the Presto™ Mini Plasmid Kit (Geneaid, New Taipei City, Taiwan) according to manufacturer's instructions. Identity of plasmids was confirmed using restriction digest and sequencing (Eurofins Genomics, Toronto, Canada).

2.2.2. Lentivirus production

For plasmid transduction into mammalian cells, a second-generation lentiviral system was used. HEK293T cells were split onto 10 cm cell culture dishes to a confluency of approximately 60 % the previous day. Then, cells were given fresh growth medium for at least one hour. Transfection mixes were prepared containing 1.2 µg pmd2.G (lentiviral envelope plasmid), 3 µg psPAX2 (lentiviral packaging plasmid), both gifted from Didier Trono (Addgene plasmid # 12259 ; http://n2t.net/addgene:12259 ; RRID:Addgene_12259, Addgene plasmid # 12260 ; http://n2t.net/addgene:12260 ; RRID:Addgene_12260) and 5.8 µg plasmid of interest in 500 µL of minimal essential

medium (MEM) before mixing with 40 µg/mL linear PEI (Polysciences, Inc. Warrington, PA USA) in 500 µl of MEM (amounts given for one 10 cm dish). Transfection mixes were incubated at room temperature for 10 min and added to the growth medium on HEK293T cells, followed by incubation for 5-6 hours. Medium was changed to full growth medium and cells were further incubated for 2 days. The virus-containing medium was collected, sterilized through a 0.45 µm syringe filter and either stored as "unconcentrated virus" at -20 °C or further concentrated using 100 kDa molecular weight cut-off centricon filters (Pall, Mississauga, Canada), according to the manufacturer's instructions, to around 1/50 of the original medium volume. "Concentrated virus" stocks were then stored at -80 °C.

2.2.3. RNA isolation and reverse transcription

Total cellular RNA, free of genomic DNA, was extracted using a 2-stage spin column approach, using the EZ-10 Total RNA Miniprep Kit (Biobasic, Markham ON, Canada). In brief, cells were lysed by a denaturing guanidine-containing buffer and gDNA was selectively absorbed on the first spin column. The RNA in the flowthrough was then adsorbed on the second spin column, washed, and eluted. No additional DNase step was needed using this kit. RNA concentrations were measured using a DS-11 spectrophotometer (DeNovix, Wilmington, DE, USA). cDNA was generated from 1 µg of RNA using the SensiFAST™ cDNA Synthesis Kit (Meridian Bioscience, Québec, Canada) according to the manufacturer's instruction.

2.2.4. Quantitative PCR

Specific mRNA levels were quantified using real time qPCR. Primers for every gene of interest were validated by serial dilution of reference cDNA and the response curve was compared to the curve for the reference gene *ACTB* to verify linear signal response. 25 ng of cDNA were then analyzed by qPCR using SsoAdvanced Universal SYBR Green Supermix (Bio-Rad Laboratories, Mississauga, Canada). Results are shown as mean of at least 3 independent experiments in duplicate ± standard deviation (SD).

Table 2: Primers for qPCR

Target gene	Animal	Forward primer (5'→3')	Reverse primer (5'→3')	Annealing temperature (°C)
ABCA1	Human	ttcctcctggtgagtgctttg	gagggcagtagcccatgttc	
ABCA3	Human	tgcaacccggaagacatctc	gcaatgcccagctctttctg	55
ACTB	Human	agccttccttcttgggtatgg	acacagagtacttgcgctcag	54.6
ARL8	Human	tctgcgatcatcctggaacac	gactgcagccttccgtaaatc	60.7
CD63	Human	caaccacactgcttcgatcctg	gactcggttcttcgacatggaag	62.9
HMGCR	Human	gtgccagcagccgagtc	cctcctttatcactgcgaacc	56.4
IGF2R	Human	caccaggcgtttgatgttgg	tttgggaatggtgccctctc	59.3
LAMP1	Human	gtgaccgtaacgctccatga	cttgtcaccgtcgtgttgtc	59.4
LDLR	Human	gtgacaatgtctcaccaagctct	gtagctgtagccgtcctggtt	60.8
NPC1	Human	catgggcagctccgtgttc	tgatggccctatgtaactgag	53.4
NPC2 3'UTR	Human	gtttcctggcagctacattc	ggtgacattgacgctgtaaga	56.4
NPC2 CDS	Human	agtggaattaactgccctatc	ggccagatgcaccgaact	52
ORP1L	Human	gaaatgccagtgccggattc	tctgatgtcaggccgtaacc	58.9
PSAP	Human	cgaacatgtctgcttcatgc	ttctggtgattcagctctgc	56
RAB5	Human	acgggccaaatacgggaaat	tcaaactttaccccaatggtactc	59.2
RAB7	Human	tgggagattctggagtcggg	ccacaccgagagactggaac	60
RAB8	Human	aacggtttcggacgatcaca	tagtcgagggccagcttttc	59.7
STARD3	Human	agcgagtggaagacaacacc	ccgacttgagcacgatgaag	58.9
VPS41	Human	tctgtgagtcgtgcctttcc	tggtccacggttcttagcac	59.4

2.2.5. Transcriptome analysis

Cellular transcription analysis was performed using microarray analysis. Cells were infected with virus expressing pGIPz shNT, shNPC1, and shNPC2 constructs. After 3 days, cells were passaged and grown for another 3 days to eliminate transcription differences base on initial infection. RNA was isolated as above and analysed by the microarray facility at The Hospital for Sick Children (Toronto, Canada). Data analysis was done using Transcriptome Analysis Console (TAC version 4.0, Thermo Fisher Scientific, Waltham, MA, USA) and significance was assumed at $p<0.05$ and a 2log fold change of 1.3.

2.2.6. Protein isolation and Western blotting

Total cellular protein was isolated by lysing cells with 0.1 % SDS in PBS with added protease inhibitors (5 µg/mL leupeptin, 5 µg/mL aprotinin, 50 µg/mL PMSF and 1 µM pepstatin) as well as phosphatase inhibitors (2 mM ortho-vanadate and 1 mM sodium

fluoride). To combat high viscosity of lysates caused by gDNA, 25 U/mL Benzonase® Nuclease (Sigma-Aldrich, Oakville, Canada) or equivalent nuclease was added to the lysis buffer directly prior to lysing of cells. After 5 mins, the lysates were collected and transferred into microcentrifuge tubes. Protein concentration was determined using Pierce™ BCA Protein Assay Kit (Thermo Fisher Scientific, Waltham, MA, USA) according to the manufacturer's instructions for 96 well plates with BSA as a standard. For storage, protein lysates were denatured by addition of sample buffer for a final concentration of 8 % SDS, 0.2 M Tris-HCl, 30 % Glycerol, 0.1 % bromophenol blue with 5 % 2-mercaptoethanol and incubation for 5 min at 95 °C. Samples were separated by SDS – polyacrylamide gel electrophoresis (SDS – PAGE) and transferred to a nitrocellulose membrane. Total protein was visualized using Pierce™ Reversible Protein Stain Kit (Thermo Fisher Scientific, Waltham, MA, USA), imaged, and destained. Blots were blocked in either 5 % skim milk powder, 2 % BSA or 2 % Polyvinylpyrrolidone (PVP) in TTBS (5 % Tween in Tris buffered saline at pH 7.4). PVP blocking was used for detection of NPC2, because NPC2 can be secreted into milk (158). Primary antibodies and working dilutions in corresponding blocking buffer plus 0.05 % sodium azide are listed in Table 3. Secondary antibodies conjugated to horseradish peroxidase, raised in donkey, against rabbit-, mouse-, or goat-IgG (Jackson ImmunoResearch) were diluted 1:10,000 in the corresponding blocking buffer. Antibody binding was detected by Clarity or Clarity Max ECL Western Blotting Substrates (Bio-Rad Laboratories, Mississauga, Canada) using the FluorChemE System (ProteinSimple, San Jose, CA, USA). Densitometry was performed using the "FIJI is just ImageJ" (FIJI) software (159) normalized to actin.

Table 3: Primary antibodies for IF and western blotting

Target	**Raised in**	**Company (Catalog #)**
Actin	Goat	Santa Cruz Biotechnology (sc-1616)
CD63	Mouse	DSHB (H5C6-s)
LAMP1	Mouse	DSHB (H4A3)
LAMP2	Mouse	DSHB (H4B4)
NPC1	Rabbit	Novus Biologicals (NB400-148)
NPC2	Mouse	Santa Cruz Biotechnology (sc-166449)
Phospho-TFEB (SER211)	Rabbit	Cell Signaling Technology (37681S)
RAB5	Rabbit	Cell Signaling Technology (3547S)
TFEB	Rabbit	Cell Signaling Technology (37785S)

2.3. Cellular and endocytic systems assays

2.3.1. Cell growth assay

For quantification of cell growth over time, the Cell Counting Kit-8 (CCK-8, APExBio, Houston, TX, USA) was used according to the manufacturer's instructions. Cells were seeded at 10,000 cells per well in 100 µL growth medium on two 96 well plates. After 24 h (day 1), 10 µL of the WST-8 (2-(2-methoxy-4-nitrophenyl)-3-(4-nitrophenyl)-5-(2,4-disulfophenyl)-2H-tetrazolium) containing CCK-8 reagent was added to one of the plates and incubated for 2 h at 37 °C and 5 % CO_2. Conversion of WST-8 to the orange formazan product by cellular dehydrogenases was measured using absorbance at 450 nM. Steps were repeated for the second plate 48 h later (day 3). Growth was quantified as absorbance delta of day 3 to day 1 of at least 5 independent experiments in quadruplicate.

2.3.2. Lactate assay

SH-SY5Y cells were washed with warm PBS before incubation with phenol red-free, glucose-free DMEM with 10 mM glucose added for 3 h. Medium was collected and cells lysed in 0.1 % SDS in PBS for protein measurement. Lactate levels in the medium were measured by fluorescence assay adapted from Shapiro et al. (160). In brief; 10 µL of collected medium were incubated with 100 µL of reaction mix (1 mM NAD+, 48 nM resazurin, 1 U/mL diaphorase, and 18.5 U/mL L-lactate dehydrogenase) in Tris/HCl Buffer (75 mM, pH 8.9 with 100 mM KCl and 0.0004% Triton X-100) for 30 min at 37 °C. Conversion of lactate and NAD^+ to pyruvate and NADH by lactate dehydrogenase is quantified by the stoichiometric turnover of resulting NADH by a diaphorase-catalyzed reaction of resazurin to resorufin and NAD^+. The resulting resorufin was detected by fluorescence measurement at 570/590 nm (excitation/emission) on a SpectraMax Gemini Microplate reader (Molecular Devices, San Jose, CA, USA) and lactate concentrations were quantified with a calibration curve on the same assay plate. Lactate in the medium was normalized to total cellular protein. Data were derived from 3 independent experiments in triplicate.

2.3.3. Cholesterol assay

To measure unesterified and total cholesterol in medium or cell lysates, a fluorometric Amplex™ Red (Thermo Fisher Scientific, Waltham, MA, USA) assay was used. Cell lysates in PBS with 0.1% SDS or medium samples were incubated for 15 min at 37 °C with reaction mix (37.5 µg/mL Amplex Red, 1 U/ml HRP, 1 U/mL cholesterol oxidase, 0.1 M potassium phosphate pH 7.4, 0.05 M NaCl, 0.1 % TritonX-100) or reaction mix including 1 U/mL cholesterol esterase, for quantification of unesterified or total cholesterol, respectively. Hydrogen peroxide released stoichiometrically by the oxidation of cholesterol reacts with Amplex Red to form fluorescent resorufin. Resorufin fluorescence was measured at 570/590 nm (excitation/ emission) over 15 min at 37 °C in 1 min intervals and averaged. Quantification was performed via a standard curve of cholesterol measured at the same time. Data were derived from at least 3 independent experiments in duplicate or triplicate.

2.3.4. NAG assay

Lysosomal exocytosis was quantified by measurement of the activity of lysosomal N-acetylglucosaminidase (NAG) in the cell culture medium, using a fluorescent assay adapted from the original protocol by Rodríguez et. al. (161–163). In brief, medium on cells grown in multiwell plates was changed to full growth medium with vehicle (dimethylsulfoxide, DMSO) or 10 µM Vacuolin-1 in DMSO for 1 h. Cells were washed once with Hepes buffered saline (HBS, 124 mM NaCl, 3 mM KCl, 5 mM D-glucose, 2 mM $CaCl_2$, 1 mM $MgCl_2$, 10 mM Hepes, pH 7.4,) and incubated for 15 min in HBS. HBS was collected, and cells were lysed using 1 % Igepal in HBS (including protease inhibitors and Benzonase) for 5 min. HBS and cell lysates were centrifuged at 10,000 g for 3 min to pellet debris. Cleared supernatants were incubated for 15 min at 37 °C with fluorescent substrate (4-methylumbellyferryl-N-acetyl-D-glucosaminide) at a final concentration of 0.75 nM. Stop solution (2 M Na_2CO_3, 1.1 M glycine) was added and fluorescence was measured (emission wavelength: 365nm, excitation wavelength: 450 nm). Lysosomal activity was expressed as the ratio of fluorescence signal in the medium to total cell lysate fluorescence of at least 3 independent experiments in quintuplicate.

2.4. Microscopy

2.4.1. Collagen-coating of coverslips

To grow SH-SY5Y on glass coverslips to be imaged using microscopy, extracellular matrices have to be applied to the glass coverslips. Coverslips were covered with 100 µg/mL collagen I from rat tail (Corning, Glendale, AZ, USA) in 30 % ethanol (~60 µL per 12 mm coverslip) and immediately neutralized by placing the dish under a box with a filter paper soaked in concentrated ammonium hydroxide for 2 minutes. The ammonia vapour gels this first layer of collagen. The coverslips were washed twice with sterile water before applying a second layer of collagen (~30 µL per 12 mm coverslip). The second layer was dried in the biosafety cabinet for 2h. Cells were plated on coverslips within a few hours after coating.

2.4.2. Cell fixation, dye- and immunostaining

Fibroblasts and SH-SY5Y cells cultured on glass coverslips or collagen-coated glass coverslips, respectively, were washed 3 times with room temperature (RT) PBS before fixation with cold 4 % paraformaldehyde (PFA) in PBS for 12 mins. Residual PFA was removed by washing the coverslips 4 times with PBS. Cells were permeabilized with 0.1 % Saponin or 50 µg/mL filipin III complex (Sigma-Aldrich, Oakville, Canada) in PBS or immunofluorescence (IF) blocking buffer (1 % BSA and 5 % goat serum in PBS) as applicable. For staining with filipin alone, cells were washed 3 times with PBS and mounted on microscope slides using AquaMount (Thermo Fisher Scientific, Waltham, MA, USA). For immunocytochemistry, coverslips were incubated with primary antibodies in IF blocking buffer (Table 3) overnight at 4 °C. Cells were washed 3 times in PBS and incubated with fluorophore-conjugated secondary antibodies, raised in donkey, against mouse-, rabbit- or goat- IgG (Jackson ImmunoResearch, West Grove, PA, USA) at 1:250 in IF blocking buffer for 2 h at RT. For nuclear staining, 4 nM of Hoechst stain in PBS was applied for 15 min following incubation with the secondary antibodies. Cells were washed 3 times with PBS and mounted onto microscope slides with AquaMount.

Rat hippocampal neurons were infected with lentiviruses to express RNAi vectors targeting NPC1, NPC2, or encoding a non-targeting control hairpin. RNAi vectors also

encoded cytosolic, green-fluorescent turbo GFP (tGFP). Two weeks after plating, neurons were fixed with 4% paraformaldehyde and stained with filipin as above.

2.4.3. Mitochondrial morphology

SH-SY5Y cells were seeded on collagen-coated glass coverslips at 50,000 cells per well on a 24 well plate and grown for 3 days. Cells were treated with or without 250 µM H_2O_2 for 6 h before fixation and immunostaining for mitochondrial TOM20 and mounting in AquaMount. Cells were imaged on a confocal microscope (acquisition details see below) and individual cells were manually circled. Images were preprocessed and analysed using the java-based Momito algorithm, first described by Ouellet et al. (164). In brief, images were preprocessed using the included tool with standard settings, applying automatic-threshold and separating individual mitochondria. Momito analysis software calculated length of individual mitochondria and counted frequency of mitochondria length in 0.5 µm bins for cell length profile. Data are from one experiment with 23 to 29 individual cells per condition.

2.4.4. DiI – LDL uptake

SH-SY5Y cells were seeded on collagen-coated glass coverslips at 50,000 cells per well on a 24 well plate and grown for 3 days. Cells were starved of cholesterol overnight by incubation in growth medium containing 5 % lipoprotein-deficient serum (LPDS) instead of FBS and Nu-Serum. Cells were then incubated in LPDS-containing medium supplemented with 50 µg/mL LDL and 10 µg/mL 3,3'-dioctadecylindocarbocyanine– LDL (DiI – LDL, Kalen Biomedical, Montgomery Village, MD, USA) for 30 min. Cells were fixed and mounted in Aquamount. Data are expressed as mean DiI signal per cell of 4 different experiments with duplicate coverslips. Significance was analysed by nested ANOVA and post-hoc test (SIDAK's MC). Graphs depict the four nested experiments, with an average of 140 cells per condition, as used for statistical analysis, and the same data in one column for all experiments together for visual representation.

2.4.5. Plasma membrane cholesterol

SH-SY5Y cells were seeded on collagen-coated glass coverslips, transduced with the green-fluorescent cholesterol sensor pLenti-CMV Clover3-D4H, and grown for another 3 days. Cells were washed 3 times with ice-cold HBS and incubated with 10 µg/mL fluorophore-conjugated wheat germ agglutinin (CF650R-WGA) for 30 min on ice. Cell were washed 3 times with ice-cold HBS, fixed, and mounted in AquaMount. Images were acquired with at 474/527 nm (ex/em) for Clover3 and 628/692 nm (ex/em) for CF650R-WGA. Using FIJI, multiple non-biased regions of interest (ROI) were defined. To obtain the plasma membrane ROI (ROI 1), WGA pictures were background subtracted (rolling ball algorithm, 10 px diameter) and auto-threshold was applied ("Moments"-algorithm). For internal D4H ROI (ROI 2), the auto-threshold algorithm "Moments" was applied to the D4H image, and then the plasma membrane ROI obtained from the WGA signal (ROI 1) was excluded. ROIs were masked for infected cells using the expression control fluorescent signal with the auto-threshold "Huang", to exclude all non-infected cells. Data is expressed as either mean ratio of D4H signal to WGA signal with ROI1 per image (PM cholesterol), or D4H signal with ROI1 per image (internal cholesterol). Significance was analysed using nested – ANOVA and post-hoc test (Tukey's MC). Graphs depict the 3 nested experiments and a one column pooled version for visual representation exclusively.

2.4.6. Endocytic vesicle analysis

To analyse distribution, size and number of endocytic vesicles, a workflow and script was developed. Cells grown on collagen-coated coverslips were fixed and immunostained for endocytic proteins of interest combined with Hoechst staining. Confocal images were taken and analysed on FIJI. Individual cells and their nuclei were circled manually using the fluorescence images of cytosolic mCherry and the Hoechst stain. Endocytic vesicle images were processed with the rolling ball algorithm (15 px radius for RAB5, 25 px radius for LAMP1, LAMP2 and CD63) to remove background and non-vesicular fluorescence and the auto-threshold algorithm "default" was applied. Images were postprocessed using the "despeckle" function for artefact removal. The

"watershed" function was then applied to break up particle clusters. The resulting image was used to obtain number and size of particles using the "particle analysis" function for each circled cell. To account for differences in cell size, the vesicle number per cell was divided by the cell area, resulting in vesicle density. The size of vesicles was averaged for each cell. To calculate particle distance to nucleus, coordinates of particles and nucleus were measured and distance calculated for each particle. Distance per particle was averaged per cell and expressed as percentage of control (shNT). Data were derived from at least 4 different experiments with duplicate coverslips, with an average of 42 cells per condition.

2.4.7. DQ – BSA assay

To quantify lysosomal proteolysis, degradation of DQ-BSA self-quenching was measured. Cells were incubated for 6 h with 100 µg/mL DQ-BSA (Thermo Fisher Scientific, Waltham, MA, USA) in full growth medium. After incubation, cells were fixed and imaged. Lysosomal proteolysis was expressed as fluorescent signal produced.

2.4.8. Image acquisition and analysis

Images of live or fixed cells were taken on a Nikon TE2000 epifluorescence microscope with a CCD camera (ORCA Hamamatsu) and 20x objective using IPLab (BD Biosciences, Franklin Lakes, NJ, USA) or ImageJ-based Micromanager 2.0.0 (165,166) software. Confocal images were taken on a Zeiss LSM 710 laser scanning microscope with 63x objective on Zen v2.3 image capture software (Zeiss, Oberkochen, Germany). All post-capture image analysis was performed using the open-source software FIJI.

Table 4: Filter settings for Nikon TE2000 epifluorescence microscope

Fluorophore	**Excitation filter [nm]**	**Emission filter [nm]**
Filipin, Hoechst	387/11	447/60
mTurquoise	427/10	472/30
Clover	474/23	527/42
mCherry, DiI, DQ-BSA	585/29	628/33
CF650R, Cy5	628/40	692/40

2.5. Radiotracer assays

2.5.1. Lipid transport between ER and mitochondria

Infected SY-SY5Y cells were plated at 600,000 cells per well of a 6 well plate and grown for 24 h in full growth medium. The day before the assay, cells were incubated with 50 µg/mL LDL overnight. Cells were incubated with serine-free DMEM for 2 h, followed by addition of 5 µCi/mL of L-[^{3}H]-serine (Perkin Elmer, Woodbridge, Canada) for 3 h. Cells were washed with PBS and harvested twice with 1 mL of methanol: dH_2O (5:4, v/v) twice after 0, 1, 2, 3, 4, and 5 h. Two hundred µL of this lysate were used for protein measurement. Six mL of $CHCl_3$:methanol (1:2, v/v) and 10 µg PS and PE standards were added to the remaining lysate and mixed vigorously before adding 3 mL of 0.58 % (w/v) NaCl and mixing again. Extracts were centrifuged at 2,500 rpm for 5 min and upper phase was aspirated. Two ml of ideal upper phase (MeOH:0.58% NaCl:$CHCl_3$, 45:47:3, v/v/v) were added, mixed and centrifuged again before aspirating the upper phase. This step was repeated once before the lower organic phase was evaporated under N_2 atmosphere and redissolved in 0.2 mL $CHCl_3$. Samples and 10 µg PS and PE standards were loaded on a TLC plate and separated using $CHCl_3$:methanol:acetic acid:dH_2O (60:40:4:1, v/v) mobile phase. Plates were stained with iodine, spots corresponding to PS and PE were scraped and L-[^{3}H]-serine incorporation was measured using a scintillation counter. Lipid transport from ER to mitochondria and conversion of PS to PE is expressed as ratio of PE to PS over the time course. Data were derived from 3 independent experiments in duplicate.

2.5.2. Cholesterol transport to ER

To measure incorporation of LDL-derived cholesterol into cholesterol esters, infected SH-SY5Y cells were seeded onto 6 well plates at 400,000 cells per well in duplicate and grown for 3 days before starving them overnight in lipoprotein-deficient serum (LPDS) growth medium (DMEM:F12, GlutaMAX™ (2mM L-alanyl-L-glutamine dipeptide), 1 mM Sodium Pyruvate, 10 % LPDS). Medium was changed to 1 mL LPDS growth medium + 10 µL [9,10-^{3}H(N)]-oleic acid (Perkin Elmer, Woodbridge, Canada) complexed to BSA (10 mM (6:1; oleate/BSA) at ~100,000 dpm/µL.) for 4 h. Cells were washed twice with warm

150 mM NaCl, 50mM Tris-HCL pH 7.4 buffer followed by washing once with 150 mM NaCl, 50 mM Tris-HCl pH 7.4 buffer and lipid were extracted with hexane:isopropanol + 0.01 % butylhydroxytoluene for 30 min with occasional mild agitation. Cell precipitate was used for protein measurement. Extracts were spiked with 10 µg cholesterol oleate (CO) and 10 µg triolein (TO) for visualization and evaporated under nitrogen atmosphere. Dried samples were reconstituted with 100 µL hexane and spotted on a silica thin layer chromatography plate (TLC; Analtech, Maynooth, Ireland) with a hexane/diethyl ether/acetic Acid (90:30:1) mobile phase. Plates were stained with iodine, spots corresponding to CO and TO were scraped and [^{3}H]-oleic acid incorporation was measured using a scintillation counter (EcoLite™+ from MPBio on Beckman LS6500 scintillation counter). Disintegrations per minutes (DPM) were normalized to total protein per sample. Data were derived from 3 different experiments in duplicate and expressed as percentage of control.

2.5.3. Cholesterol biosynthesis

Infected SY-SY5Y cells were plated at 600,000 cells per well of a 6 well plate and grown for 24 h in growth medium. Medium was then changed to LPDS-containing medium, LPDS medium + 50 µg/mL LDL, or full growth medium for 24 h, after which medium was changed to LPDS medium + LDL, LPDS medium, or full growth medium, each with 2 µCi/mL [2-^{14}C]-acetic acid (Perkin Elmer, Woodbridge, Canada) for another 24 h. Cells were washed and lipids extracted using hexane:isopropanol + 0.01 % butylhydroxytoluene for 30 min. Cell precipitate was used for protein measurement. Extracts were evaporated under N_2 atmosphere before resuspension in 1 mL NaOH (0.1 M) and addition of 10 µg cholesterol standard. Three mL of anhydrous ethanol was added before saponification of samples by addition of 0.5 mL of 50 % KOH (v/v) and incubation for 1 h at 60 °C. Samples were cooled to RT and sterols extracted twice with 3 mL hexane. Organic phase was evaporated under N_2 atmosphere, redissolved with 100 µL chloroform and separated using TLC alongside cholesterol standard using cyclohexane: ethyl acetate (3:2) mobile phase. Plates were stained with iodine, spots corresponding to cholesterol were scraped, and [^{14}C]-acetic acid incorporation was

measured using a scintillation counter. DPM were normalized to total protein and expressed as a percentage of non-targeting control. Data were derived from 3 independent experiments in duplicate.

2.6. Statistics

Statistical analysis was done using Microsoft Excel (Redmond, WA, USA) or Graphpad Pro Prism (San Diego, CA, USA) software. Significance between three or more groups was calculated using ANOVA testing with Tukey's multiple comparison for post-hoc testing, unless otherwise indicated. Bar graphs depict mean ± SEM. Box and whisker graphs are median with 95 percentile box and Min/Max whiskers. Significance was assumed at $p < 0.05$ and indicated as *$p<0.05$, **$p<0.01$ and *** $p<0.001$.

3. CHAPTER 3 RESULTS: ER – MITOCHONDRIA CONTACTS

Previous studies published by the Karten lab and others have shown that depletion of NPC1 causes cholesterol accumulation in LE/L and leads to NPC2- and STARD3-mediated increased cholesterol transport to the mitochondria (155,167). This increased cholesterol influx to mitochondria can cause mitochondrial dysfunction. Building on these insights, this chapter aimed to elucidate the influence of mitochondrial cholesterol on various mitochondrial characteristics, such as morphology and ER-mitochondria contact sites. NPC disease is a neurodegenerative disease, so the human neuroblastoma cell line SH-SY5Y was chosen to study this relationship in a disease-related cell line (168).

3.1. Micro RNA-induced depletion of NPC1 leads to cholesterol accumulation in LE/L

For depletion of NPC1 and STARD3, miRNA silencing was chosen. Hairpins were based on mir-30 and mirGE design with a pGIPz lentiviral expression vector. Lentiviral infection was chosen for RNAi vector expression because the high transduction efficiency allowed acute effects of protein depletion. Moreover, the heterogeneity and plasticity of SH-SY5Y cells make it impractical to establish stable, monoclonal lines derived from SH-SY5Y cells. To achieve depletion of two proteins at the same time, several microRNA hairpins were concatenated within one vector.

Quantitative PCR showed a reduction in NPC1 mRNA by approximately 70% in SH-SY5Y cells transduced with vectors targeting NPC1 or NPC1 and STARD3 together compared to non-targeting control (**Figure 3.1** A). Similarly, mRNA levels for STARD3 in STARD3-depleted cells, with and without co-depletion of NPC1, showed a reduction of 70 % to control levels (**Figure 3.1** B). Co-depletion did not alter effectiveness of the individual depletions based on residual mRNA levels.

To investigate the effectiveness of NPC1 depletion to induce cholesterol accumulation in LE/L, cells were loaded with LDL overnight and filipin staining was performed. Cells depleted of either NPC1 alone or co-depleted with STARD3 showed punctate filipin staining in LE/L-like compartments, indicating strong cholesterol accumulation at a similar level as expected (**Figure 3.1** D). STARD3 depletion by itself did not induce

cholesterol accumulation in SH-SY5Y cells. These patterns were observed in both SH-SY5Y subtypes, the neuron-like (n-type) and epithelial-like (s-type) cells.

Previous studies in CHO cells from the Karten lab showed increased lactate production in NPC1-depleted cells, and that STARD3 co-depletion prevented this effect (155,169). To study the effects of NPC1 and STARD3 depletion in SH-SY5Y cells, lactate assays were performed. NPC1-deficient SH-SY5Y cells showed higher lactate secretion, while depletion of STARD3 alone did not affect the formation of lactate (**Figure 3.1** C). SH-SY5Y cells depleted of both, NPC1 and STARD3, showed significant lactate production. This observation was in contrast to previous results in CHO cells, where co-depletion of STARD3 and NPC1 normalized lactate secretion compared to NCP1-deficient cells (155).

Taken together, these results show that the miRNA-based approach succeeds in depleting endogenous NPC1 and STARD3 levels as well as to induce cholesterol accumulation in LE/L and increased lactate secretion with NPC1 depletion. However, STARD3 co-depletion did not normalize lactate production in NPC1 depleted cells, in contrast to previous results in CHO cells (155).

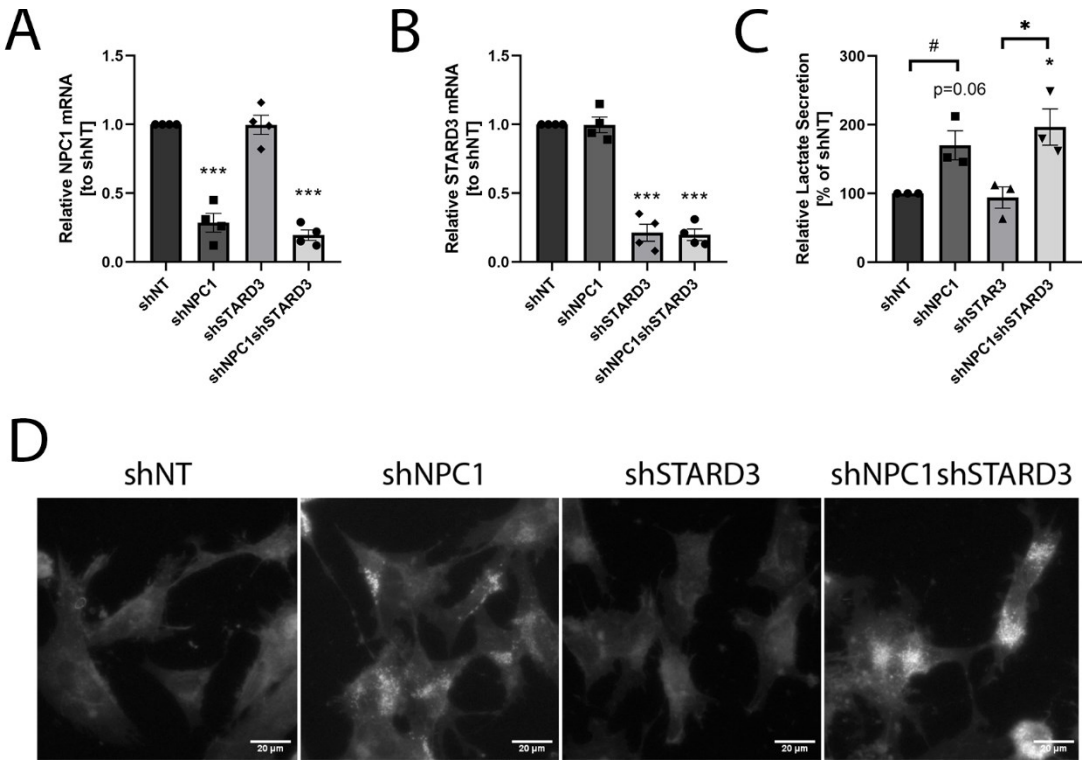

Figure 3.1: NPC1 depletion causes cholesterol accumulation in SH-SY5Y cells. SH-SY5Y were transduced with pGIPz shNT, shNPC1, shSTARD3, and shNPC1shSTARD3 (**A – B**) SH-SY5Y RNA was isolated and NPC1 and STARD3 expression levels analysed by qPCR using ACTB as reference gene. (**C**) Lactate secretion into the medium during 5 h incubation. # indicates significance by students t-test of $p < 0.05$ (**D**) Cells were incubated with LDL overnight before fixation and staining with filipin.

3.2. Mitochondria length distribution algorithm "Momito" struggles with SH-SY5Y morphological heterogeneity.

NPC1-depletion has been shown to induce mitochondrial dysfunction, which could be prevented by STARD3-co-depletion in some cases (155,170). However, in SH-SY5Y cells, increased lactate secretion could not be prevented by STARD3-co-depletetion. To further investigate how NPC1-depletion affects mitochondria health and the protective capabilities of STARD3-co-depletion, mitochondria morphology was investigated as a major indicator for mitochondrial health (171,172).

Mitochondrial length distribution in SH-SY5Y was investigated using a recently published algorithm named "Momito" (164). To evaluate the algorithm in SH-SY5Y cells, mitochondrial fragmentation was induced by H_2O_2 treatment, and cells were immunostained for the mitochondrial TOM20 protein. Images were analyzed using the

Momito algorithm (**Figure 3.2** A). H_2O_2-treated SH-SY5Y cells showed clear mitochondrial fragmentation and the Momito analysis length distribution showed a significant shift to shorter mitochondria in the H_2O_2-treated SH-SY5Y cells (**Figure 3.2** B). However, considering the severe mitochondrial fragmentation, the difference between the curves for control and H_2O_2-treated SH-SY5Y cells appeared small, and statistical significance was low; possibly due to the high morphological heterogeneity of SH-SY5Y cells (**Figure 3.2** C).

Next, mitochondria length distribution of SH-SY5Y cells depleted of NPC1 and/or STARD3 was analysed. Fluorescence images of mito-mTurquoise showed no overt differences in mitochondrial morphology or distribution (**Figure 3.2** D-E). Analysis with the Momito algorithm showed a trend to shorter mitochondria length compared to control in all other groups. This trend was most apparent in the NPC1-depleted cells having the highest number of short mitochondria fragments, but differences were not statistically significant. Graph shown depicts one representative experiment including all miRNA constructs. Other experiments with different combinations of vectors showed similar results but were not combined as due to slight experimental setup variations such as infection time, image acquisition and data analysis.

Taken together, these results show no difference in mitochondria length distribution between genotypes. However, SH-SY5Y morphological heterogeneity might limit the efficiency of the Momito algorithm.

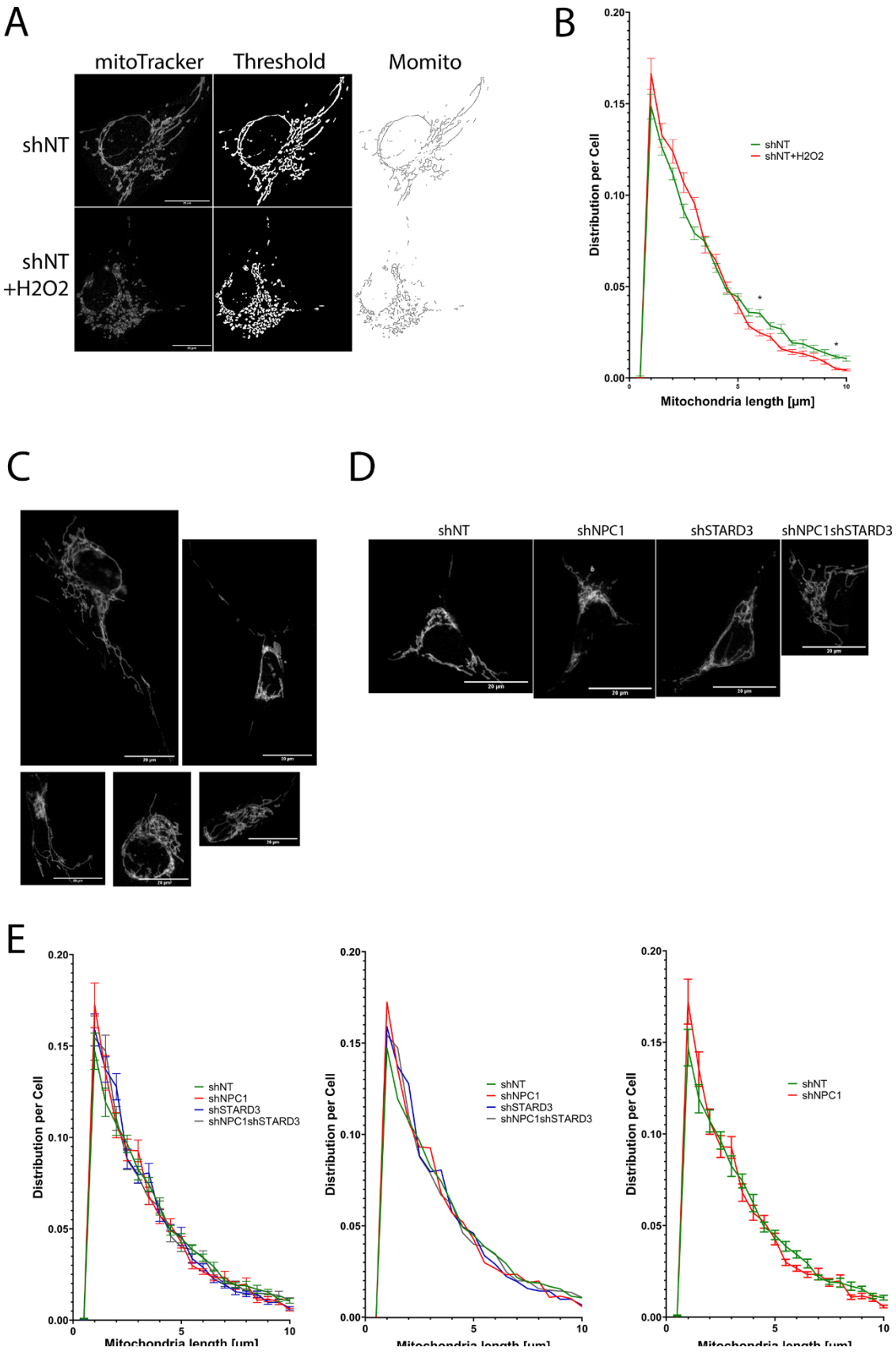
A
mitoTracker
Threshold
Momito
shNT
shNT
+H2O2
B
Distribution per Cell
Mitochondria length [µm]
shNT
shNT+H2O2
C
D
shNT
shNPC1
shSTARD3
shNPC1shSTARD3
E
Distribution per Cell
shNT
shNPC1
shSTARD3
shNPC1shSTARD3

Figure 3.2: High morphological variability of SH-SY5Y diminishes mitochondrial length differences. (**A-C**) SH-SY5Y treated with or without H_2O_2 were immunostained with TOM20 antibodies. Images were acquired on a confocal microscope and processed with the Momito algorithm. (A) Workflow of Momito algorithm, showing raw, preprocessed, and analysed images of SH-SY5Y cells with or without H_2O_2. (B) Mitochondrial length distribution profile. Data are from one experiment with SEM. (C) Representative images showing cellular heterogeneity of non-treated SH-SY5Y cells. (**D-E**) SH-SY5Y were transduced with shNT, shNPC1, shSTARD3, or shNPC1shSTARD3. Cells were grown on collagen-coated coverslips for 3 days before fixation and immunostaining for TOM20 (D). (E) Images were analysed using Momito algorithm. Data are from one experiment presented with SEM (left panel), without SEM (middle panel) and only comparing shNT and shNPC1 data with SEM (right panel).

3.3. NPC1 depletion has no effect on mitochondria associated membrane mediated lipid transfer.

MERC are a major regulator of mitochondria fission and fusion as well as calcium and lipid exchange (173,174). Cholesterol is enriched at these locations and alterations of cholesterol levels have been shown to alter ER and mitochondria association (175).

To investigate the functionality of MERC in NPC1-depleted cells, MERC phospholipid transfer was quantified. Radiolabelled serine is converted in the ER to PS, transported to mitochondria via MERC and converted to PE. The conversion of PS to PE only occurs in mitochondria; therefore, radiolabeled PE reflects the import of PS into mitochondria. The ratio of PE to PS over time was used to quantify MERC-associated lipid transfer. The PS to PE ratio increased linearly over the course of the 5 h experiment in control cells, indicating a steady transport of PS to the mitochondria. However, no difference in PS transport was measured for NPC1-depleted SH-SY5Y compared to control cells at any timepoint, indicating that mitochondrial cholesterol does not affect the rate of MERC-mediated transport of phospholipids (**Figure 3.3** A). Similarly, depletion of NPC2 in SH-SY5Y cells did not change phospholipid transfer between the ER and mitochondria (**Figure 3.3** B). Absolute values of PS and PE radioactivity at t = 0 were similar between conditions, but varied between experiments and were therefore expressed as percentage of control.

These findings indicate that mitochondrial dysfunction caused by depletion of NPC1 does not interfere with MERC associated lipid transfer between the ER and mitochondria.

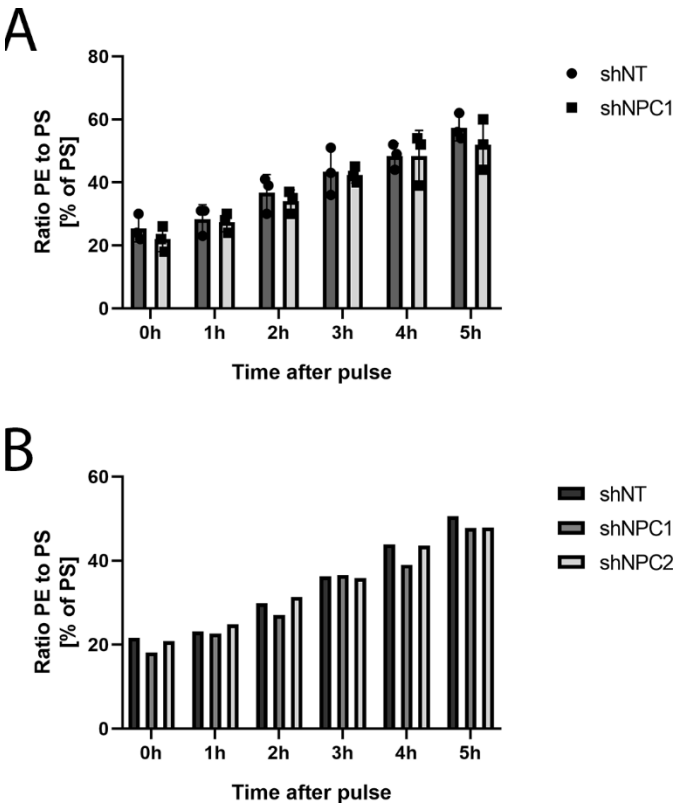

Figure 3.3: SH-SY5Y cells depleted of NPC1 or NPC2 show normal ER-M-CS mediated phospholipid transfer. (**A**) SH-SY5Y cells were transduced with pGIPz shNT and shNPC1. Cells were loaded overnight with LDL before pulsing with [^{14}C]-serine for 3 h. Cells were harvested over a 5 h chase and radiolabelled PS and PE were measured. ER to mitochondria lipid transfer was quantified as percentage of radiolabelled PE converted from PS over time. (**B**) Individual experiment of (A) including SH-SY5Y cells transduced with pGIPz shNT, shNPC1, and shNPC2.

4. CHAPTER 4 RESULTS: NPC2

Chapter 3 showed that although STARD3 mRNA was depleted in SH-SY5Y cells, it did not have the same effect on lactate production as previously seen in CHO cells. Furthermore, studies done by colleagues indicated that depletion of STARD3 decreased growth of SH-SY5Y cells, while SH-SY5Y cells co-depleted of NPC1 and STARD3 showed increased growth and a tendency to form floating spheroid cultures reminiscent of neurospheres, indicating additional effects of STARD3 not manifesting in CHO cells. These additional not yet described effects would make it challenging to directly associate any observed phenotype of these cells to mitochondrial cholesterol or dysfunction.

An alternative model to study elevated mitochondrial cholesterol without direct interference with STARD3 is to use NPC2 depletion and expression of NPC2 variants, as previously published by the Karten lab (62). Depletion of NPC2 led to accumulation of cholesterol in LE/L in CHO cells, without increase in mitochondrial cholesterol. However, it was shown that additional expression of an NPC2 variant with a missense mutation (V81D), which is unable to bind to NPC1, can increase mitochondrial cholesterol by selective shuttling of cholesterol via STARD3 to mitochondria. Expression of an NPC2 variant (Y119A) unable to bind sterols did not show this increased mitochondrial cholesterol. This model was chosen as an alternative approach to study the effects of mitochondrial cholesterol in SH-SY5Y cells.

4.1. NPC2 depletion does not induce filipin accumulation in SH-SY5Y cells

To elucidate the effect of NPC2 depletion on cholesterol transport in SH-SY5Y cells, endogenous NPC2 was targeted with miRNA-mediated RNA interference. Silencing vectors based on the pGIPz backbone were delivered using lentiviral particles with an infection efficiency of ~90%, based on fluorescent marker expression. Quantitative PCR of cDNA obtained from infected SH-SY5Y cells showed a reduction of mRNA levels of endogenous NPC1 and NPC2 to 30 % and 10 %, respectively (**Figure 4.1** A-B). Quantification of NPC2 mRNA levels in fibroblast revealed similar depletion levels as in SH-SY5Y cells (**Figure 4.1** C). Compared to a previous study in CHO cells, residual NPC2

mRNA levels were similar or even lower in SH-SY5Y after miRNA-induced silencing (62). Protein levels of endogenous NPC1 and NPC2 were also markedly reduced (**Figure 4.1** D-E) by the miRNA vectors. Total protein staining and β-actin band intensity indicated equal loading across the lanes. Immunoblotting for NPC2 required nearly fourfold higher levels of protein loading, indicating low antibody binding or low abundance of the protein in SH-SY5Y cells. Two bands were observed for NPC2, likely corresponding to the apoprotein and the glycosylated protein as previously suggested (42,60,158).

One of the major hallmarks of NPC1 and NPC2 depletion is the accumulation of cholesterol and sphingolipids in LE/L (176,177). To determine if NPC2 depletion leads to this characteristic cholesterol accumulation in SH-SY5Y cells, cells infected with the pGIPz miRNA vectors shNT, shNPC1, and shNPC2 were incubated with human LDL overnight. Filipin staining showed a strong signal in LE/L- like compartments in the perinuclear area in shNPC1 SH-SY5Y cells, indicating accumulation of unesterified cholesterol in LE/L. However, shNPC2 SH-SY5Y consistently failed to produce any sign of endosomal cholesterol accumulation compared to control (**Figure 4.1** F). These observations were consistent for both, n- and s-type SH-SY5Y cells. In contrast, transduction of fibroblasts with the same shNPC1 and shNPC2 pGIPz lentiviral vectors produced strong endosomal cholesterol accumulation even in the absence of LDL (Figure 4.1 E), similar to reports in the literature for NPC1 and NPC2 patient fibroblast (178,179).

Taken together, these results show that despite robust depletion of NPC2, SH-SY5Y cells did not accumulate cholesterol, in contrast to the strong accumulation in fibroblasts. With NPC1-depleted SH-SY5Y cells clearly showing accumulation, these results represent an aberration to the usual cholesterol “hand-off” model, and led to further investigation of cholesterol transport in NPC2-depleted SH-SY5Y cells

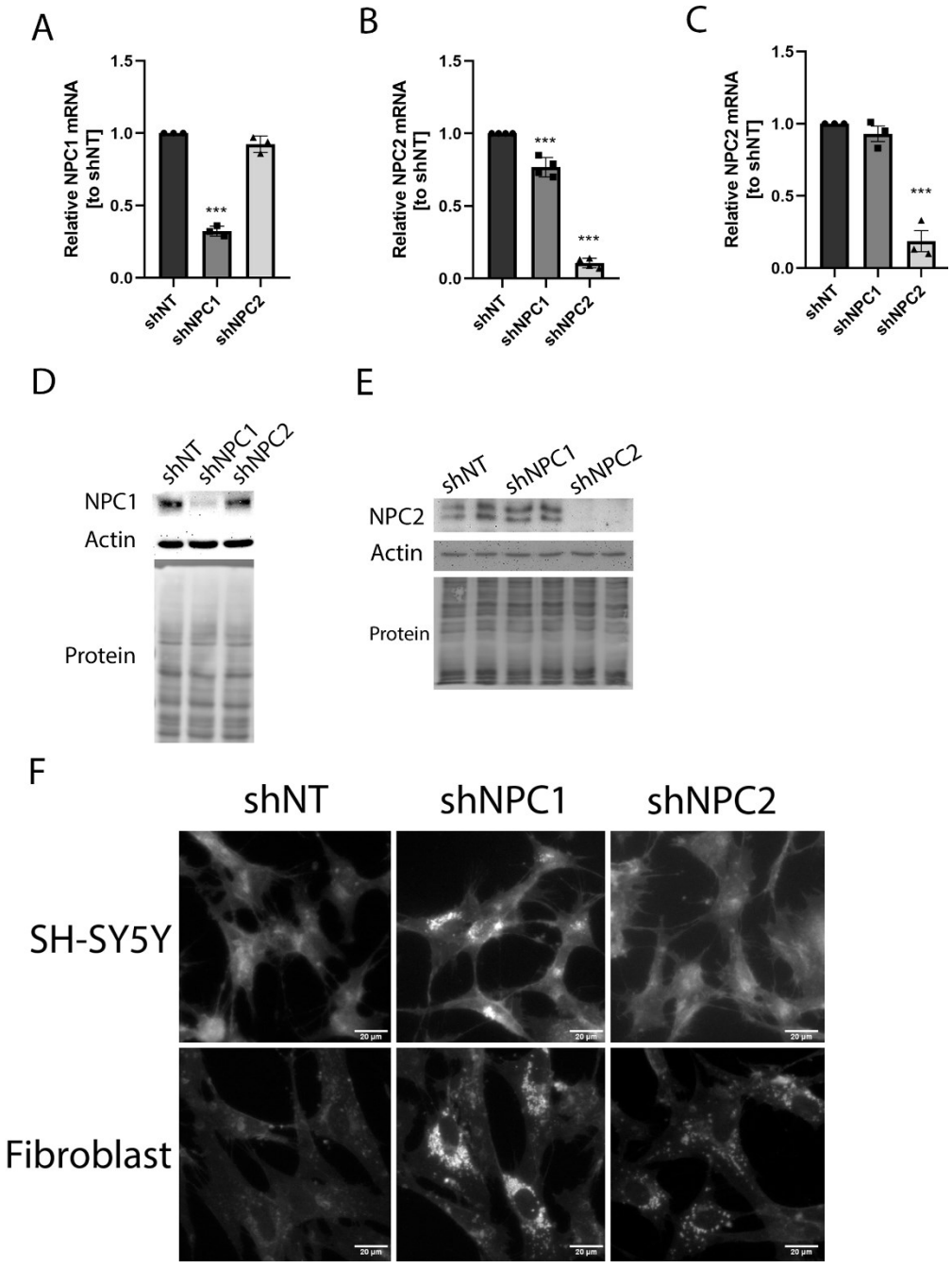

Figure 4.1: ***NPC2 depletion in SH-SY5Y cells does not lead to cholesterol accumulation in LE/L.*** SH-SY5Y cells or fibroblasts were transduced with pGIPz shNT, shNPC1, or shNPC2 for 3 days. (**A – B**) SH-SY5Y RNA was isolated and NPC1 and NPC2 mRNA levels analysed by qPCR using ACTB as reference gene. (**C**) Fibroblasts were transduced with with pGIPz shNT, shNPC1, or shNPC2 for 3 days. RNA was isolated and NPC2 mRNA levels analyzed by qPCR using ACTB as reference gene. (**D – E**) SH-SY5Y total cell lysates were immunoblotted for NPC1 or NPC2 followed by actin as a loading control. (**F**) SH-SY5Y cells, but not fibroblasts, were incubated with LDL overnight before fixation and staining with filipin.

4.2. NPC2 depletion impairs cholesterol transport to ER, similarly to NPC1 depletion

Another well-known characteristic of NPC1- or NPC2-deficient cells is the defective transport of LDL-derived cholesterol to the ER for esterification by SOAT1.

To investigate whether NPC2-depletion leads to impaired cholesterol esterification, SH-SY5Y cells infected with shNT, shNPC1 or shNPC2 vectors were starved overnight in LPDS before refeeding with LDL and [^{3}H]-Oleic acid/BSA for 4 h. Under these conditions, incorporation of the radiolabeled oleic acid into cholesterol esters reflects transport of LDL-derived cholesterol to SOAT1 in the ER. NPC1-depleted cells showed a 50% reduction in radiolabeled CE compared to control. This reduction is comparable to reports in NPC1 patient fibroblasts (180). NPC2-depleted cells also had reduced esterification, but not to the same extent as NPC1-depletion, with 40% reduction compared to control (**Figure 4.2** A). Furthermore, NPC2-depleted cells also showed decrease in radiolabeled triacylglycerol (TAG) (**Figure 4.2** B). Given the high fatty acid (FA) quantity added and that FA transport into the cell is usually not rate-limiting, these results likely reflect a decrease in TAG synthesis. Reduced rates of FA uptake as the limiting factor cannot be completely disregarded, but were not further investigated in this work.

To further investigate the cholesterol transport defect in NPC2-depleted cells, the ability of endocytosed cholesterol to down-regulate cholesterol biosynthesis was measured. To measure the response to changing levels of available LDL-cholesterol in the medium, cells were incubated according to the treatment time-line in **Figure 4.2** C, thereby inducing a starved, refed, and fed response profile. Cells were incubated with [2-^{14}C]-acetic acid during the last incubation step. NPC1-depleted cells exhibited increased cholesterol synthesis during starvation and re-feeding (**Figure 4.2** D). However, NPC2-depleted cells showed no difference to control cells. In normal growth conditions (fed), cholesterol biosynthesis was the same for all cells.

Mirroring the conditions of the cholesterol biosynthesis measurement, total RNA was isolated and HMGCR mRNA levels were quantified. HMGCR expression levels are

regulated by cholesterol reaching the ER through the SREBP/SCAP complex. HMGCR transcription is activated when ER cholesterol is low and reduced during increasing ER cholesterol. HMGCR mRNA levels were significantly higher in NPC1-depleted SH-SY5Y cells, similarly to cholesterol biosynthesis. However, although cholesterol biosynthesis levels stayed up during refeeding, HGMCR levels in NPC1-depleted cells were similar to control cells. NPC2-depleted cells showed no change in HMGCR levels compared to control, indicating NPC2 does not control sterol dependent regulation of SREBP in the ER. During fed conditions, HMGCR mRNA levels were similar in all cells.

These results indicated that, although NPC2-depleted cells show no endosomal cholesterol accumulation, cholesterol transport from the endosome to regions in the ER responsible for esterification is deficient. However, cholesterol biosynthesis and HMGCR mRNA levels indicate that de-novo cholesterol synthesis is still regulated according to LDL-cholesterol availability similarly to control cell.

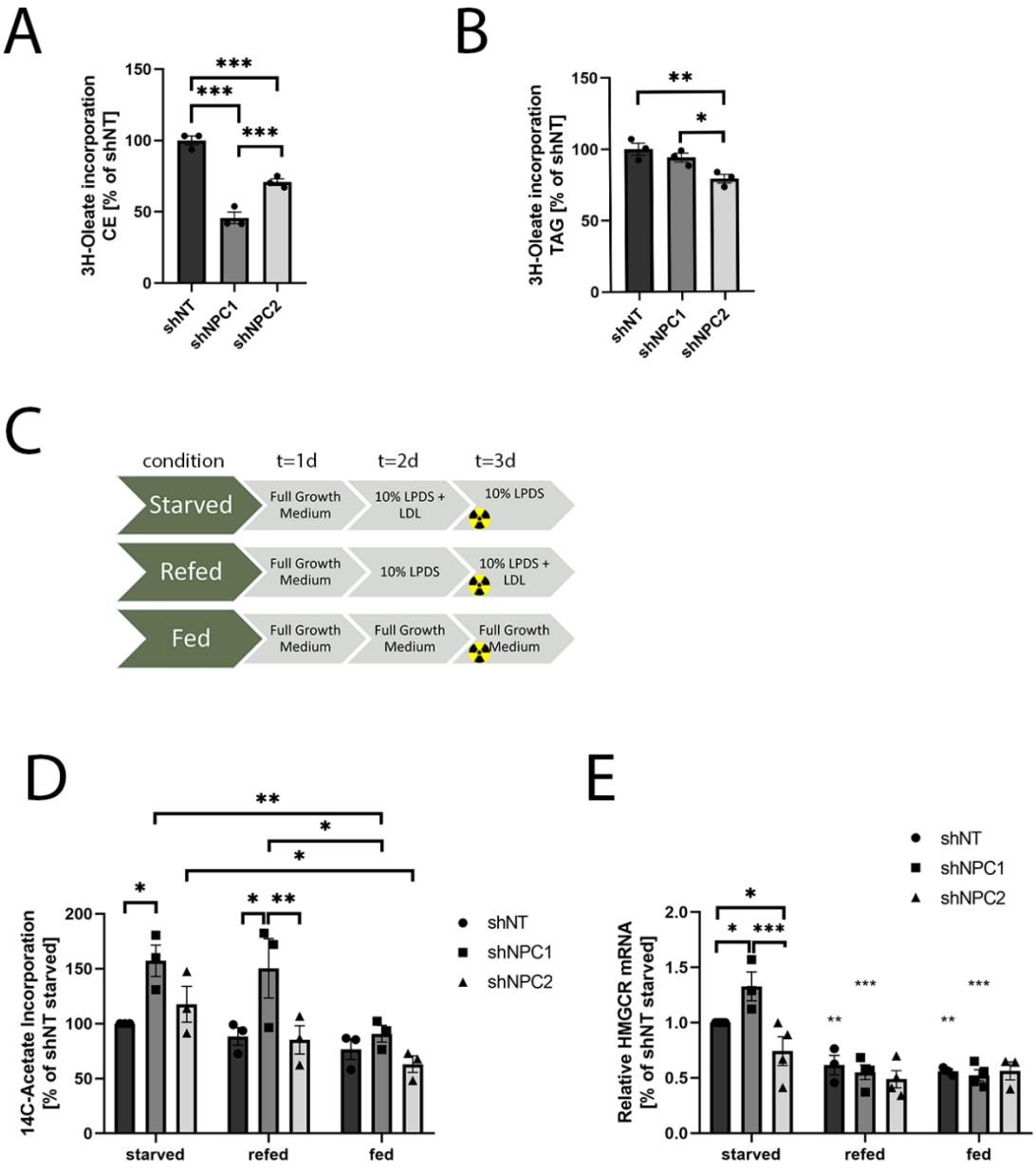

Figure 4.2: NPC2 depletion impairs cholesterol transport from LE/L to the ER for esterification but not for the SREBP response. SH-SY5Y cells were transduced with pGIPz shNT, sNPC1 or shNPC2 for 3 days. (**A – B**) Cells were starved overnight in LPDS medium before treatment with [9,10-^{3}H(N)]-oleic acid for 4 h. Lipids were extracted, separated, and [9,10-^{3}H(N)]-oleic acid incorporation into CE (A) and TAG (B) was measured. Data are normalized to total cell protein and expressed as percentage of control (shNT). (**C-E)** SH-SY5Y cells were transduced with pGIPz shNT, sNPC1 or shNPC2 for 3 days. Medium was changed in 24 h intervals with radiolabelled [2-^{14}C]-acetic acid added at as depicted in (C). (D) Lipids were extracted, separated and [2-^{14}C]-acetic acid incorporation into cholesterol was measured. (E) Same timeline as depicted in (C) without radiotracer. RNA was isolated and HMGCR mRNA levels analysed by qPCR using ACTB as reference gene. Significance stars without bars are compared to the starved condition of the same transduced cells.

4.3. Cholesterol levels in NPC2-depleted SH-SY5Y cells after LDL loading are similar to control, but decrease after subsequent starvation

To further investigate the effect of NPC2 depletion on cellular cholesterol in SH-SY5Y cells, total cellular cholesterol was measured after incubation for 16 h with LDL. Compared to control cells, cholesterol levels were unchanged in NPC2-depleted cells (**Figure 4.3** A), while NPC1-depleted cells showed a significant increase in cellular cholesterol. Furthermore, only a small proportion of total cholesterol was esterified, approximately 9 % across all cells, indicating that cholesterol ester storage is not a major pathway in SH-SY5Y cells.

To investigate how cholesterol levels change during subsequent cholesterol withdrawal, LDL loading was followed by a 24 h incubation in the absence of exogenous cholesterol (lipoprotein-deficient serum, LPDS). Only unesterified cholesterol was measured, as it is the majority of the total cholesterol mass in SH-SY5Y cells. NPC1-depleted cells showed similar cholesterol levels compared to control (**Figure 4.3** B). However, following removal of exogenous cholesterol, NPC2-depleted cells had lower cholesterol levels than control cells.

These studies also revealed differences in cell growth between transduced SH-SY5Y cells. As serum cholesterol availability can influence cellular proliferation especially in cancer cells (181), growth assays were performed. NPC1-depleted cells showed a nearly 40 % higher cell proliferation compared to control over a 3-day period (**Figure 4.3** C). In contrast, NPC2-depleted cells grew comparably to control cells during the same period.

Taken together, these results indicate NPC2 depletion does not affect cholesterol level or growth during high LDL conditions compared to control, but leads to reduction in cellular cholesterol following starvation. Moreover, NPC1 and NPC2 depletion had different effects on cellular cholesterol homeostasis and growth of SH-SY5Y cells.

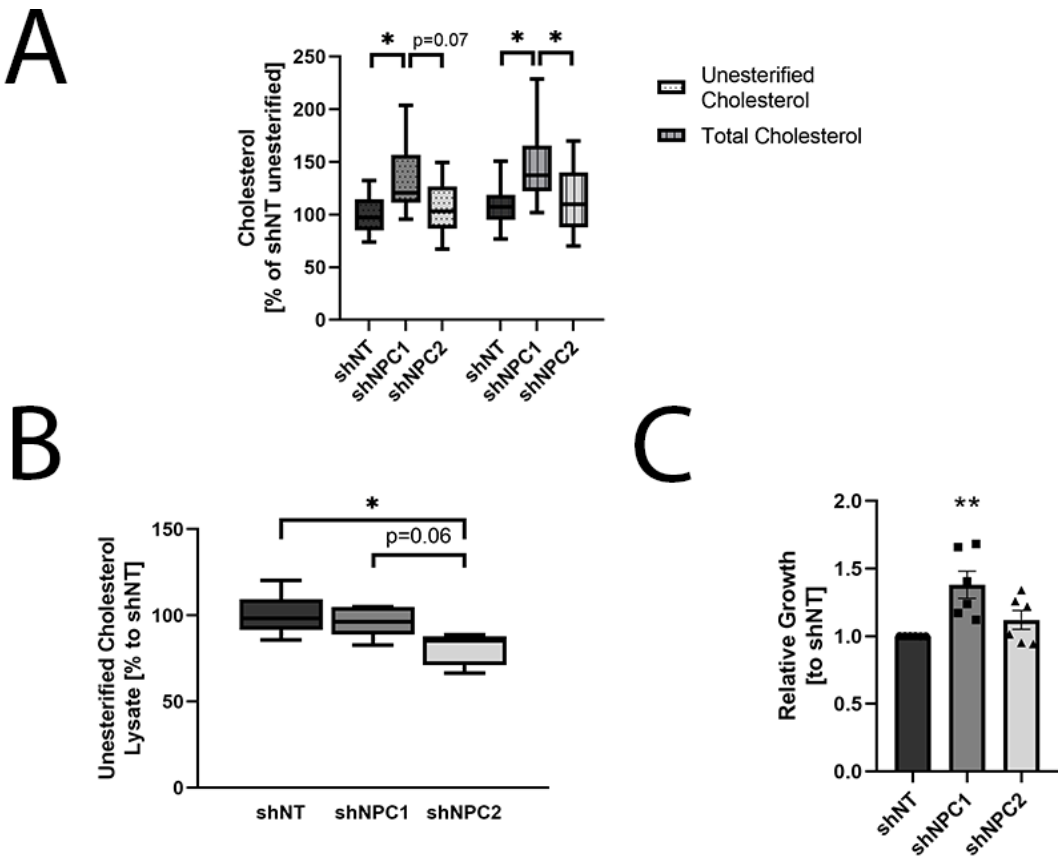

Figure 4.3: Cellular cholesterol levels in NPC2-depleted SH-SY5Y cells are normal after LDL loading but reduced following incubation in LPDS compared to control. (**A**) SH-SY5Y cells transduced with pGIPz shNT, shNPC1, and shNPC2 were loaded with LDL overnight, and unesterified and total cholesterol were measured. Data are expressed as percentage of shNT unesterified cholesterol. (**B**) SH-SY5Y transduced with pGIPz shNT, shNPC1 and shNPC2 were loaded with LDL overnight, then treated with LPDS medium for 24 h and unesterified and total cholesterol were measured. Data are expressed as percentage of shNT. (**C**) SH-SY5Y cells were transduced with pGIPz shNT, shNPC1, or shNPC2 and growth assays were performed. Data shows growth over 2 days relative to control.

4.4. Cholesterol secretion is decreased in NPC2-depleted SH-SY5Y cells compared to control.

Lysosomal exocytosis, the process of fusion of LE/L with the PM and secretion of lumenal content into the medium, has been indicated as a mechanism to circumvent the lysosomal cholesterol trafficking block and ameliorate cholesterol accumulation in NPC patient fibroblast cells and CHO cells (182).

To explore whether NPC2-depleted SH-SY5Y cells can avoid cholesterol accumulation by cholesterol secretion into the medium, cells were loaded with LDL overnight and then incubated in the absence of exogenous cholesterol in LPDS-containing medium for 24 h.

If NPC2-depleted SH-SY5Y cells prevented LE/L cholesterol accumulation through increased secretion, higher medium cholesterol levels could be expected. However, NPC2-depleted SH-SY5Y cells had less unesterified cholesterol in the medium compared to control and NPC1-depleted cells (40 % and 20 %, respectively) (**Figure 4.4** A). NPC1-depleted cells also had 20% less unesterified cholesterol in the medium than control cells. These findings are in line with previous findings that depletion of NPC1 blocks the anterograde transport and expulsion of LE/L content into the medium (183–185). The strong decrease in medium cholesterol suggested that the lack of cholesterol accumulation in LE/L of NPC2-depleted cells was not due to increased secretion of cholesterol. Overall, medium cholesterol was only 2-3 % of total cellular cholesterol.

To confirm that the lower levels of cholesterol in the medium of NPC2-depleted cells were associated with decreased lysosomal exocytosis, the secretion of the lysosomal enzyme NAG into the cell culture medium was measured. The commercially available NAG assay kit (Sigma) based on colorimetric detection was not sensitive enough for SH-SY5Y cells, suggesting generally low lysosomal exocytosis or weak NAG activity in these cells. Therefore, a fluorescent detection assay based on a method described by Rodríguez et. al was necessary (161). Cells were pretreated for 1 h with or without Vacuolin-1, a specific inhibitor of calcium-induced lysosomal exocytosis (162,186), before adding the efflux buffer for 15 min. Both, shNPC1 and shNPC2, showed a 50 % decrease in the ratio of enzymatic activity in medium to cell lysate compared to control cells, indicating impaired lysosome fusion with the PM following depletion of either NPC1 or NPC2 (**Figure 4.5**, **Figure 4.4** B). However, Vacuolin-1 treatment only marginally reduced lysosomal exocytosis and failed to show significance in the compiled data for control cells. Studies in HeLa cells have shown that vacuolin-1 effects last for at least 1 h after its removal (187), indicating that the lack of significant effects of Vacuolin-1 was not due to its absence in the efflux buffer. Instead, these results suggest generally low levels of calcium-dependent lysosomal exocytosis in SH-SY5Y cells.

Taken together, these results show that NPC1 and NPC2 depletion in SH-SY5Y cells leads to reduction of lysosomal exocytosis and cholesterol secretion into the medium. At the

same time, these observations fail to explain the absence of cholesterol accumulation in NPC2-depleted cells.

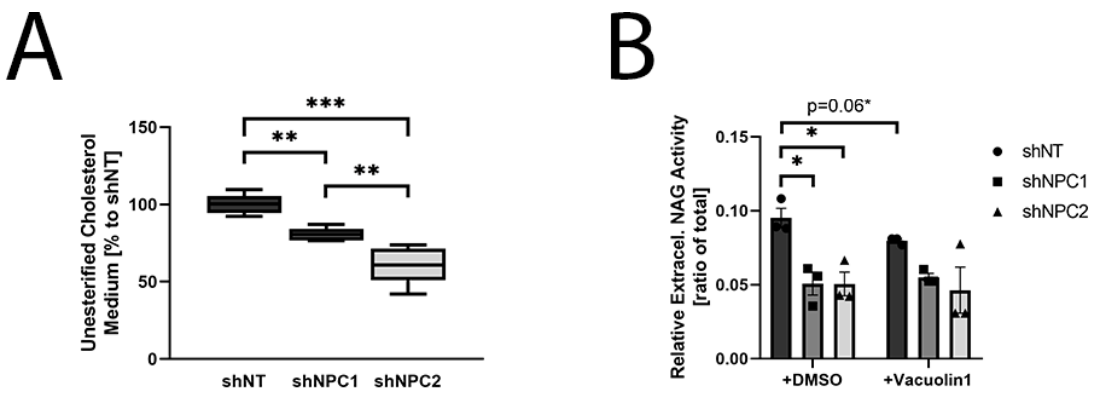

Figure 4.4: Cholesterol secretion is decreased in NPC2-depleted SH-SY5Y cells. (**A**) SH-SY5Y transduced with pGIPz shNT, shNPC1 and shNPC2 were loaded with LDL overnight. Cells were then treated with LPDS medium for 24 h and unesterified and total cholesterol in the medium were measured. Data are the ratio of medium to cellular cholesterol expressed as percentage of shNT control. (**B**) SH-SY5Y transduced with FUGW shNT, shNPC1 and shNPC2. Cells were pretreated with or without 10 µM Vacuolin-1 for 1 h and incubated for 15 min in HBS. NAG enzyme activity was measured in HBS and cells by fluorescent assay. Data are the ratio of medium to cellular fluorescence.

4.5. Cellular LDL uptake is unaltered in NPC1- and NPC2-depleted cells.

A major source of cholesterol for cells are LDL particles taken up by the LDLR. A reduction in uptake of LDL could explain the absence of cholesterol accumulation in NPC2-depleted SH-SY5Y cells.

To measure uptake of LDL, SH-SY5Y cells were incubated with LDL particles labelled with the lipophilic fluorescent marker DiI. A preliminary time course experiment with DiI-LDL incubation for 15, 30, 45, 60, and 120 min showed the strongest DiI signal without diffusion of the fluorophore at 30 min. This incubation time was therefore chosen for further experiments.

SH-SY5Y cells incubated with DiI-LDL for 30 min showed strong DiI signal as punctate patterns scattered through the cell. Signal pattern was very indicative of endocytic vesicles, with small clustered particles at various distance to the nucleus (**Figure 4.5** A). The distribution of DiI-positive vesicles seemed similar in control and NPC2-depleted

cells but showed perinuclear clustering for NPC1-depleted cells, similar to filipin staining patterns (seen in **Figure 4.1** E). Quantification of total DiI-LDL uptake revealed no difference in either NPC1- or NPC2-depleted cells (**Figure 4.5** B). However, the heterogeneity of SH-SY5Y morphology led to high variability in measurements, as seen in the broad distribution of measurements for each condition, potentially masking subtle differences. Quantitative analysis of LDLR mRNA expression levels showed no difference between control cells or NPC1- and NPC2-depleted cells (**Figure 4.5** C).

These results show that uptake of LDL particles in NPC1- and NPC2-depleted cells was comparable to that of control and indicate that the reduced cholesterol mass and lack of cholesterol accumulation in LE/L after NPC2 depletion was not due to decreased cholesterol uptake.

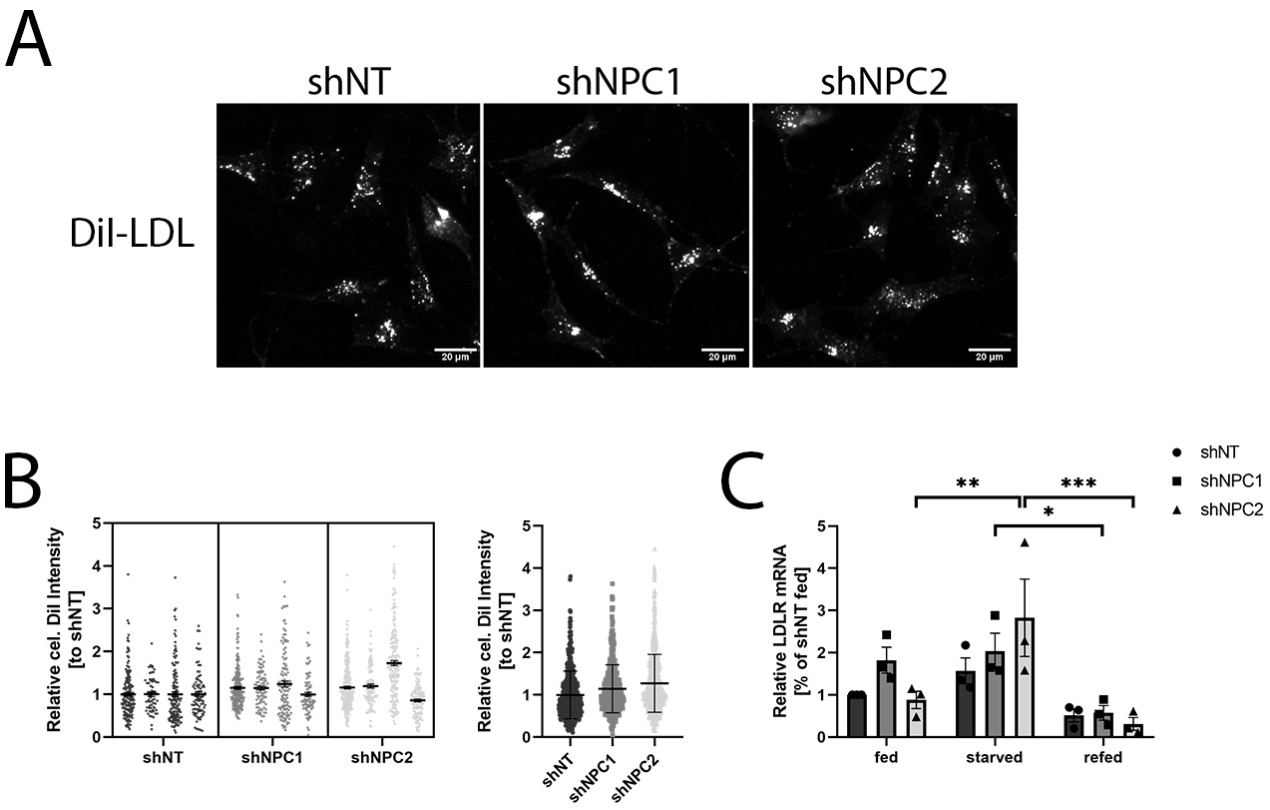

Figure 4.5: LDL uptake is unaltered in NPC2-depleted SY-SY5Y cells. (**A**) SH-SY5Y cells transduced with pGIPz shNT, shNPC1, and shNPC2 were starved overnight in LPDS medium. Cells were then incubated with DiI-LDL for 30 min. (**B**) Quantification of DiI LDL fluorescence per cell. Data are shown as individual experiments or pooled in one column and expressed as ratio to shNT. (**C**) SH-SY5Y RNA was isolated after incubation in full growth medium (fed), after 30 h in LPDS medium (starved), or 24 h in LPDS medium followed by 6 h in LPDS medium + LDL (refed) and LDLR mRNA levels analysed by qPCR using ACTB as reference gene.

4.6. Plasma membrane cholesterol is significantly lower in NPC2-depleted SH-SY5Y cells compared to NPC1-depleted cells, but not to control cells.

The PM is the organelle with the highest cholesterol content in the cell. The absence of LE/L cholesterol accumulation in NPC2-depleted cells with normal LDL uptake could indicate transport alterations, potentially leading to alter PM cholesterol.

To further characterize the cholesterol profile of SH-SY5Y cells during NPC2 depletion, the D4H cholesterol sensor (188) was employed. D4 is the cholesterol-binding domain of the bacterial cytolysin perfringolysin O, and has been previously used as a recombinant, exogenous sensor (D4) or as the higher affinity, ectopically expressed version – D4H. In contrast to filipin, D4H tagged with a fluorescent protein allows visualization of

intracellular cholesterol in live cells with low photobleaching and without permeabilizing membranes.

SH-SY5Y cells transduced with FUGW shNT, shNPC1, or shNPC2 were infected again with virus containing the clover3-D4H expression construct. Fluorophore-conjugated WGA was used as a PM stain and ROIs to separate PM and internal vesicular D4H signal were generated using a nonbiased approach (**Figure 4.6**). Areas of high WGA signal, indicating PM, were marked and the ratio of D4H to WGA signal was calculated (ROI1). To measure the vesicular D4H signal, high D4H signal to noise areas were isolated and the PM signal area was excluded (ROI2).

The D4H signal showed strong internal vesicular patterns, probably corresponding to endocytic vesicles, as well as signal patches along the cell periphery (**Figure 4.7** A). Neither the D4H nor WGA signals showed a continuous ring of PM around the cells, possibly caused by a flattening of SH-SY5Y cell morphology along the edges, making the PM appear discontinuous in epifluorescence images. However, neither NPC1- nor NPC2-depleted cells showed a significant difference of D4H localization to the PM relative to control cells, although a trend towards more extensive D4H fluorescence in NPC1-depleted cells and lower D4H fluorescence in NPC2-depleted cells was observed(**Figure 4.7** B). A comparison of NPC1- and NPC2-depleted cells to each other showed significantly lowerD4H fluorescence fluorescence in the PM ROI in NPC2-depleted cells. These findings indicate that there are no significant differences in PM cholesterol in either NPC1- or NPC2-depleted cells compared to control, although NPC2-depleted cells may have lower PM cholesterol than NPC1-depleted cells. One caveat to this conclusion is that D4H binding to membranes is also influence by the phospholipid composition, and that D4H can bind some cytosolic proteins. The internally clustered D4H signal, corresponding to vesicular cholesterol pools, showed no difference between the groups (**Figure 4.7** C). However, without preincubation with LDL, cholesterol accumulation is not pronounced even in NPC1-depleted cells.

Although no significant difference in PM cholesterol was seen compared to control, these results further indicate that NPC1- and NPC2- depleted SH-SY5Y cells do not show

the same cholesterol phenotype, even at the PM. Moreover, it seems unlikely that NPC2-deficient SH-SY5Y cells avoid endosomal cholesterol accumulation by redistributing this cholesterol to the PM.

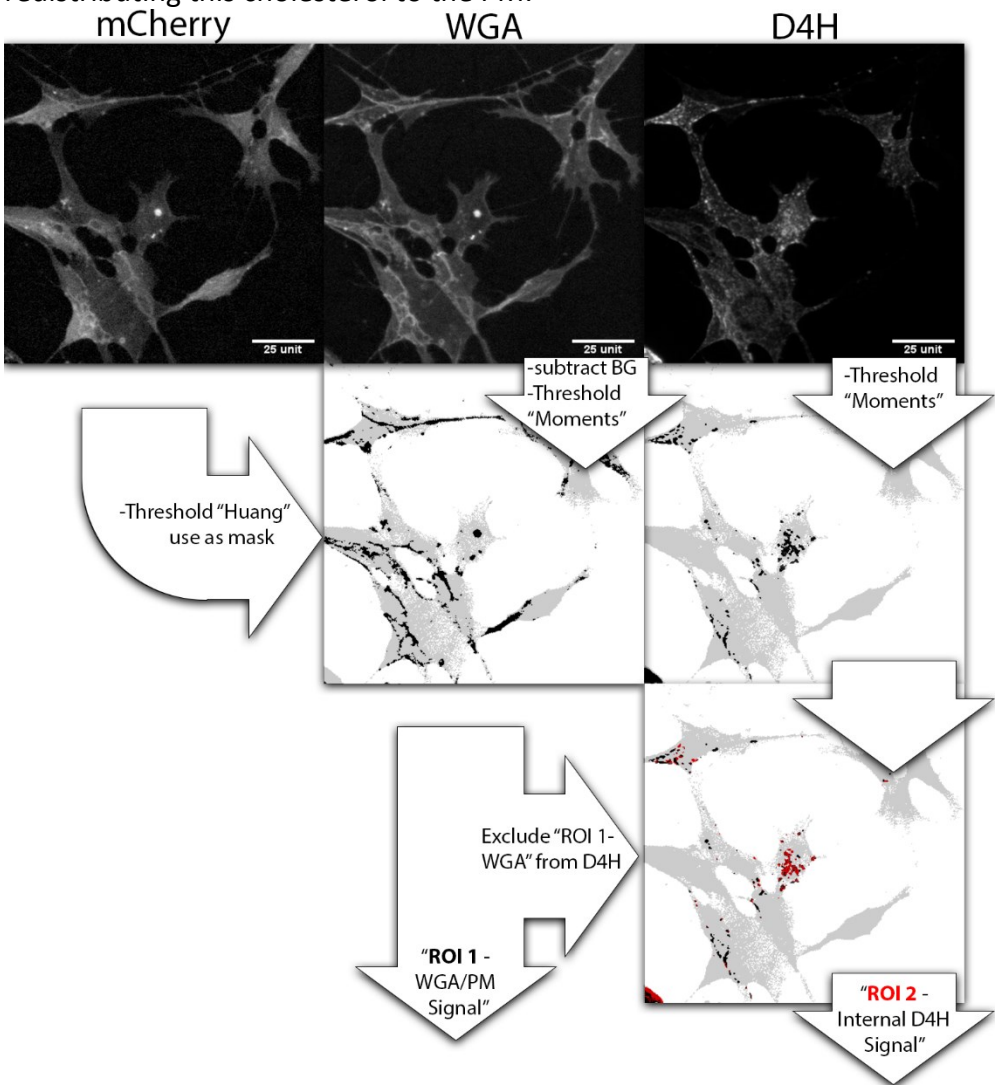

Figure 4.6 Overview of PM cholesterol analysis workflow. PM cholesterol was analyzed using Clover3-D4H and fluorescently-labelled WGA that binds to the PM. The D4H signal was quantified at the PM using a ratio of D4H signal to WGA signal at high WGA signal locations, specified by ROI1. Internal versicular cholesterol was quantified as D4H signal corresponding to high D4H signal clusters, exluding the signal from the PM (ROI2).

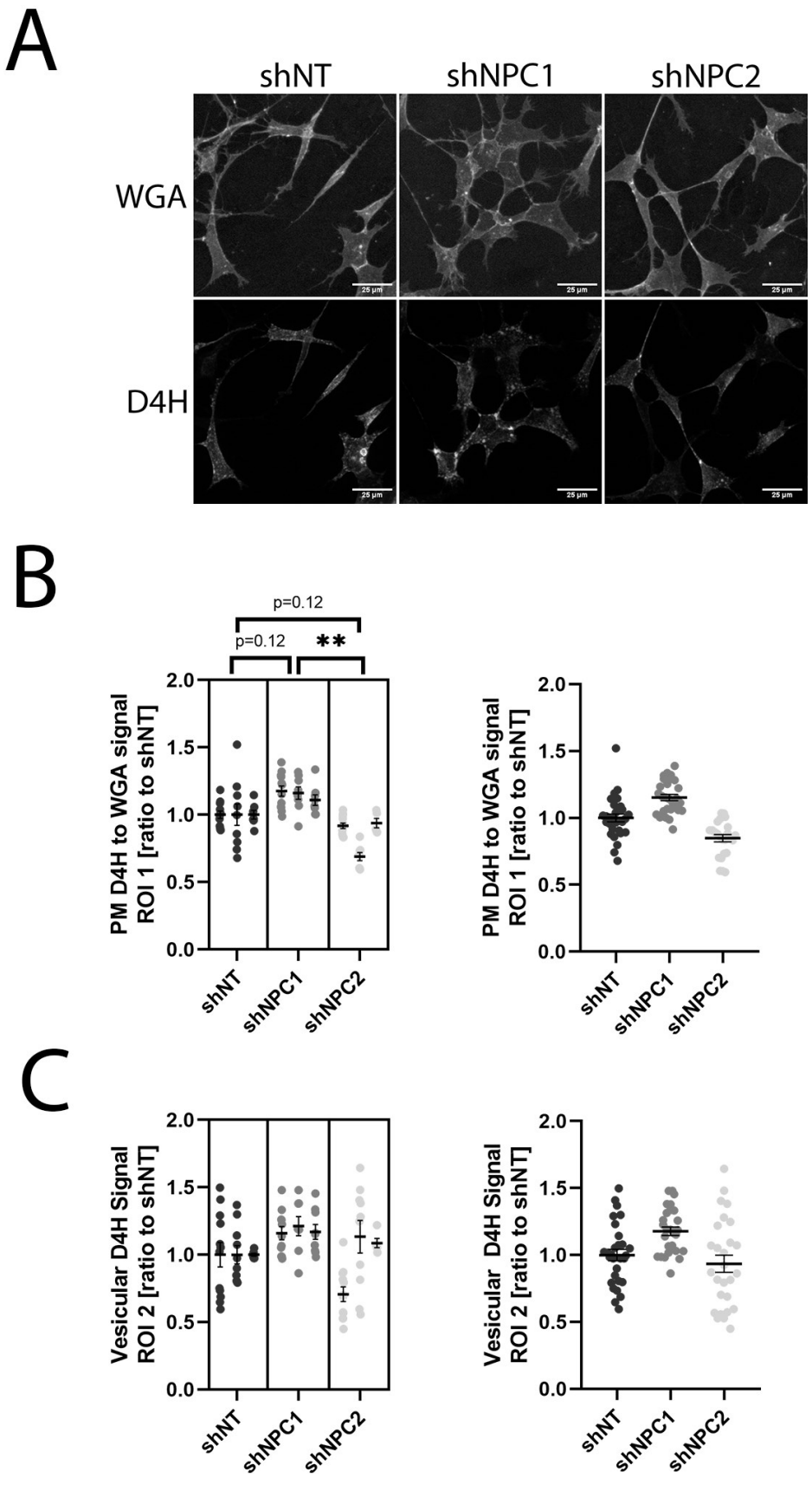
A
shNT
shNPC1
shNPC2
WGA
D4H
25 µm
B
p=0.12
p=0.12
**
PM D4H to WGA signal
ROI 1 [ratio to shNT]
2.0
1.5
1.0
0.5
0.0
shNT
shNPC1
shNPC2
C
Vesicular D4H Signal
ROI 2 [ratio to shNT]

Figure 4.7 PM cholesterol levels in NPC2-depleted SH-SY5Y cells are significantly lower compared to NPC1-depleted cells, but not compared to control. (**A**) SH-SY5Y cells transduced with FUGW shNT, shNPC1, and shNPC2 were seeded on collagen-coated coverslips and transduced with Clover3-D4H vectors. After 3 days, cells were stained with CF650R-WGA, a fluorescent PM stain. (**B-C**) Images were analysed using an unbiased FIJI workflow and presented as (B) ratio of D4H signal to WGA signal compared to control (PM cholesterol) and (C) internal vesicular D4H signal compared to control (endocytic cholesterol).

4.7. No compensatory pathways in absence of NPC2 were identified

Compensatory or complementary pathways as well as redirection through other pathways could explain the absence of cholesterol accumulation in NPC2-depleted SH-SY5Y cells. Alternative pathways in NPC1-depleted cells for transport of cholesterol out LE/L have been shown (60,61,189–195) and alternative candidates for NPC2 in lysosomal cholesterol transport have been suggested (196).

A list of candidate genes playing a role in cholesterol transport or the endocytic system was created (**Table 5**) and RNA interference vectors with two concatenated miRNA hairpins, targeting the candidate cholesterol transporter with either a non-targeting hairpin or a hairpin targeting NPC2 were generated. Cells were transduced with miRNA expression vectors, loaded with LDL and stained with filipin.

Quantitative PCR was used to verify the effectiveness of the RNAi vector and showed ~90 % reduction of mRNA levels for ARL8, IGF2R, RAB3, VPS41, ORP1L and PSAP (**Figure 4.8**).

NPC1-depleted SH-SY5Y cells showed strong accumulation of cholesterol in the perinuclear area, whereas NPC2-depletion failed to induce accumulation as before (**Figure 4.9** and **Figure 4.10**). Depletion of candidate genes ARL8, IGF2R, RAB3, VPS41, ORP1L and PSAP failed to induce cholesterol accumulation with or without co-depletion of NPC2. Interestingly, PSAP-depletion consistently showed reduced viability of SH-SY5Y cells after transduction, across different lentivirus preparations. Viability of cells seemed to improve slightly in PSAP- and NPC2-co-depleted cells. Loss of neurons in the brain has been seen in PSAP-depleted brain tissue, emphasizing importance of PSAP for neuronal viability, but this observation was not further pursued in the scope of this thesis (197). Depletion of IGF2R, the receptor responsible for NPC2 delivery to the endocytic system,

was previously shown to induce cholesterol accumulation in fibroblasts, because NPC2 is secreted rather than delivered to endosomes in the absence of IGF2R (60). However, in SH-SY5Y cells depletion of IGF2R did not lead to visible endosomal cholesterol accumulation, further emphasizing the differences between SH-SY5Y and fibroblast cholesterol transport. Similarly, ORP1L-depleted HeLa cells have been shown to accumulate cholesterol in endosomes (198), while ORP1L-depleted SH-SY5Y cells failed to do so with or without NPC2-co-depletion.

In contrast to SH-SY5Y cells, fibroblasts accumulated cholesterol following depletion of NPC1 or NPC2 (**Figure 4.9** and **Figure 4.10**). Furthermore, IGF2R- and ORP1Ldepletion led to cholesterol accumulation as reported (198). Compared to SH-SY5Y, PSAP-depletion did not have any adverse effects on cell viability in fibroblast. NPC2 co-depletion caused strong accumulation across all candidates, indicating the importance of NPC2 in fibroblast for cholesterol transport out of the lysosome.

Taken together these results indicate that no single candidate alone takes over the function of NPC2, as depletion of none of the candidates induced overt cholesterol accumulation as visualized by filipin staining by itself or together with NPC2 depletion. However, a more detailed analysis of filipin intensity a distribution, and additional methods, such as esterification assays or measurement of SREBP activation, would be required to detect more subtle changes in cholesterol trafficking. Furthermore, these findings emphasize the apparent difference of cholesterol transport in SH-SY5Y and fibroblasts, as even the depletion of OPR1L or IGF2R failed to induce cholesterol accumulation in SH-SY5Y cells.

Table 5: Compensatory pathway candidates

Candidate	**Proposed role and reference**
ARL8	Lysosome fusion and anterograde transport (192)
IGF2R	Delivery of NPC2 in the endocytic system (60)
ORP1L	LE motility and LE-ER-contact sites (91,92)
PSAP	Cholesterol egress from lysosomes (189,199)
RAB3	Secretory vesicle release and lysosomal exocytosis (112,200)
VPS41	LE and lysosome fusion and secretion (96,195,201)

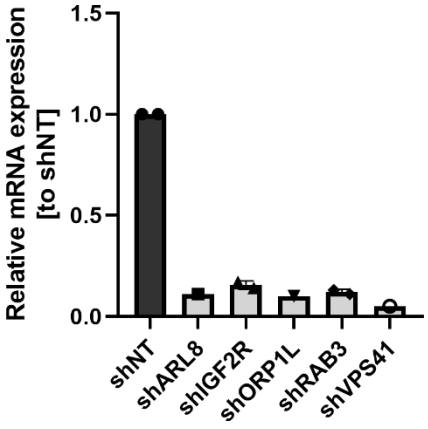

Figure 4.8: RNA interference vectors decrease candidate gene expression. SH-SY5Y cells transduced with pLenti shNT, shARL8, shIGF2R, shOPR1L, shRAB3A/B, and shVPS41 were grown for 3 days before harvesting total cellular RNA and quantification by qPCR. Data are from 1 or 2 experiments.

A

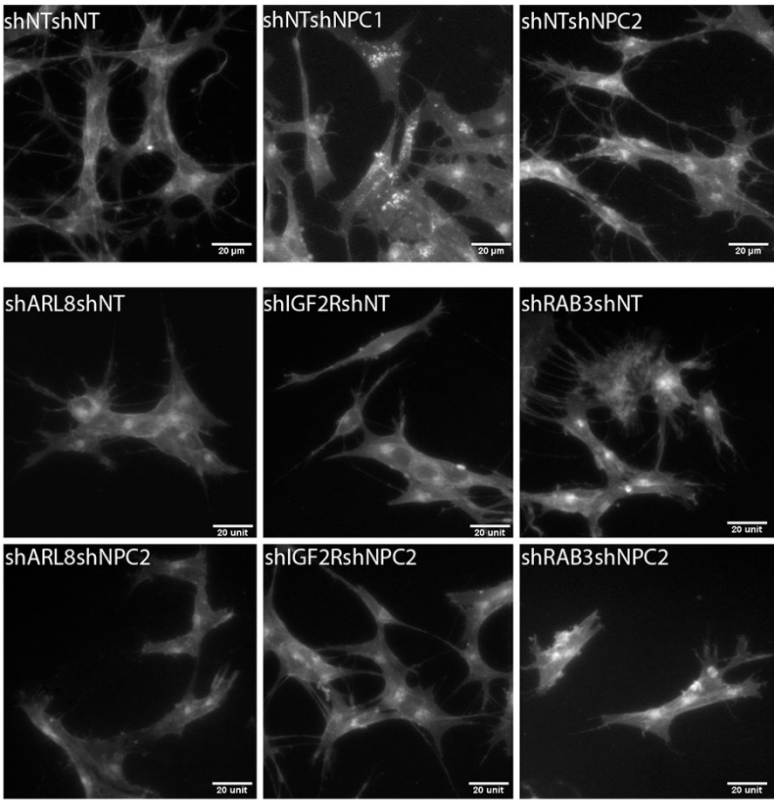
shNTshNT
shNTshNPC1
shNTshNPC2
shARL8shNT
shIGF2RshNT
shRAB3shNT
shARL8shNPC2
shIGF2RshNPC2
shRAB3shNPC2
20 µm
20 unit

B

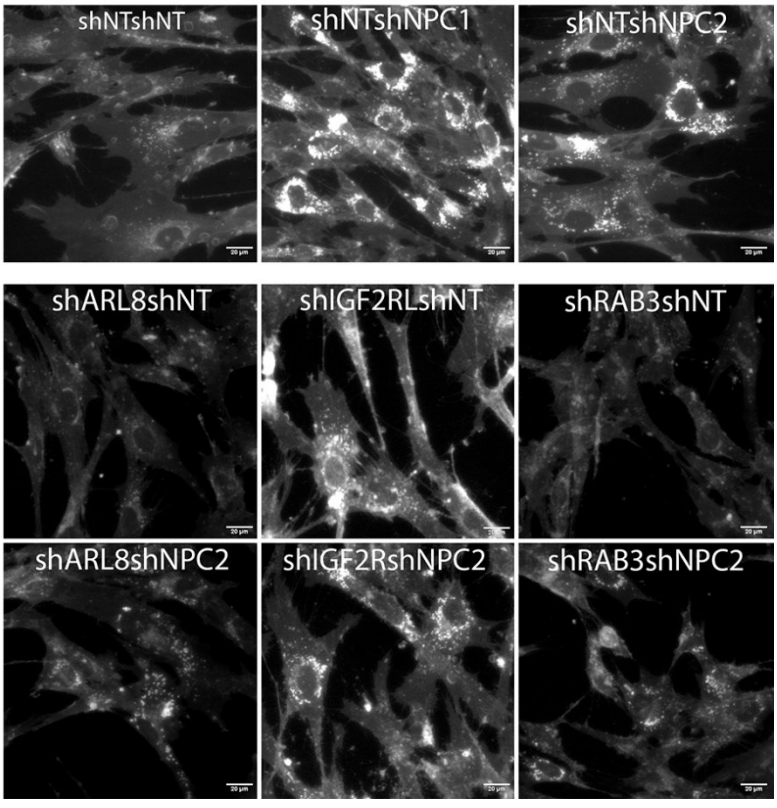
shNTshNT
shNTshNPC1
shNTshNPC2
shARL8shNT
shIGF2RLshNT
shRAB3shNT
shARL8shNPC2
shIGF2RshNPC2
shRAB3shNPC2

Figure 4.9: Knock down of ARL8, IGF2R or RAB3A/B with or without simultaneous NPC2 depletion does not induce cholesterol accumulation in SH-SY5Y cells. SH-SY5Y cells (A) or fibroblasts (B) were seeded on coverslips and transduced with pLenti miRNA constructs targeting ARL8, IGF2R, or RAB3 with or without NPC2. SH-SY5Y cells were incubated overnight with LDL before filipin staining. Images are representative of 3 independent experiments.

A

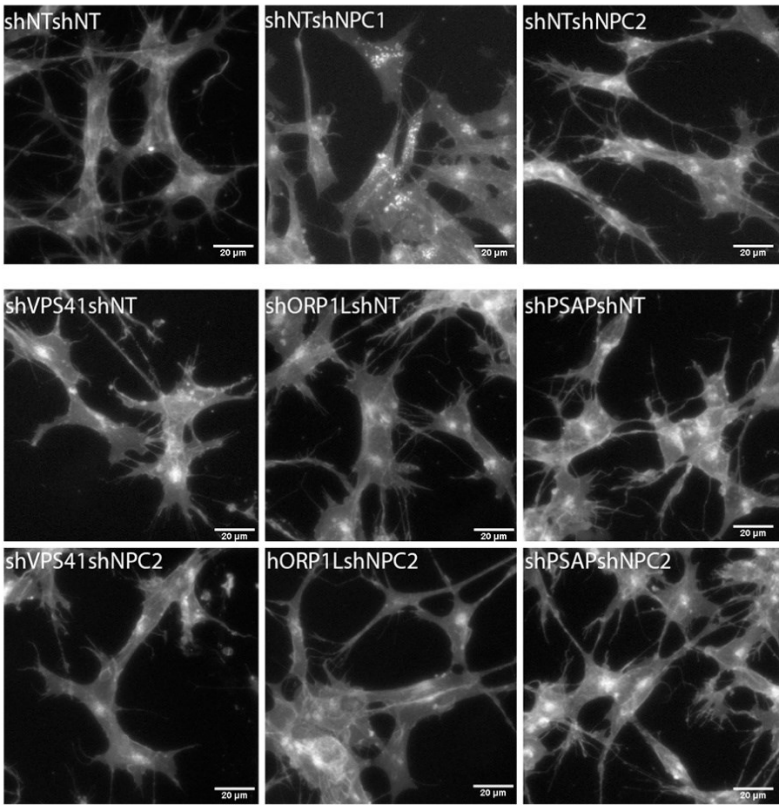
shNTshNT
shNTshNPC1
shNTshNPC2
shVPS41shNT
shORP1LshNT
shPSAPshNT
shVPS41shNPC2
hORP1LshNPC2
shPSAPshNPC2

B

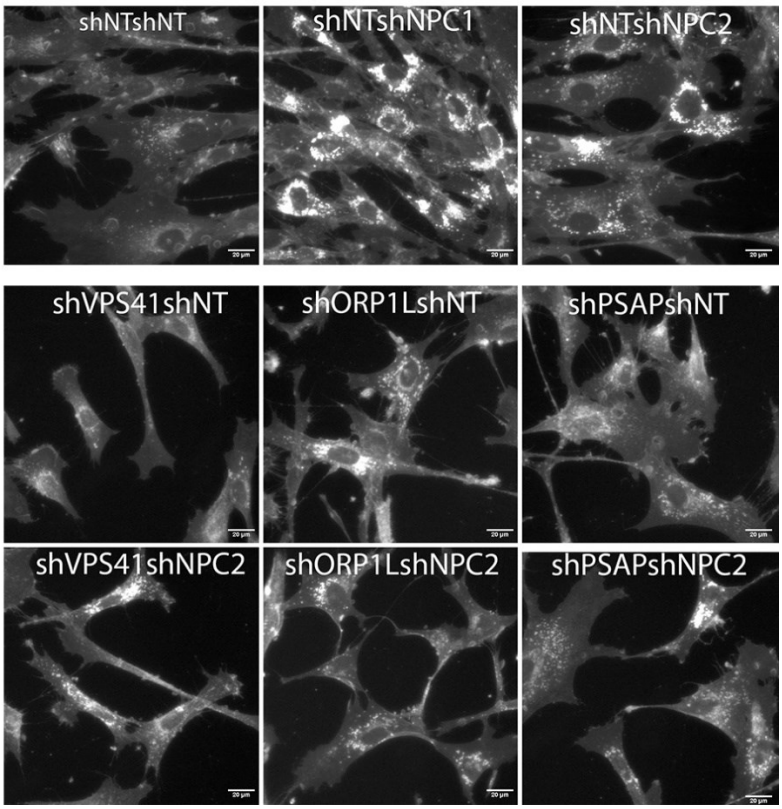
shNTshNT
shNTshNPC1
shNTshNPC2
shVPS41shNT
shORP1LshNT
shPSAPshNT
shVPS41shNPC2
shORP1LshNPC2
shPSAPshNPC2

Figure 4.10 Knock down of VPS41, ORP1L or PSAP with or without simultaneous NPC2 depletion does not induce cholesterol accumulation in SH-SY5Y cells. SH-SY5Y cells (A) or Fibroblasts (B) were seeded on coverslips and transduced with pLenti miRNA constructs targeting VPS41, ORP1L, or PSAP with or without NPC2. SH-SY5Y cells were incubated with LDL before filipin staining. Images are representative of 3 independent experiments.

4.8. SH-SY5Y exhibit low lysosomal activity compared to fibroblasts

Although no compensatory pathway could be identified, the previous results indicated alterations in the endocytic system, given that OPR1L depletion also did not cause cholesterol accumulation in SH-SY5Y cells. To assess endosome maturation, quantification of lysosomal proteolytic activity was attempted.

DQ-BSA is a fluorescently tagged BSA molecule with self-quenching properties. During proteolysis, the quenching effect is disrupted and the fluorescence signal can be measured. However, SH-SY5Y cells incubated with DQ-BSA did not show fluorescence activity above background levels could (**Figure 4.11** A), while fibroblasts showed strong DQ-BSA fluorescence in parallel experiments The difference in DQ-BSA fluorescence suggested low levels of lysosomal proteolysis in SH-SY5Y cells compared to fibroblasts, although differences in pinocytosis, which is responsible for uptake of DQ-BSA, could also play a role.

The differences seen in lysosomal activity between SH-SY5Y cells and fibroblasts could indicate different lysosomal regulation. A master regulator of the endocytic and lysosomal system is TFEB, which controls lysosomal biogenesis through translocation into the nucleus. This translocation is controlled through TFEB phosphorylation (202,203). To investigate if the low lysosomal activity in SH-SY5Y cells could be explained by lower TFEB activation, phosphorylation levels of TFEB in SH-SY5Y cells and fibroblasts were investigated. Cell were grown in normal growth medium before analysis, so steady-state levels of phosphorylation could be analysed and not the response to changed nutritional levels in the medium. Antibodies recognized TFEB phosphorylated at Ser211, which is retained in the cytosol and is unable to act as a transcription factor or total TFEB. SH-SY5Y cells had less phosphorylated TFEB as a ratio to total TFEB

compared to fibroblasts (**Figure 4.11** B). However, fibroblasts appeared to have higher overall levels of TFEB.

Taken together these data indicate that SH-SY5Y cells have low lysosomal activity compared to fibroblasts. However, this difference cannot be explained by low lysosomal biogenesis activation through TFEB.

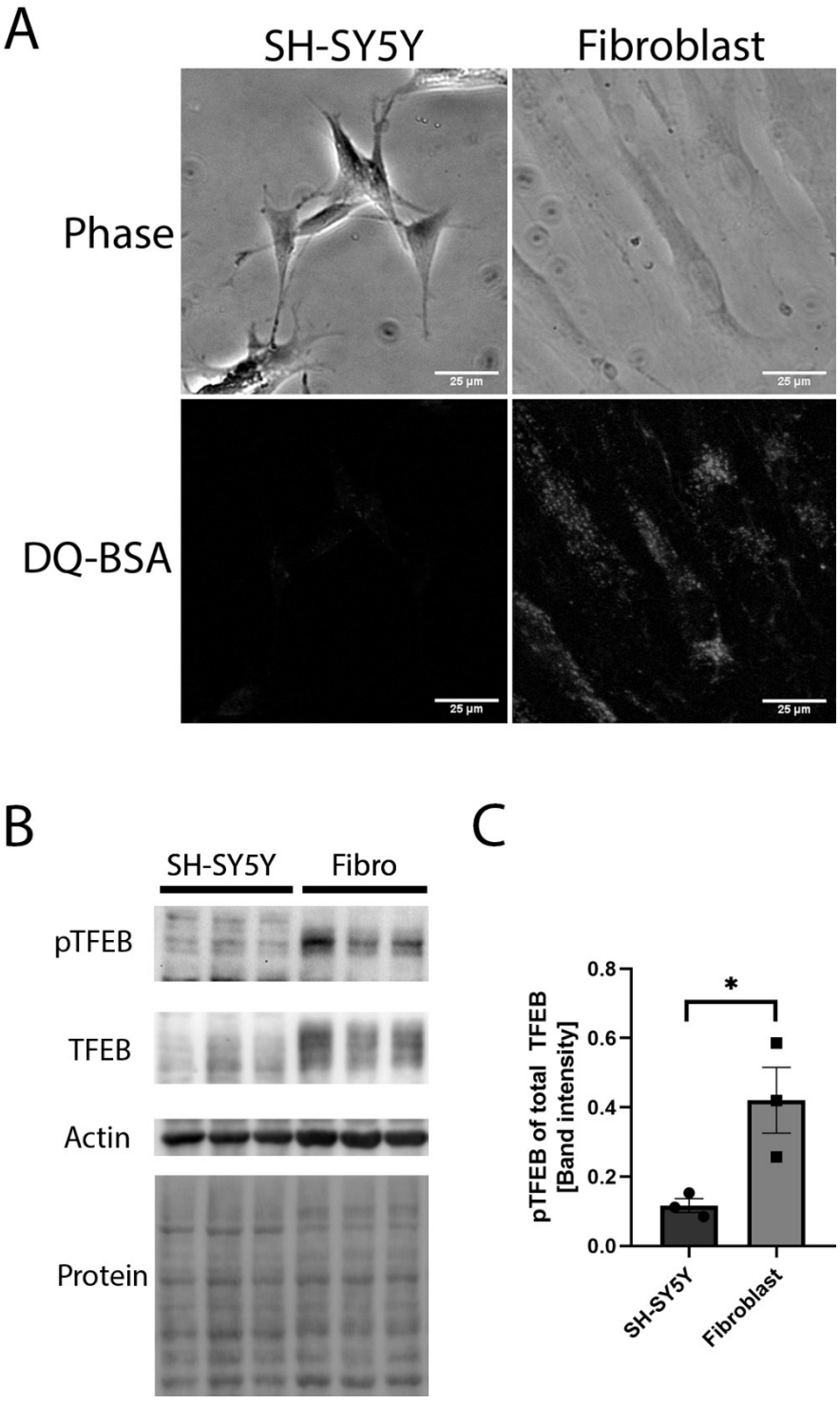

Figure 4.11 SH-SY5Y cells exhibit low steady-state TFEB phosphorylation (Ser233) and very low lysosomal DQ-BSA degradation. (**A**) SH-SY5Y cells and fibroblasts were incubated with DQ-BSA for 6 h, fixed, and phase and fluorescence images were acquired. (**B-C**) SH-SY5Y cells and fibroblasts were grown for 3 days before harvesting total protein and separation by SDS-PAGE. Phosphorylated TFEB and total TFEB signals were normalized to actin.

4.9. Transcriptome analysis did not reveal clear candidates for compensatory pathways

Throughout this work, NPC1- and NPC2-depleted SH-SY5Y cells showed differences in many aspects of cholesterol homeostasis, although these two proteins are generally thought to act in the same pathway, causing the same phenotype. For an unbiased, general comparison between NPC1- and NPC2-depleted cells, microarray transcriptome analysis was performed.

Microarray analysis of SH-SY5Y cells transduced with pGIPz shNT, shNPC1, and shNPC2 revealed only limited differences. NPC1-depleted cells showed a total of 267 differentially expressed genes compared to control, with only 108 genes being annotated (**Figure 4.12** A). NPC2-depleted cells showed a similar number of differentially expressed genes compared to control of 250, with 115 being annotated (**Figure 4.12** B). Of those gene lists, roughly half were uncharacterized gene locations, microRNA, or small nuclear RNA, without clear indication of affecting one or more pathways specifically. Genes that showed differential transcription were analysed by the TAC pathway analysis, but with only 1-2 hits per pathway no pattern emerged. DAVID gene enrichment analysis (https://david.ncifcrf.gov (204,204)), PANTHER expression analysis (http://www.pantherdb.org (205,206)), and STRING protein-protein interaction network analysis (https://string-db.org, (207)) were performed but no significant differences could be observed.

Comparing the differentially expressed gene list of NPC1- and NPC2-depleted cells to each other, only a few overlapping genes could be identified. A quantitative Venn diagram was created using BioVenn (208). Comparison revealed only 35 genes being affected by both, NPC1- and NPC2-depletion, in SH-SY5Y cells (**Figure 4.12** C). Of those genes, 19 were annotated and are shown in

Table 6. Panther expression analysis of these genes revealed no shared pathways and STRING protein interaction analysis showed no interaction.

These results indicate that although NPC1 and NPC2 act in the same pathway, their depletion in SH-SY5Y cells leads to very different expression profiles with only few genes affected in both.

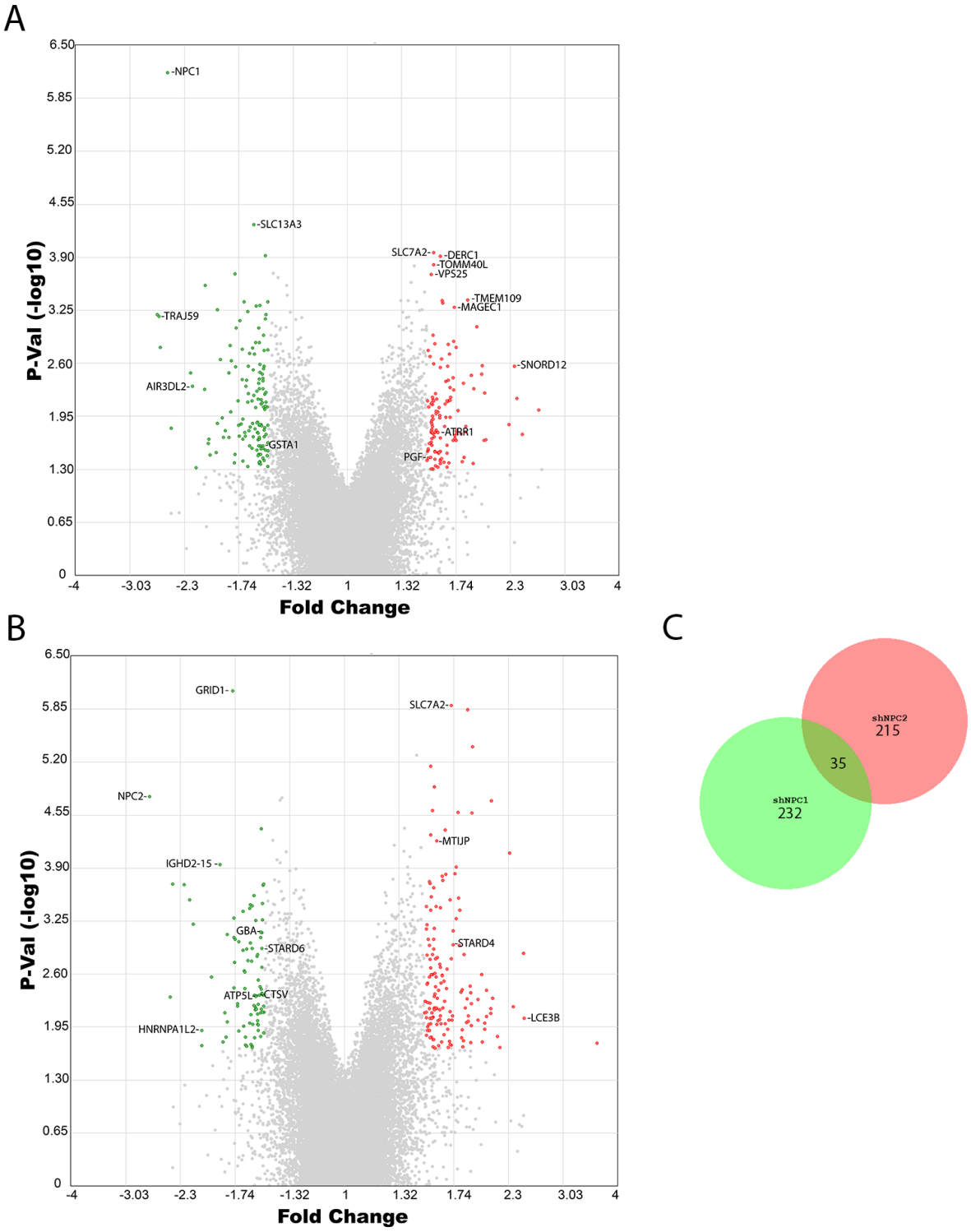

Figure 4.12: No compensatory pathways for the absence of cholesterol accumulation in NPC2 depleted SH-SY5Y cells could be identified by transcriptome analysis. SH-SY5Y cells transduced with pGIPz shNT, shPC1, and shNPC2 were grown for 3 days and RNA isolated in 3 independent experiments for microarray transcriptome analysis. (A) shNPC1 vs. shNT (B) shNPC2 vs shNT. (**C**) Quantitative Venn diagram comparing shNPC1 and shNPC2 differential expression.

Table 6: Genes differentially expressed in NPC1- and NPC2-depleted cells

Gene Symbol	Name
C3orf62	chromosome 3 open reading frame 62
FAM66D	family with sequence similarity 66, member D
FBXO28	F-box protein 28
GOLGA2P11	golgin A2 pseudogene 11
KIR3DL2	killer cell immunoglobulin-like receptor, three domains, long cytoplasmic tail, 2
KRTAP21-1	keratin associated protein 21-1
LOC105370733	uncharacterized LOC105370733
MIR431	microRNA 431
MIR4324	microRNA 4324
SLC7A2	solute carrier family 7 (cationic amino acid transporter, y+ system), member 2
SNORA12	small nucleolar RNA, H/ACA box 12
SNORA14A	small nucleolar RNA, H/ACA box 14A
SNORD12; ZFAS1	small nucleolar RNA, C/D box 12; ZNFX1 antisense RNA 1
SNORD124	small nucleolar RNA, C/D box 124
SNORD12C	small nucleolar RNA, C/D box 12C
SNORD46	small nucleolar RNA, C/D box 46
SNORD9	small nucleolar RNA, C/D box 9
STARD4	StAR-related lipid transfer domain containing 4
TIFAB	TRAF-interacting protein with FHA domain-containing protein B

4.10. NPC2 depletion did not induce cholesterol accumulation in primary rat neurons or IMR32 neuroblastoma cells.

Previous work on NPC2 has been mostly done on fibroblast and CHO cells, which reproducibly exhibit cholesterol accumulation after depletion of NPC2 (62,209). To investigate the effects of NPC2 depletion in other neuron-like cells, the neuroblastoma cell line IMR32 and primary rat neurons were transduced with NPC2 miRNA vectors and filipin staining performed.

Primary rat neurons and IMR32 cells showed strong filipin staining in LE/L-like compartments after NPC1 depletion, indicating cholesterol accumulation (**Figure 4.13**). However, primary neurons, as well as IMR32 cells, failed to produce any filipin staining that would indicate cholesterol accumulation after NPC2 depletion, even after incubation of IMR32 cells with LDL overnight.

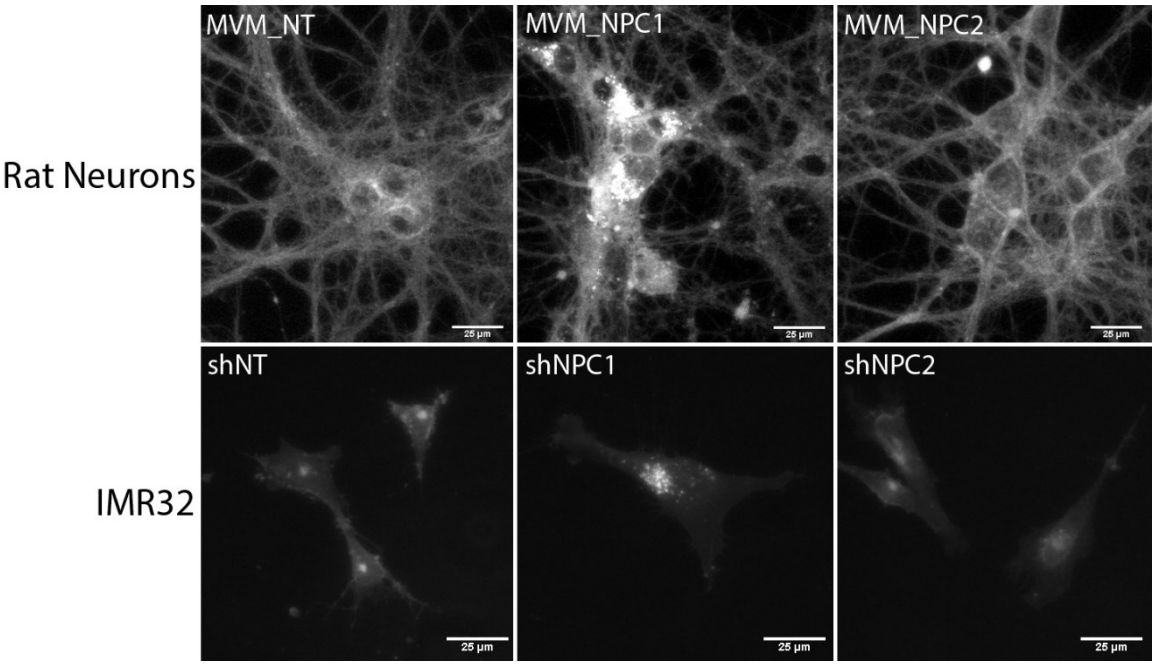

Figure 4.13: Rat primary neurons and IMR32 neuroblastoma cells do not show cholesterol accumulation after NPC2 depletion. (**A**) Rat hippocampal neurons were seeded on PLL-coated coverslips and transduced with lentiviral vectors expressing miRNA targeting NPC1, NPC2, or non-targeting control (NT) under control of the neuron-specific human synapsin promoter. Cells were fixed and cholesterol was visualized using filipin staining. (**B**) IMR32 neuroblastoma cells transduced with pGIPz shNT, shNPC1 and shNPC2 were seeded on coverslips, loaded overnight with LDL, before fixation and filipin staining.

4.11. NPC2 depletion decreases the number of endocytic vesicles while vesicle size is unchanged

LDL is endocytosed and shuttled through the endocytic system to the LE/L before its cholesterol esters are hydrolyzed and cholesterol transported to the rest of the cell. Absence of cholesterol accumulation in NPC2-depleted cells despite normal cholesterol uptake could indicate a cholesterol transport defect along the endocytic system, leading to altered trafficking or maturation of the endocytic system, which could explain the absence of LE/L cholesterol accumulation

To investigate if NPC2 depletion causes alterations to the endocytic system in SH-SY5Y cells, different endocytic compartments were visualized by immunofluorescence, and size, quantity, and localization of endocytic particles were analysed using an automated, nonbiased approach.

Immunostained images revealed differences in vesicle sizes for NPC1-depleted cells (**Figure 4.14**). While vesicles positive for the EE marker RAB5 were of similar size in NPC1-depleted cells compared to control and NPC2-depleted cells, vesicles positive for the LE markers LAMP1, LAMP2, or CD63 were significantly larger in NPC1-depleted compared to control and NPC2-depleted cells, with no differences between those two groups. Notably, many NPC1-depleted cells showed the increased size of late endosomes in NPC1-depleted SH-SY5Y cells is in line with the cholesterol transport defect and accumulation of lipids (210). EE are not affected by this defect, in agreement with the normal Rab5(+) vesicle size. In contrast, NPC2-depleted cells showed no alterations in apparent size of endocytic vesicles. However, NPC2-depleted cells showed a significant decrease in the number of vesicles positive for EE and LE markers RAB5, LAMP2, and CD63 per cell area compared to control cells and NPC1-depleted cells. Furthermore, compared to control, NPC1- and NPC2-depleted SH-SY5Y cells seem to show clustering of LE markers around the perinuclear area.

To quantify these apparent differences, a nonbiased approach was developed (**Figure 4.15**). Individual cells were circled and automated threshold applied. Images were then post-processed by removal of speckles and de-aggregating vesicle clusters. Size and number of endocytic marker positive vesicles was analysed. The number of vesicles was divided by cell area to compensate for different cell sizes. Furthermore, the individual distance of these vesicles to the centre of the nucleus was measured and averaged per cell.

Quantification confirmed the size increase for LE vesicles in NPC1-depleted SH-SY5Y cells, with a 50-70 % increase of LAMP1-, LAMP2-, CD63-positive vesicles size compared to control (**Figure 4.16**). Vesicle size in NPC2-depleted cells was not different from control cells. However, NPC2-depleted cells showed a marked decrease in the vesicle number per area, except for LAMP1-positive vesicles (**Figure 4.17**). This reduction was especially apparent in CD63-positive vesicles, showing a 40 % decrease mean vesicle number per area compared to control. NPC1-depleted cells showed no difference in vesicles number per area compared to control, except for CD63-positive vesicles, which

showed a 20 % decrease compared to control. CD63 is implicated in LE/L anterograde transport from the perinuclear area to the PM, a process known to be impaired in NPC1 depleted cells (183,184,211), which would explain the reduced number of CD63-positive vesicles in NPC1-depleted cells. Interestingly, the decrease in CD63-positive vesicles in NPC2-depleted cells was significantly more severe compared to NPC1-depleted cells during individual experiments. However, this significant difference disappeared in the compiled data ($p=0.051$), only suggesting a subtle difference between NPC1- and NPC2-depleted cells. Investigating the relative distance of endocytic vesicles compared to the nucleus revealed no difference of either NPC1- or NPC2- depleted cells compared to control SH-SY5Y cells (**Figure 4.18**).

Analysis of mRNA and protein levels of endocytic system markers RAB5, RAB7, RAB8, LAMP1, LAMP2, and CD63 showed no changes in NPC1- or NPC2-depleted cells compared to control (**Figure 4.19**).

Taken together, these results reveal clear differences in the consequences of NPC1 and NPC2 depletion in SH-SY5Y cells on the size and quantity of endocytic vesicles. While NPC1 depletion affected mostly the size of LE/L vesicles, NPC2 depletion led to significant reduction of the number of EE and LE/L vesicles without changing their size. Furthermore, this difference was not due to differential expression of endocytic vesicles markers.

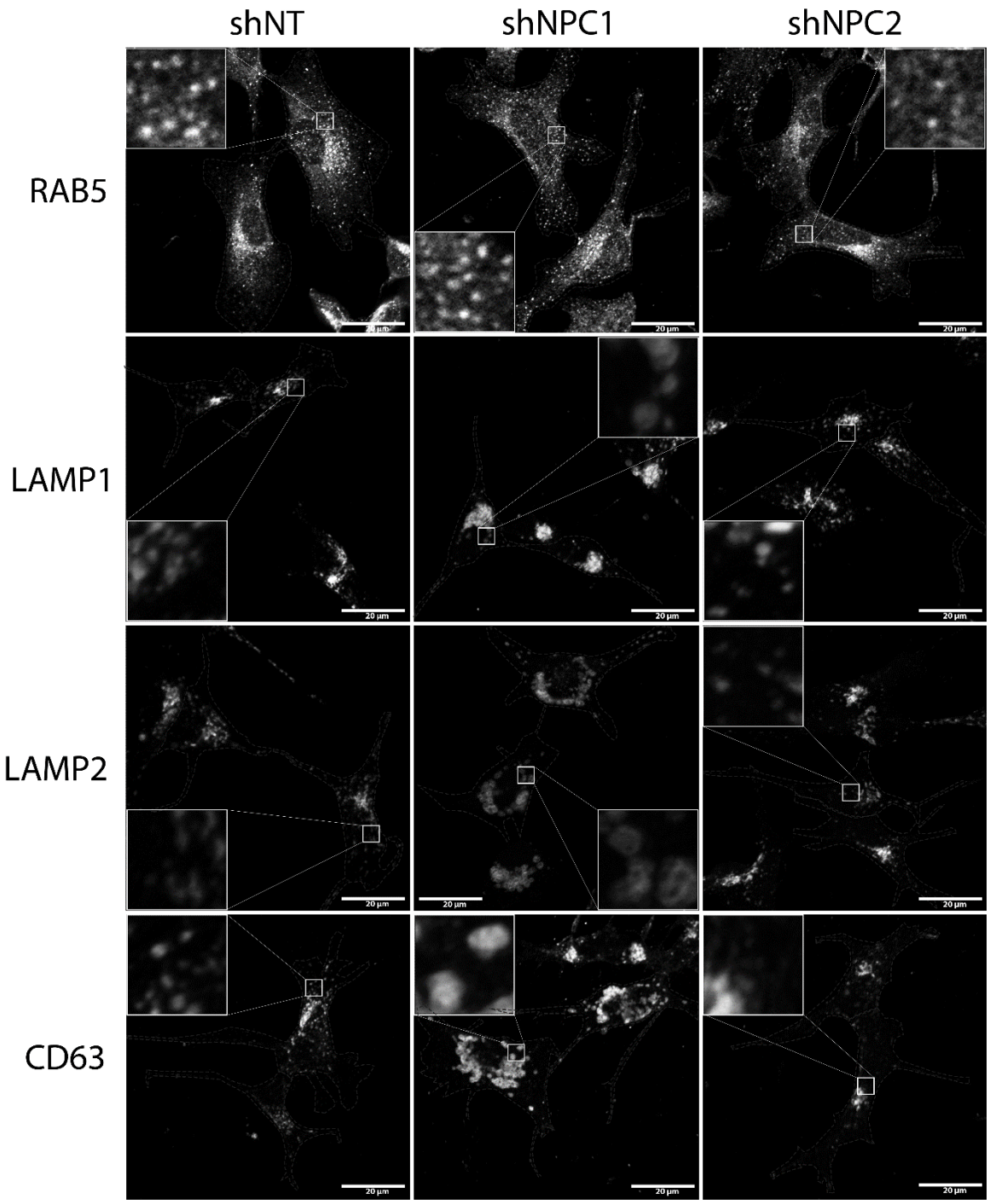

Figure 4.14: Representative images of endocytic vesicle analysis. SH-SY5Y transduced with pGIPz shNT, shNPC1 and shNPC2 were seeded on collagen-coated coverslips and immunostaining for RAB5, LAMP1, LAMP2, or CD63 was performed after 3 days. Shown are representative confocal images. Inserts show enlargements of image area marked by a white square. Dotted lines outline the shape of a cell, based on the co-expressed fluorescent protein.

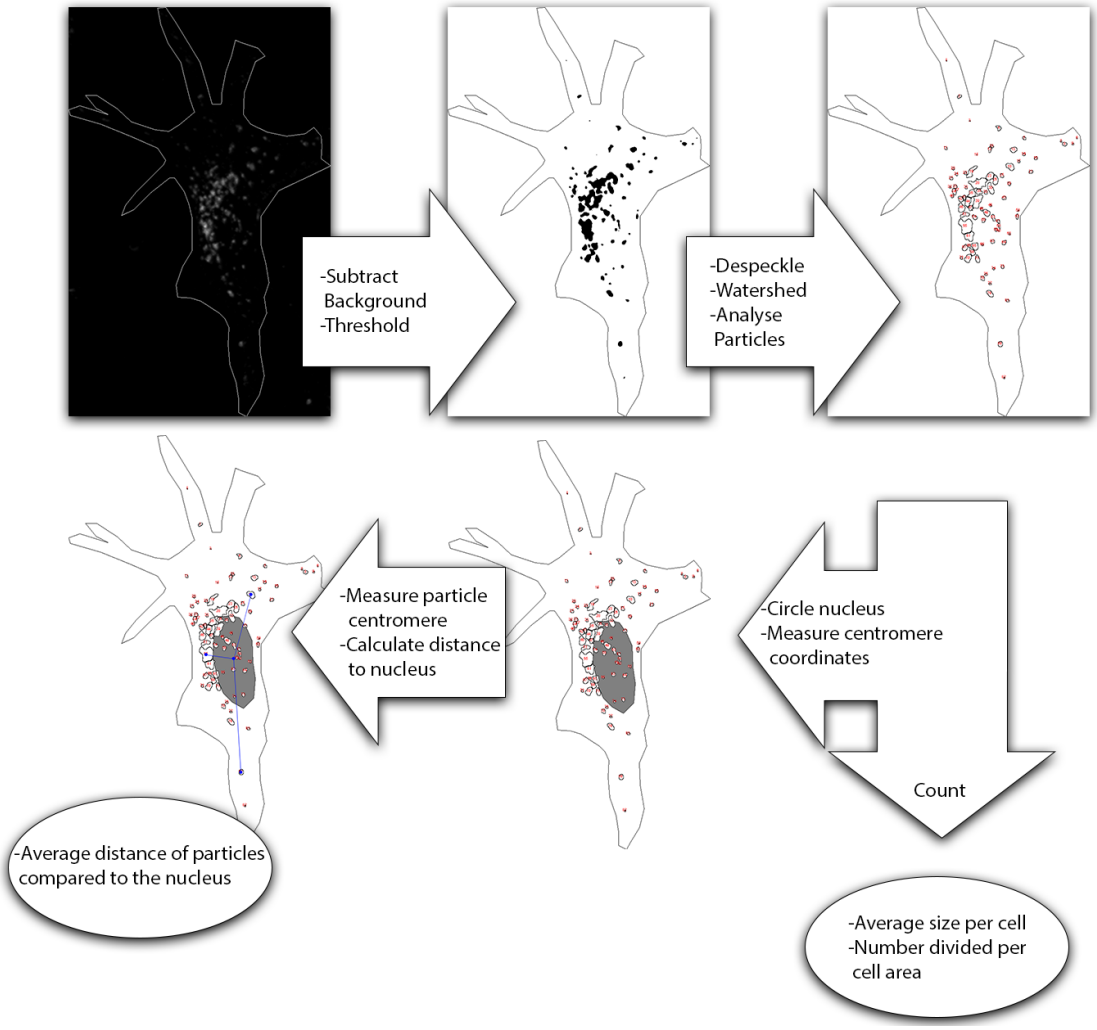

Figure 4.15: Overview of endocytic vesicles analysis workflow. To investigate endocytic system morphology, confocal IF images of SH-SH5Y using antibodies against RAB5, LAMP1, LAMP2, or CD63 were analysed using a nonbiased approach in FIJI. Cells were individually circled using the images of the co-expressed fluorescent protein. Vesicle images were background subtracted and auto-threshold applied. Signals were cleaned up using the "Despeckle" tool and de-aggregated with the "Watershed" algorithm, before particle size and number per cell were analysed. Coordinates of particle and the nucleus were used to calculate the distance between as a measure of particle distribution.

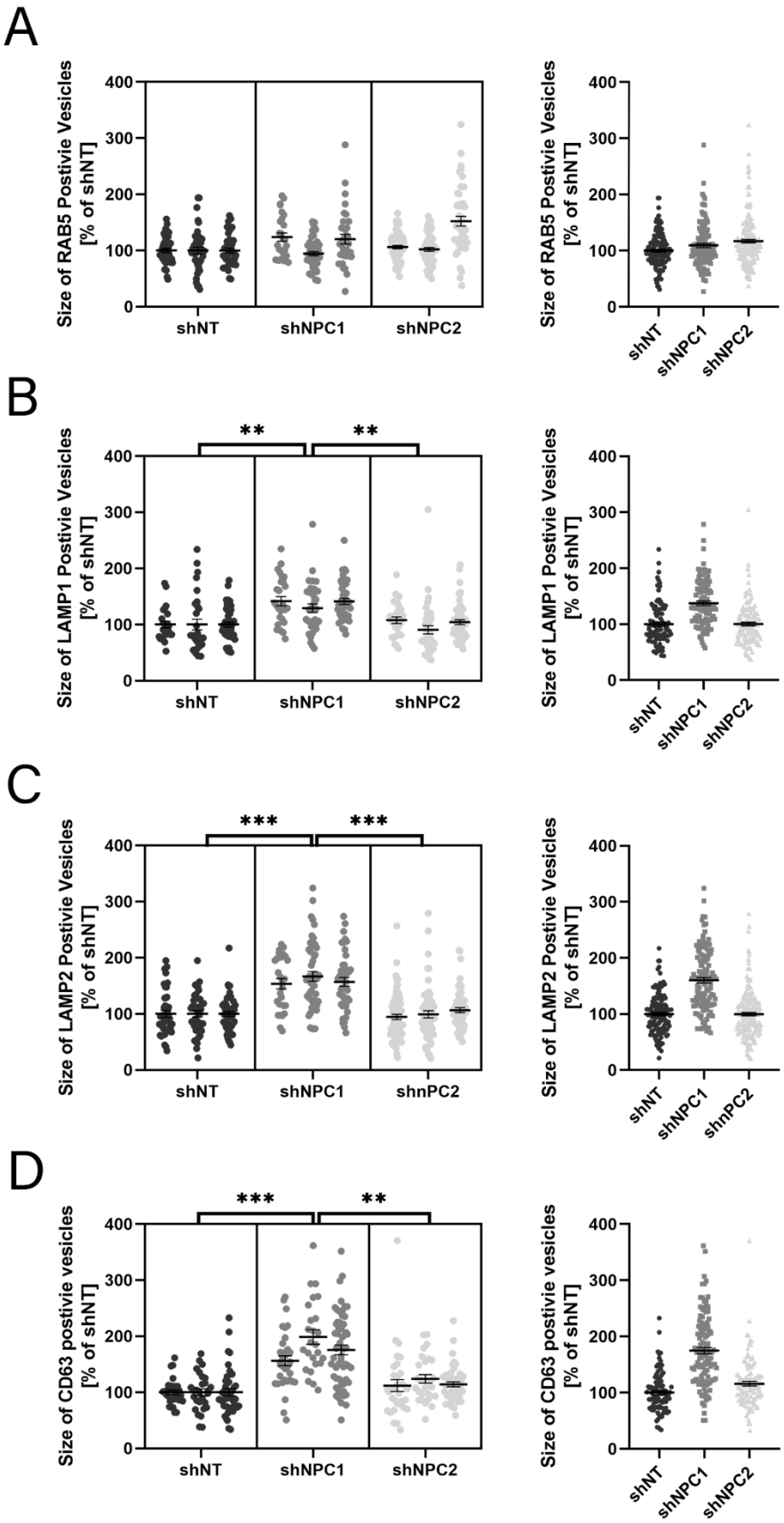
A
Size of RAB5 Postivie Vesicles [% of shNT]
400
300
200
100
0
shNT
shNPC1
shNPC2
B
**
**
Size of LAMP1 Postivie Vesicles [% of shNT]
C
***
***
Size of LAMP2 Postivie Vesicles [% of shNT]
shnPC2
D
***
**
Size of CD63 postivie vesicles [% of shNT]

Figure 4.16: Late endocytic and lysosomal vesicles of NPC1-depleted SH-SY5Y cells have increased volume compared to NPC2-depleted and control cells. SH-SY5Y transduced with pGIPz shNT, shNPC1 and shNPC2 were seeded on collagen-coated coverslips and immunostained for RAB5 (**A**), LAMP1 (**B**), LAMP2 (**C**), or CD63 (**D**) after 3 days. Images were analysed using a nonbiased approach in FIJI. Each data point represents the average size of marker-positive vesicles for an individual cell, expressed as percentage of the mean of shNT control.

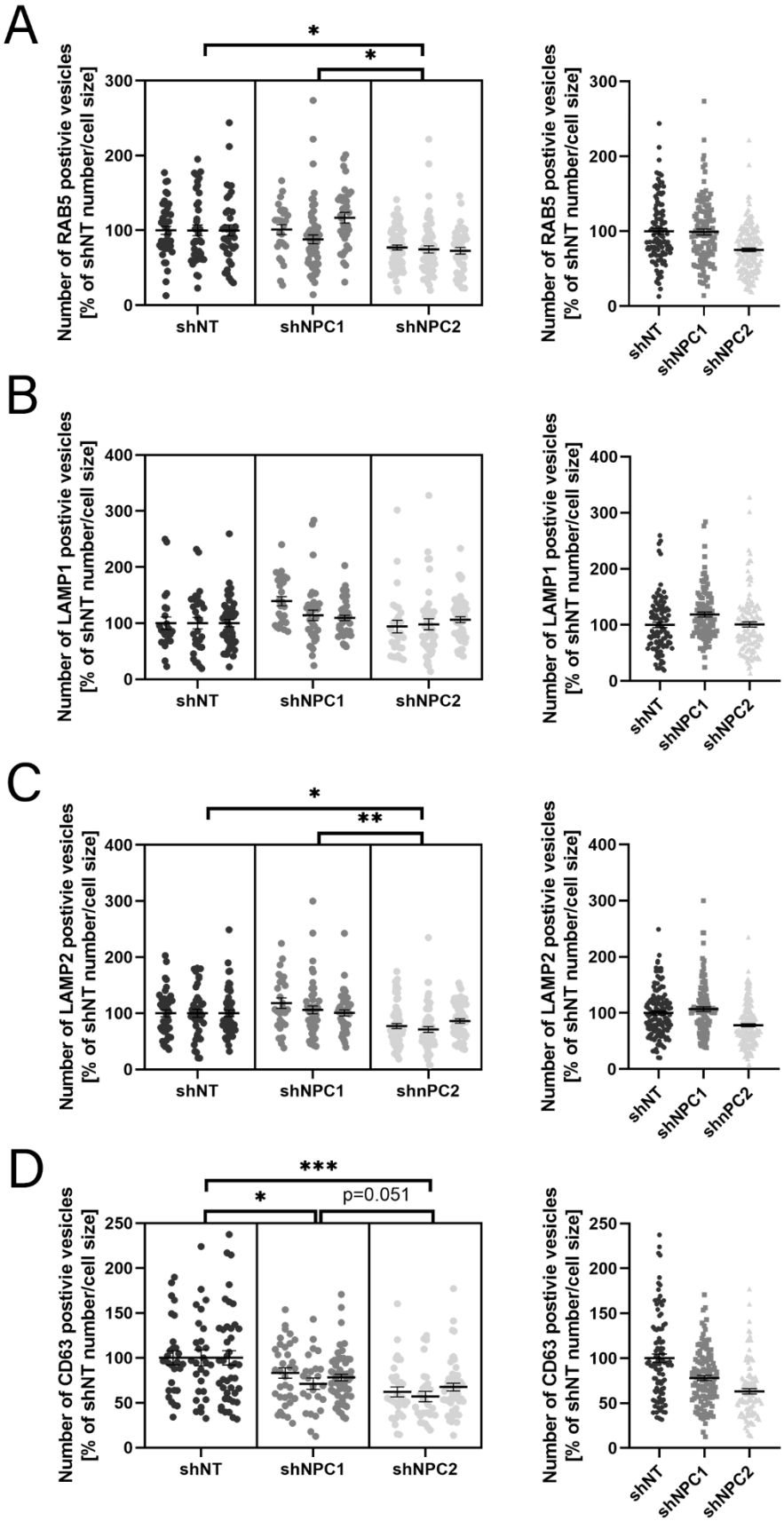
A
Number of RAB5 postivie vesicles [% of shNT number/cell size]
shNT
shNPC1
shNPC2
B
Number of LAMP1 postivie vesicles [% of shNT number/cell size]
C
Number of LAMP2 postivie vesicles [% of shNT number/cell size]
shnPC2
D
Number of CD63 postivie vesicles [% of shNT number/cell size]
p=0.051

Figure 4.17: NPC2-depleted SH-SY5Y cells have fewer late endocytic and lysosomal vesicles per cell compared to NPC1-depleted and control cells. SH-SY5Y transduced with pGIPz shNT, shNPC1 and shNPC2 were seeded on collagen-coated coverslips and immunostained for RAB5 (**A**), LAMP1 (**B**), LAMP2 (**C**), or CD63 (**D**) after 3 days. Images were analysed using a nonbiased approach in FIJI. Each data point is the number of marker-positive vesicles per area for one individual cell, expressed as percentage of the mean of shNT control.

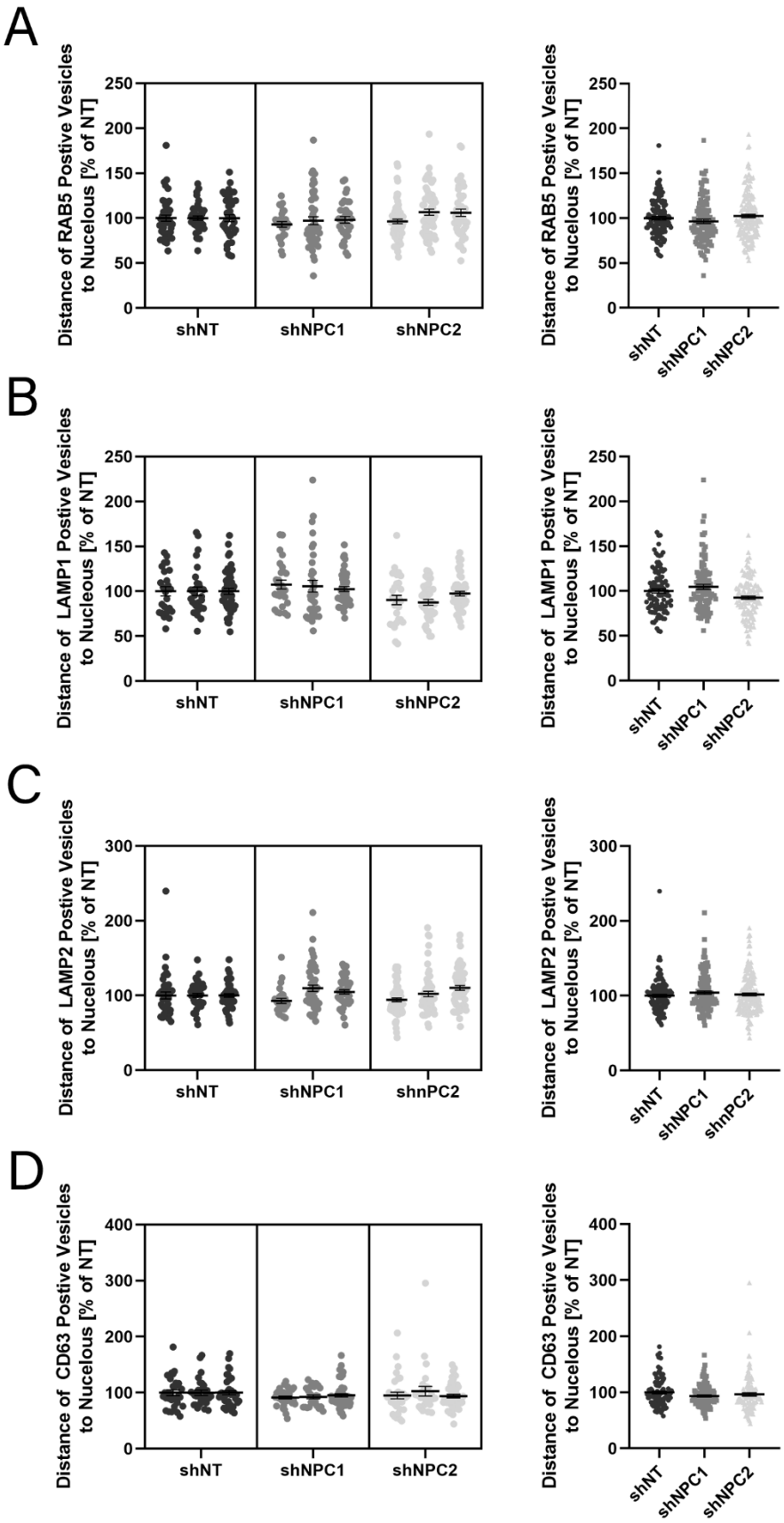
A
Distance of RAB5 Postive Vesicles to Nucelous [% of NT]
250
200
150
100
50
0
shNT
shNPC1
shNPC2
B
Distance of LAMP1 Postive Vesicles to Nucleous [% of NT]
C
Distance of LAMP2 Postive Vesicles to Nucelous [% of NT]
300
shnPC2
D
Distance of CD63 Postive Vesicles to Nucelous [% of NT]
400

Figure 4.18: Late endocytic and lysosomal vesicles of NPC1- or NPC2-depleted SH-SY5Y cells show no difference in distribution compared to control cells. SH-SY5Y transduced with pGIPz shNT, shNPC1 and shNPC2 were seeded on collagen-coated coverslips and immunostained for RAB5 (**A**), LAMP1 (**B**), LAMP2 (**C**), or CD63 (**D**) after 3 days. Images were analysed using a nonbiased approach in FIJI. Every data point is the average distance of marker-positive vesicles to the nucleus for one individual cell, expressed as percentage of mean of shNT control.

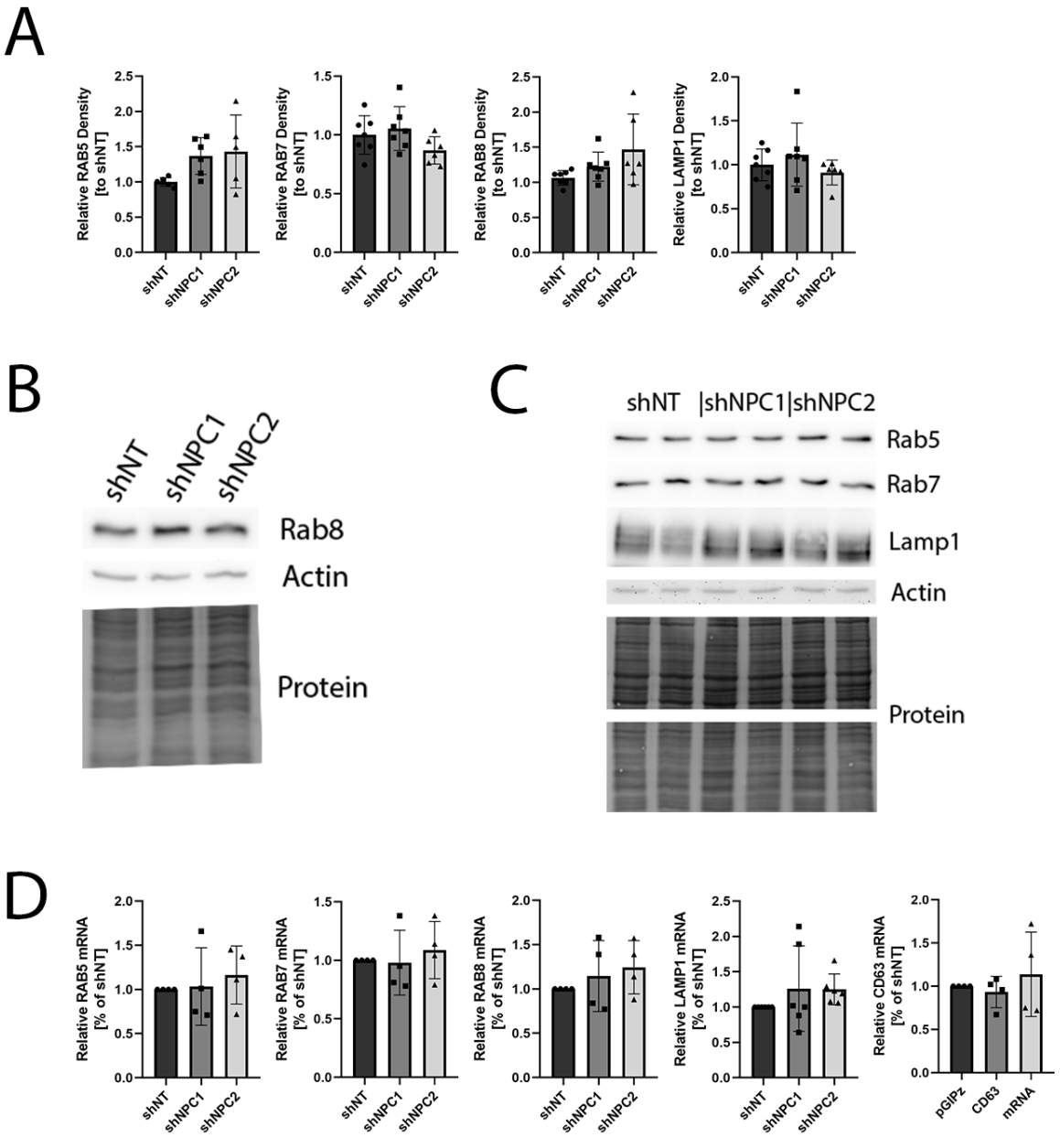

Figure 4.19: Unchanged expression of endocytic markers in NPC1- and NPC2-depleted SH-SY5Y cells. SH-SY5Y cells transduced with pGIPz shNT, shNPC1, and shNPC2 were grown for 3 days. (**A-C**) Total cell lysates were immunoblotted for RAB5, RAB7, RAB8, and LAMP1 followed by actin as a reference gene. Band intensity was quantified using FIJI and normalized to actin band intensity (**D**) Total cellular RNA was isolated and RAB5, RAB7, RAB8, LAMP1, and CD63 expression levels analysed by qPCR using ACTB as reference gene.

4.12. UBC promoter vectors provide robust RNAi with moderate overexpression of NPC2 variants

To investigate if the decrease in endocytic vesicle number cause by the depletion of NPC2 in SH-SY5Y could be rescued by the expression of wild-type NPC2 or functional variants of NPC2, new pGIPz expression vectors were designed. Wild-type NPC2 (NPC2.WT), NPC2 with the point mutation Y119A unable to bind sterols (NPC2.Y119A)(62,156), and NPC2 with the point mutation V81D unable to interact with NPC1 (NPC.V81D)(62,156) were chosen as candidates.

Quantitative mRNA analysis of SH-SY5Y cells showed strong depletion of endogenous NPC2 (**Figure 4.20** A-B). However, NPC2 variants were overexpressed 100 to 200-fold compared to endogenous NPC2 due to strong CMV promotor activity. Localization analysis of NPC2 variants C-terminally fused to mCherry fluorescent protein showed endocytic-system-like vesicular signal, similar to LAMP2 localization patterns, indicating delivery of recombinant protein to the LE/L (**Figure 4.20** C).

Although these results indicate depletion of endogenous protein and correct localization of recombinant protein, the strong overexpression of NPC2 variants could skew further experiments. Furthermore, aggregates of overexpressed fluorescent protein was seen in the medium. To address these artificially high expression levels of NPC2 variants by the pGIPz CMV vectors, the expression cassette was transferred into a FUGW vector with a weaker UBC promoter. One additional NPC2 variant was included, a glycosylation mutant that is not retained by the cell and secreted (NPC2.N58A)(60).

Depletion efficiency and level of overexpression with UBC vectors in SH-SY5Y cells showed reduction of NPC1 to 40 % of control in shNPC1 and reduction of endogenous NPC2 in shNPC2 and NPC2 variant expressing cells to 15 – 30 % compared to control (**Figure 4.21** A-B). NPC1 levels in NPC2 variant expressing cells were similar to control. However, NPC1-depleted cells showed a significant increase in NPC2 expression levels of 50 %. Total NPC2 mRNA levels in NPC2 variant expressing cells were 2 – 8 fold higher than control (**Figure 4.21** C).

NPC2 immunoblotting of total SH-SY5Y protein showed no band for endogenous NPC2 in NPC2-depleted cell, indicating robust depletion (**Figure 4.21** D). NPC2.WT, NPC2.Y119A and NPC2.V81D expressing cells revealed strong overexpression of recombinant protein with bands corresponding to the full length mCherry tagged protein (arrow), the cleaved glycosylated (hollow arrow head) and un-glycosylated (full arrow head) NPC2. The NPC2.N58A variant only exhibited bands for the full length mCherry tagged NPC2 and the cleaved un-glycosylated forms, as expected. Furthermore, the band intensities of this variant were much lower, as the lack the post-translational glycosylation leads to secretion of most of the protein (60).

In fibroblasts, transduction with the UBC promotor vectors still led to robust cholesterol accumulation in NPC1- and NPC2-depleted cells, as seen previously with the pGIPz vectors (**Figure 4.21** E). Expression of NPC2.WT restored normal filipin staining patterns compared to control, whereas other NPC2 variants failed to rescue the accumulation phenotype and exhibited strong filipin staining similar to NPC2 and NPC1 depleted cells, as expected. However, none of the SH-SY5Y cells experienced cholesterol accumulation, except for NPC1-depleted cells, as seen with the pGIPz vectors.

Investigating the localization of the mCherry-tagged recombinant proteins revealed similar endocytic system-like patterns as seen after transduction with the pGIPz vectors, closely co-localizing with the LE/L maker LAMP2 (**Figure 4.22**).

Taken together, these results show that the weaker UBC promoter is still able to cause robust depletion of NPC1 and NPC2. Furthermore, sterol binding, the ability to interact with NPC1, and glycosylation of NPC2 are crucial for proper cholesterol transport in fibroblasts, whereas only NPC1 depletion, but not NPC2 depletion, leads to defects in cholesterol transport in SH-SY5Y cells.

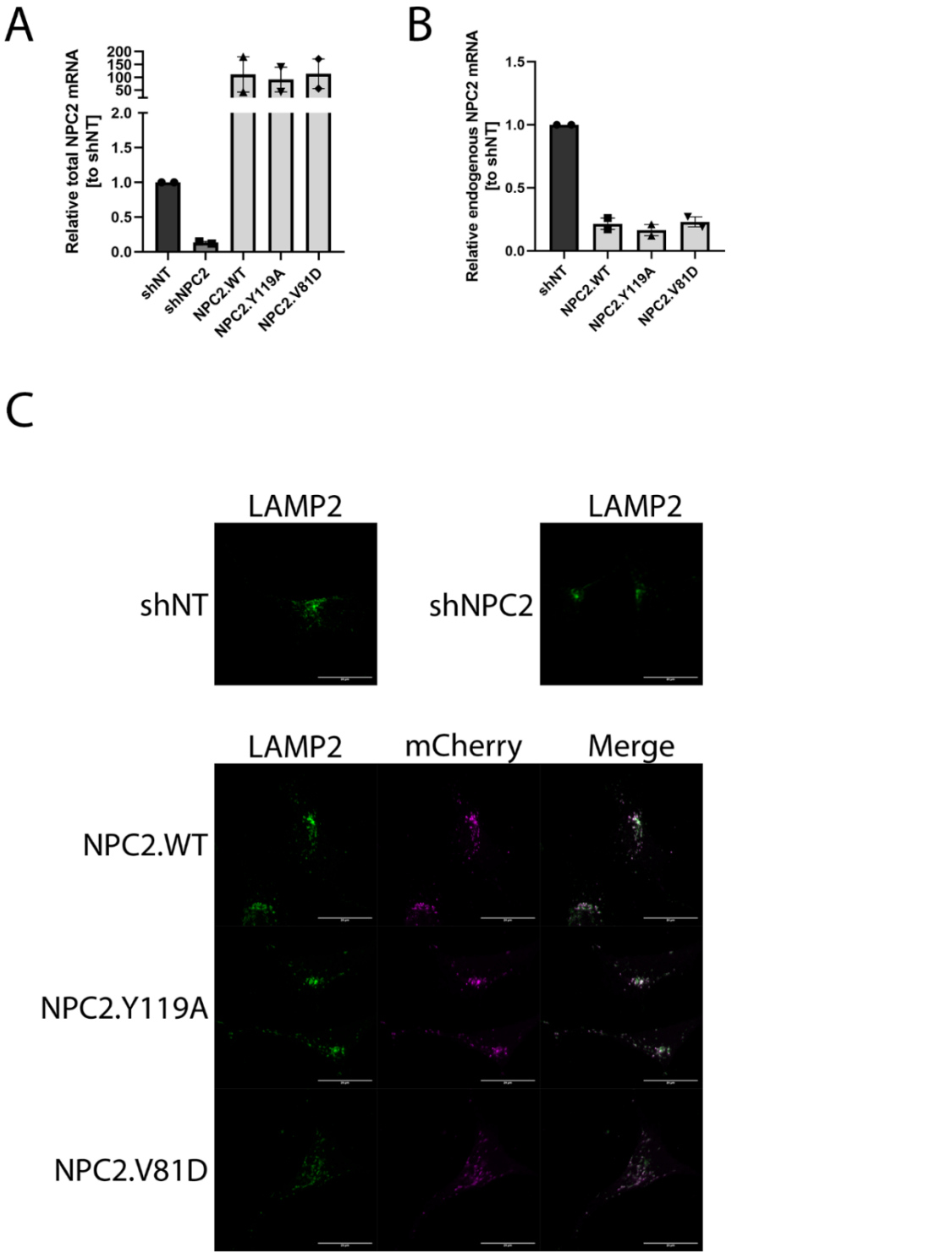

Figure 4.20: CMV promoter-driven NPC2 variant mRNA levels are up to 200-fold higher than endogenous levels. SH-SY5Y cells were transduced with pGIPz shNT, shNPC2, or NPC2 variant vectors (**A – B**) SH-SY5Y RNA was isolated and total (A) and endogenous (B) NPC2 expression levels analysed by qPCR using ACTB as reference gene. (**C**) SH-SY5Y were grown on collagen-coated coverslips and immunostained for LAMP2. LAMP2 signal, NPC2 variant mCherry signal, and a merge of the channels are shown.

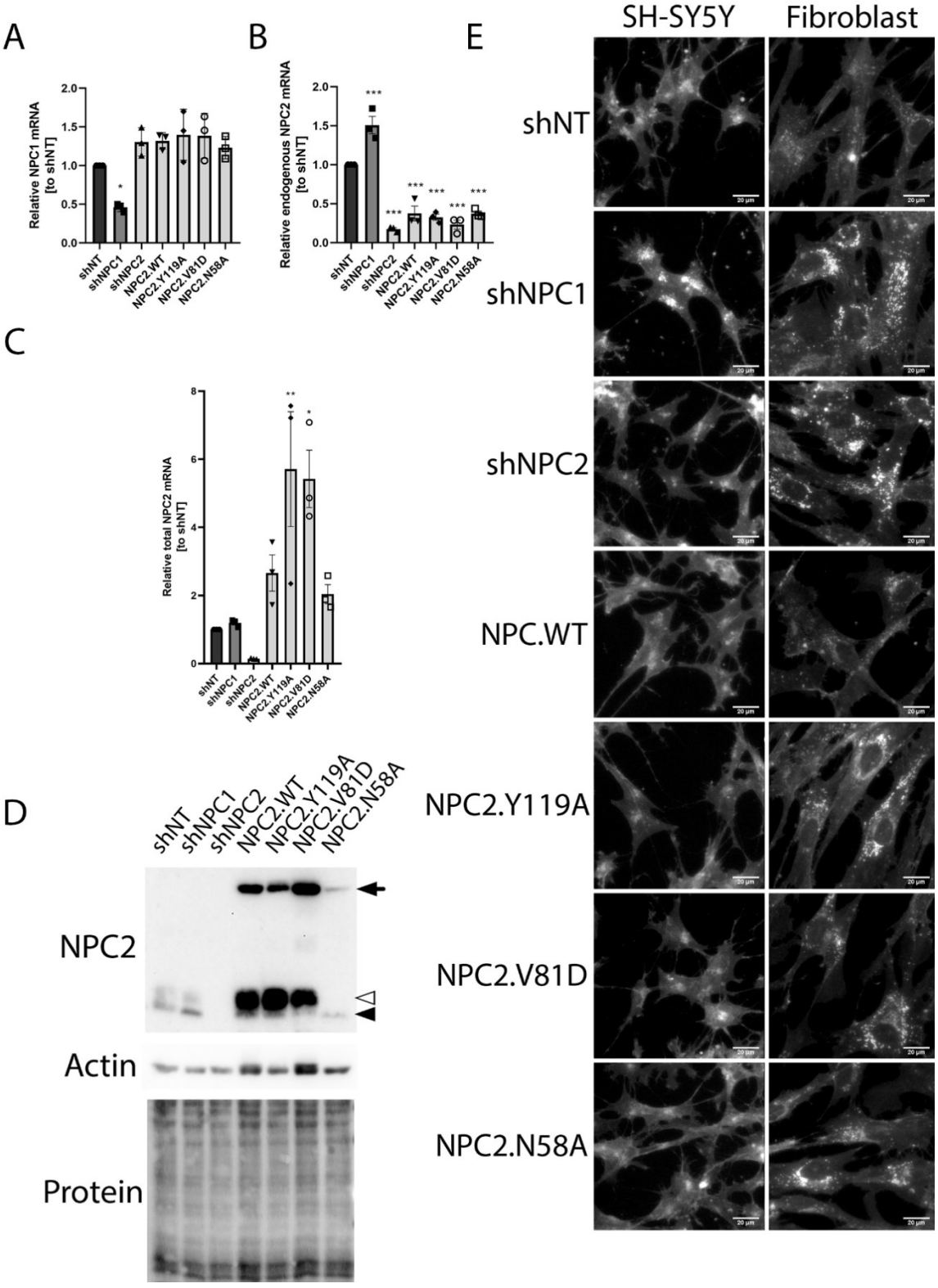

Figure 4.21: UBC promoter driven expression provides strong depletion of endogenous NPC2 while providing moderate NPC2 variant overexpression. SH-SY5Y cells or fibroblasts were

transduced with FUGW shNT, shNPC1, shNPC2, or NPC2 variant constructs for 3 days. (**A – B**) NPC1 and NPC2 mRNA levels in SH-SY5Y cells analysed by qPCR using ACTB as reference gene. (**C – D**) SH-SY5Y total cell lysates were immunoblotted for NPC2 followed by actin as a reference. Arrow: full length NPC2 variant with mCherry tag. Hollow arrowhead: NPC2 glycosylated. Arrowhead: NPC2 un-glycosylated (**E**) SH-SY5Y cells, but not fibroblasts were loaded with LDL overnight before fixation and staining with filipin.

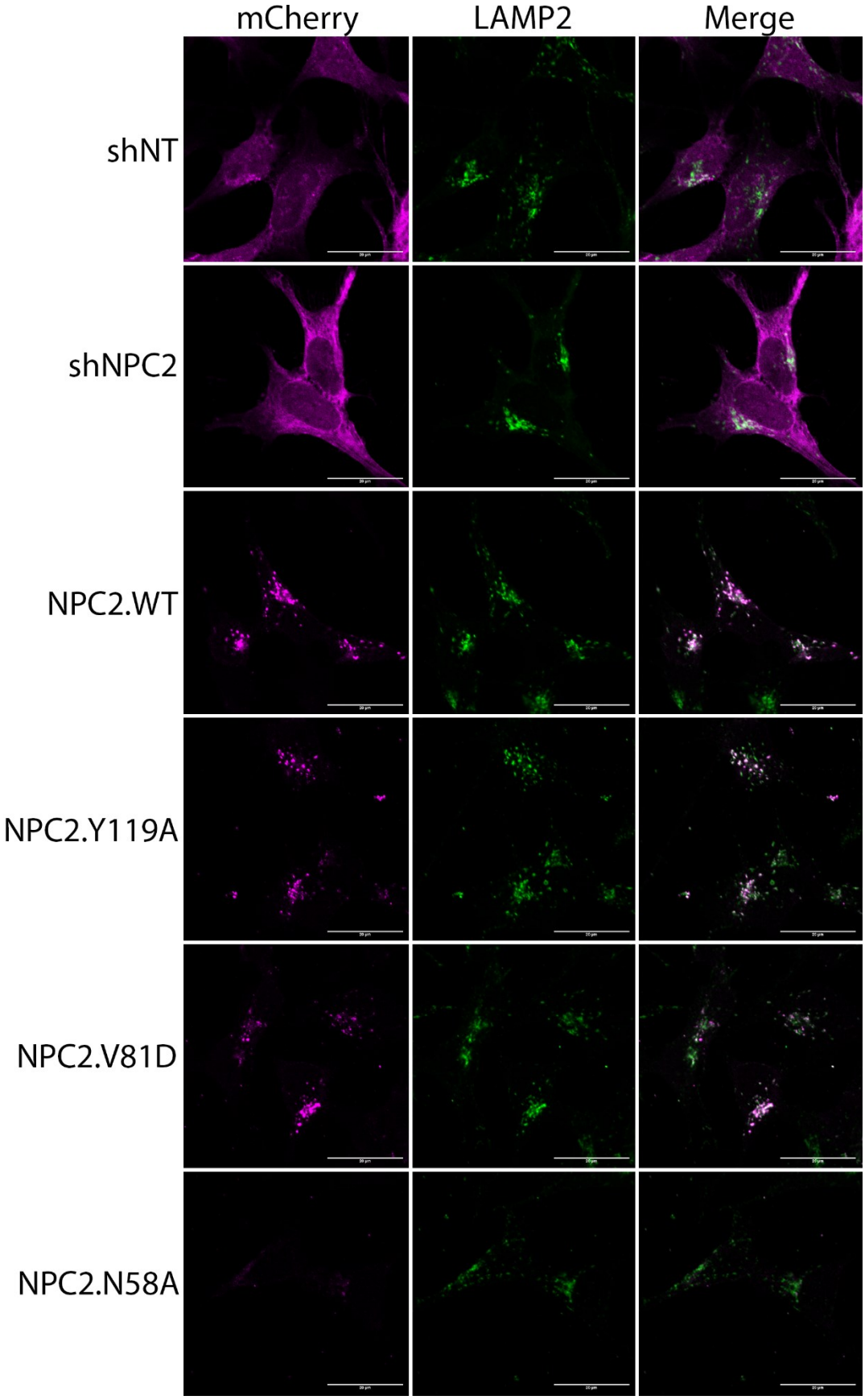
mCherry
LAMP2
Merge
shNT
shNPC2
NPC2.WT
NPC2.Y119A
NPC2.V81D
NPC2.N58A

Figure 4.22: NPC2 variants colocalize with Lamp2. SH-SY5Y cells transduced with FUGW shNT, shNPC2, or NPC2 variant constructs were grown on collagen-coated coverslips. Cells were immunostained for LAMP2. Images show LAMP2, NPC2 variant mCherry, and a merge of the channels.

4.13. All NPC2 variants prevent the decrease in the number of endosomes.

To investigate if the effects of NPC2 depletion on the endocytic system can be prevented by expression of wild-type NPC2 or functional NPC2 variants, the endocytic system vesicle number analysis for LAMP2 and CD63 were repeated in SH-SY5Y cells depleted of endogenous NPC2 while expressing NPC2 variants driven by the UBC promoter.

Vesicle number analysis for LAMP2 and CD63 show that UBC promoter-based knock down of NPC2 leads to a similar reduction in CD63- and LAMP2-positive vesicles as seen with the CMV promoter-based vectors (**Figure 4.23** A-B). Co-expression of wild-type NPC2 prevented this phenotype, as expected. However, expression of NPC2 variants prevented this phenotype as well, independent of their functional domains. Unexpectedly, the NPC2.N58A glycosylation variant showed the strongest and most consistent protection of vesicle number across all variants.

Quantitative expression analysis of endocytic vesicles markers RAB5, LAMP2, and CD63 revealed no differences in mRNA levels of these genes in cells expressing the NPC2 variants compared to NPC2-depleted cells expressing only mCherry (**Figure 4.23** C-E). CD63 mRNA levels were slightly increase in shNPC2 and shNPC2/NPC2.V81D cells compared to control, whereas LAMP2 and RAB5 mRNA levels were similar to control in all groups. The lack of any differences in mRNA levels of endocytic markers in NPC2-depleted cells expressing mCherry or expressing NPC2 variants suggests that the decreased number of endocytic vesicles caused by NPC2 depletion was not due to transcriptional regulation.

Together these data further suggest a role of NPC2 in the regulation of the endocytic system that is not based on any yet know function of NPC2.

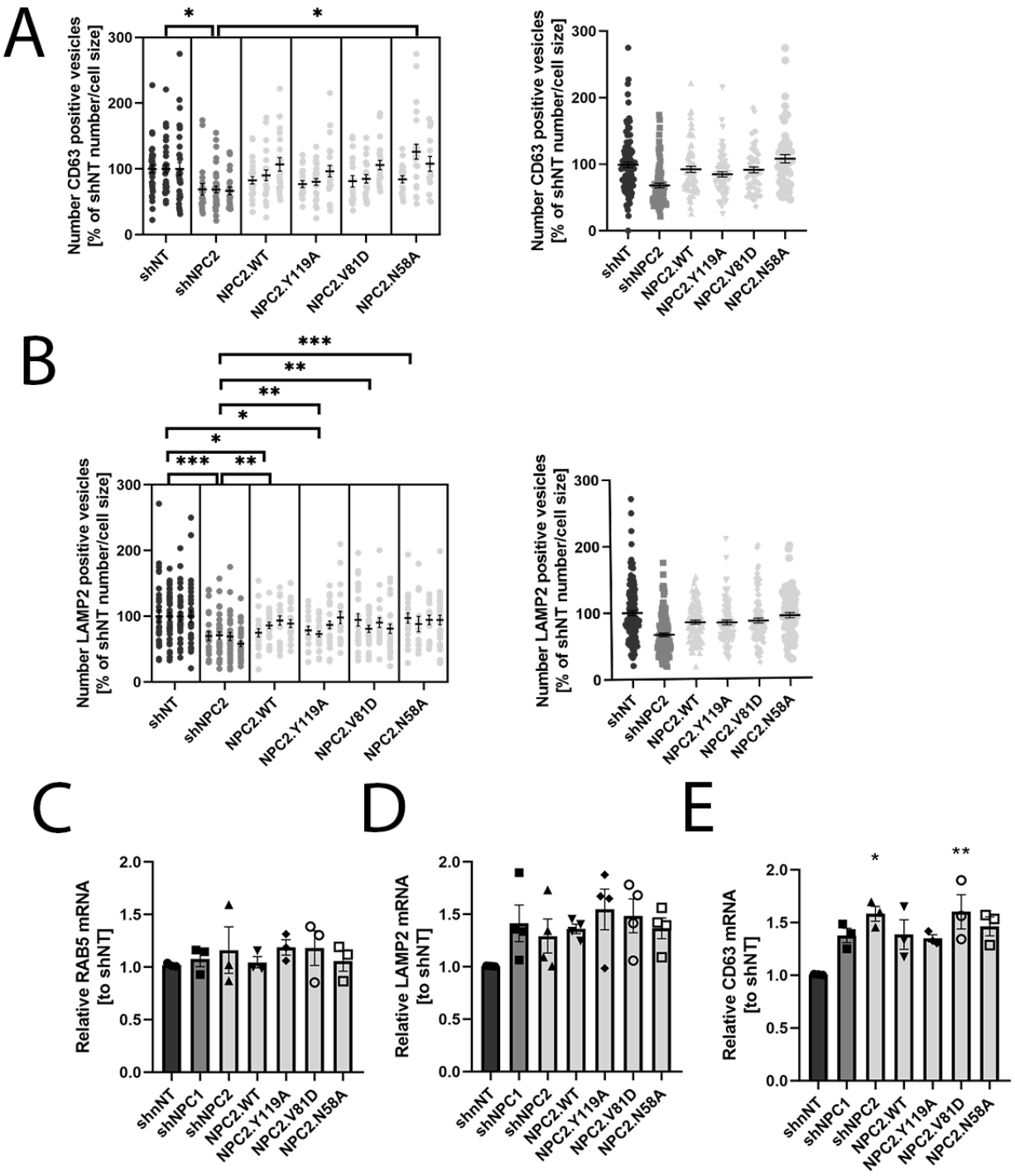

Figure 4.23 NPC2 variant expression prevents the decrease in endocytic vesicles in NPC2-depleted SH-SY5Y cells. SH-SY5Y transduced with FUGW shNT, shNPC2 and NPC2 variants were seeded on collagen-coated coverslips and immunostained for CD63 (**A**) and LAMP2 (**B**) after 3 days. Images were analysed using a nonbiased approach in FIJI to determine the average number of marker positive vesicles per cell. Data are expressed as percentage of shNT control and shown as individual experiments (left) and pooled in one column (right). (**C-D**) SH-SY5Y RNA was isolated and RAB5, LAMP2 and CD63 mRNA levels were analysed by qPCR using ACTB as reference gene.

4.14. NPC2 variant expression increases cell proliferation

During the endocytic vesicle analysis, differences in cell growth were noticed, with the NPC2 variant expressing cells showing faster proliferation after transduction. To quantify these observations, growth assays were performed.

SH-SY5Y cells transduced with FUGW expression vectors showed similar growth patterns for NPC1- and NPC2-depleted cells as seen after transduction with the pGIPz vectors (**Figure 4.3**), namely that NPC2-depletion did not alter cell growth, while NPC1-depletion increased growth by 30 % compared to control (**Figure 4.24**). Expression of NPC2 variants also increased cell growth compared to either shNT or shNPC2 cells, regardless of known functional defects of these variants. All observed growth was positive over time, but no statement could be made if changes seen between conditions are due to increased cell growth or increased cell longevity.

These results indicate that NPC2 variant expression might affect cellular growth in SH-SY5Y cells in a way not dependent on any function yet know in NPC2.

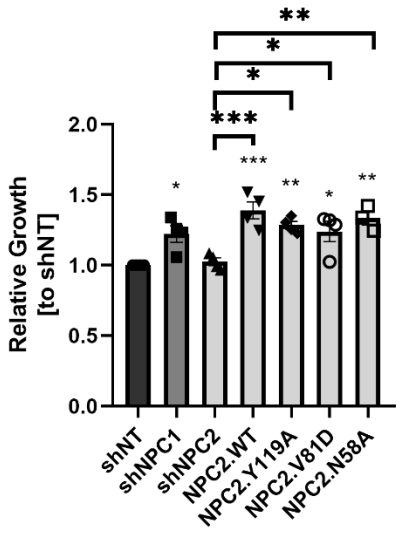

Figure 4.24: NPC2 variants expression increases cell growth compared to control. SH-SY5Y cells were transduced with FUGW shNT, shNPC1, shNPC2, and NPC2 variants and growth assays were performed. Data show growth over 2 days relative to control.

5. CHAPTER 5 DISCUSSION

The goal of this thesis originally was to investigate the effects of increased mitochondrial cholesterol import on mitochondrial and cellular health. NPC disease, characterized by increased endosomal cholesterol accumulation, has been shown to also detrimentally affect mitochondrial health (170,212,213). Studies done by the Karten lab revealed that during NPC1 depletion, cholesterol accumulating in the endosome can be transported to the mitochondria by NPC2 and STARD3 (62,155). This cholesterol import leads to increased mitochondrial cholesterol levels, which in turn could be linked to increased ROS production, also found in other studies (214). Mitochondrial cholesterol has been further implicated as a factor contributing to Alzheimer disease pathology (215,216). However, most studies looking at mitochondrial cholesterol in the context of NPC disease were done in non-neuronal cells, like fibroblasts, HeLa, or CHO cells. For this study, the aim was to investigate the functional implications of increased mitochondrial cholesterol in the context of neurodegenerative disease. Therefore, the human neuroblastoma cell line, SH-SY5Y was chosen for this work. To induce increased cholesterol in mitochondria, two models were chosen to be tested, both relying on

STARD3-mediated cholesterol egress from cholesterol-laden endosomes. The first model relies on induction of cholesterol accumulation in the LE by depletion of NPC1. Previous studies had shown that this cholesterol transport pathway is inhibited by depletion of STARD3, so that cells co-depleted of NPC1 and STARD3 still have endosomal cholesterol accumulation, but normal mitochondrial cholesterol. The second model induces cholesterol accumulation by depletion of NPC2, the protein acting in concert with NPC1 for cholesterol egress from endosomes. Furthermore, depletion of NPC2 also blocks cholesterol egress to mitochondria, as NPC2 is needed for STARD3-mediated cholesterol transport to mitochondria (62). An NPC2 variant (NPC2.V81D) that can bind cholesterol but is not able to transfer it to NPC1 is able to facilitate cholesterol transport to mitochondria when STARD3 is present. Thus, expression of this variant in NPC2-depleted cells causes increased mitochondrial cholesterol, without mobilizing the bulk of endosomal cholesterol. Expression of NPC2 wild-type, to prevent endosomal cholesterol accumulation altogether, and the NPC2.Y119A variant, not able to bind sterols, blocking either transport out of the endosome serve as controls. Later, the NPC2.N58A variant was included in this model, which is not glycosylated properly and therefore secreted from the cell.

In this chapter, I will discuss observations made while studying these two models in SH-SY5Y cells in the context of the literature and discuss their implications on mitochondrial health as well as the canonical cholesterol “hand-off” model proposed for endosomal cholesterol egress mediated by NPC2 and NPC1. My findings indicate that mitochondria morphology was not altered and ER to mitochondria contact sites were not affected during NPC1-depletion in SH-SY5Y cells. I found that depletion of NPC2 did not lead to endosomal cholesterol accumulation although endosomal cholesterol egress for esterification in the ER was diminished. I showed that the lack of accumulation could not be explained by increased cholesterol secretion or reduced cholesterol uptake. However, I provide evidence that depletion of NPC2 in SH-SY5Y cells influenced the endocytic system by decreasing endocytic vesicle number across various stages, a process prevented by an as yet unknown function of NPC2. These findings provide

insight into an alternative role of NPC2 in the endocytic system and shine a light on the functional differences between NPC1 and NPC2, even though these proteins are usually implicated only in cholesterol egress from the endocytic compartment.

5.1. NPC1 and mitochondrial health

The topic of mitochondria dysfunction and its involvement in various diseases is moving more and more into the spotlight. Mitochondria dysfunction has been implicated in neurodegenerative diseases like Alzheimer's, Parkinson's, and Huntington's disease (213). In the Karten lab, one disease in particular is in the center of research, namely NPC disease. Studies in CHO cells identified cholesterol transport to the mitochondria to be a major player in the development of mitochondrial dysfunction manifested by increased lactate production, decreased mitochondrial respiration and decreased ATP transport across mitochondrial membranes (155). However, the exact mechanisms for how mitochondrial cholesterol affects mitochondrial health remained elusive. In the first part of the study, the aim was to further elucidate the consequences of altered cholesterol levels in mitochondria and investigate how they could play a role in the regulation of mitochondria.

5.1.1. NPC1 and STARD3 in SH-SY5Y

The human neuroblastoma cell line, SH-SY5Y was chosen for this thesis, due to the close connection of mitochondrial health and neurodegenerative disease (213). Previous studies on the subject from the Karten lab were done in CHO cells and mouse models and showed that NPC1 depletion leads to STARD3-mediated cholesterol import to the mitochondria. In my thesis, I aimed to apply this approach to SH-SY5Y cells, to further investigate mitochondrial dysfunction in a neuronal cell line. As seen in **Figure 3.1**, miRNA-mediated RNAi markedly decreased endogenous NPC1 and STARD3 mRNA levels. Furthermore, depletion of NPC1 led to the characteristic, punctate filipin staining, indicative of endosomal cholesterol accumulation seen in NPC patients, similarly to other studies depleting NPC1 in SH-SY5Y cells (217). Previously, the Karten lab provided evidence that NPC1 depletion leads to mitochondrial dysfunction that can manifest by increased lactate production which could be prevented by STARD3 co-depletion

(145,155). In SH-SY5Y cells, NPC1 depletion led to increased lactate production, a potential sign of mitochondrial dysfunction and reduced mitochondrial pyruvate processing, leading to increased production of lactate for regeneration of nicotinamide adenine dinucleotide (218). However, while lactate secretion was not increased in STARD3-depleted cells, co-depletion of STARD3 did not prevent the increase in lactate production induced by NPC1-depletion. This was in contrast to previous results in CHO cells. The lack of this protective effect might be explained a few ways. Although STARD3 mRNA levels were significantly reduced through RNAi, we were unable to verify the depletion of STARD3 protein, due to technical difficulties with the antibodies. Thus, the lack of this protective effect could have also been caused by insufficient depletion. Furthermore, it could be that the increase in lactate production is either not due to STARD3-mediated cholesterol import to mitochondria in SH-SY5Y cells as seen before in CHO cells, or the mitochondria might import cholesterol through another pathway, so that STARD3 co-depletion would not prevent this phenotype. SH-SY5Y cells are also cancer cells which are known to have increased glycolytic activity (219). SH-SY5Y cells could have already higher mitochondria cholesterol, inducing higher glycolysis levels, further increased by NPC1-depletion but not completely preventable by STARD3-co-depletion. Additionally, STARD3- and NPC1-co-depletion increased cellular proliferation and induced spontaneous formation of neurosphere-like cell clusters. NPC1 was recently shown to impair neuronal self-renewal and differentiation through altered cholesterol homeostasis while high STARD3 expression in breast cancer has been linked to cancer aggressiveness and has become an promising target in cancer therapy (220–222). These observations led to a separate investigation into the role of NPC1 and STARD3 in growth and dedifferentiation of SH-SY5Y cells by colleagues (data not yet published).

5.1.2. Mitochondrial length in NPC1-depleted SH-SY5Y

As STARD3-depletion affected SH-SY5Y proliferation and induced growth in spheroid, unattached clusters, I decided to focus primarily on the effects of NPC1-depletion on mitochondrial health. Mitochondria are dynamic organelles, able to rapidly change size, interconnectedness, and activity. Mitochondrial size, regulated by fission and fusion

events, is associated with metabolic activity, where the presence of longer mitochondria is often a sign of metabolically active cells (172,223). Furthermore, mitochondrial oxidative stress has been shown to induce fragmentation (224). As mentioned previously, studies in the Karten lab have associated NPC1-depletion with an increase in ROS production. To investigate whether NPC1-depletion leads to changes in mitochondrial morphology in SH-SY5Y cells, I employed an algorithm recently developed by Ouellet et al., which is able to separate mitochondrial networks and quantify mitochondrial length and interconnectedness (164). Although the induction of mitochondrial fragmentation through oxidative stress in SH-SY5Y cells was clearly successful, the algorithm did not show significant differences between the treated and untreated cells (**Figure 3.2**). Plotting the size distribution of mitochondria showed a tendency to shorter mitochondria after peroxide treatment, but this difference was not as pronounced as one would expect based on the mitochondrial fluorescence images. SH-SY5Y are a heterogeneous population of cells, containing n-type as well as s-type cells, which can be vastly different in their morphology (168,225). N-type cells appear small and elliptical in cell shape with many neurite-like outgrowths. S-type cells on the other hand are comparably big, round, and flat. Although fragmentation was clearly visible in individual cells, the heterogeneity of SH-SY5Y cells led to a masking of this effect during quantification with the algorithm. Although this could have been mitigated through isolation of cell types, selection would have introduced bias to the results and created SH-SY5Y sub-cell-lines. SH-SY5Y cells depleted of either NPC1, STARD3, or both, did not show significant differences. Although NPC1 depletion resulted in a similar mitochondria length distribution to the fragmented mitochondria in the stress-induced conditions, with a tendency to shorter mitochondrial length compared to control, no significance could be shown. Fragmentation of mitochondria in NPC1-deficient neurons generated from human stem cells has been reported (226).

5.1.3. NPC1 and ER-mitochondria association

A major hub for mitochondrial regulation, including mitochondrial fusion and fission, are the MERC. ER membranes that are part of MERC have relatively higher levels of

cholesterol compared to the rest of the ER, and it was proposed that they also function in cholesterol transport between ER and mitochondria (175,227). For example, truncation of ATAD3 linker domain, which is important for the tethering of membranes in MERCs, decreased steroid formation in steroidogenic cells, due to decreased mitochondrial cholesterol import (228). SH-SY5Y are steroidogenic cells; therefore, import of cholesterol into mitochondria in these cells could alter steroid production (168). Formation of MERC is also dependent on the cholesterol levels of the membranes forming the contact site, shown by increased phospholipid transfer to mitochondria in CHO cells upon depletion of cholesterol at MERC membranes with cyclodextrin (175). Furthermore, MERC cholesterol has recently been the focus of several studies involving mitochondrial DNA (mtDNA) (229,230). In those studies, mtDNA was associated with the cholesterol-rich MERC membranes as well as ATAD3 and this association was important for replication. Given that cholesterol transport from the endosome to the ER affects cholesterol homeostasis at the ER and, by extent, could affect MERC cholesterol content, I investigated effects of NPC1-depletion in SH-SY5Y cells on MERC. For quantification, the well-established transport of PS over MERC to mitochondria for PE synthesis was followed through radiolabelling (**Figure 3.3**). However, over the course of the 5 h experiment, no differences in PE synthesis could be detected between NPC1-depleted cells and control cells, indicating that the cholesterol transport defect in NPC1-depleted cells did not affect the formation of MERC. Although formation of MERC is dependent on membrane cholesterol levels, these membranes are also enriched in cholesterol synthesis proteins (231,232). NPC1-depletion impairs cholesterol transport from the endosome to the ER, which could affect MERC cholesterol content. However, as no adverse effects on PS transport along MERC were measured, it seems likely that cholesterol biosynthesis keeps MERC cholesterol levels steady. Published studies in CHO cells and primary rat neurons, and my own results in SH-SY5Y cells (**Figure 4.2**), have shown that cholesterol biosynthesis is increased, or at least not decreased, in NPC1-deficient cells, due to reduced transport of endocytosed cholesterol to SREBP in the ER (233,234). If newly synthesized cholesterol can be transported across the MERC to mitochondria, the increased cholesterol synthesis in NPC1-deficient cells might also

increase cholesterol transport to the mitochondria, and in turn lead to increased mitochondrial cholesterol, even during STARD3 depletion. Further investigation into mitochondrial cholesterol levels would be needed, however, especially to verify mitochondrial cholesterol levels. The measurement of mitochondrial cholesterol levels in SH-SY5Y was attempted in the Karten lab. However, the amount of mitochondria needed using acute depletion was problematic and the generation of monoclonal, stable SH-SY5Y cell lines would lead to selection of individual morphologies and was therefore avoided.

The ER regulates many functions of the mitochondria through the MERC. One functional analysis of MERC is not sufficient for a full functional assessment of the association of the organelles. Through the course of this thesis, I attempted other readouts, such as ER-mitochondria calcium transport or quantification of proximity of ER and mitochondria through split fluorescent proteins. However, technical difficulties, and the characteristics of the SH-SY5Y cell line limited the application of these approaches and they were, therefore, not further pursued.

5.1.4. Conclusion

In conclusion of this subchapter, this study aimed to elucidate the role of NPC1-depletion on mitochondrial health through cholesterol level regulation at mitochondria and the ER. I found that although NPC1-depletion lead to endosomal cholesterol accumulation and increased lactate secretion, STARD3 co-depletion did not prevent this effect, as seen previously, and caused additional effects on growth and dedifferentiation in SH-SY5Y cells. Mitochondrial length distribution appeared to be normal in NPC1-depleted cells, but limitations of methodology and the heterogeneity of the SH-SY5Y cell population could have masked differences. Furthermore, NPC1-depletion does not seem to affect MERC formation even though cholesterol transport to the ER is disrupted. Further experiments would have to be undertaken to verify these statements through other means, however, due to unexpected effects of STARD3 as well as technical limitations, this line of inquiry was not further pursued. Instead, it was decided to

further investigate mitochondrial cholesterol through an alternative model involving NPC2.

5.2. NPC2 and cholesterol in SH-SY5Y

The transport of endosomal cholesterol to mitochondria by STARD3 requires binding of cholesterol to the lumenal protein NPC2 and delivery to the perimeter membrane (62). In previous work by the Karten lab, it was shown that by employing a NPC2 variant (mutation V81D) that is not able to interact with NPC1 but still able to bind cholesterol, one can direct cholesterol from the endosome to mitochondria and induce increased cholesterol levels. Furthermore, the sterol binding-deficient NPC2 variant (mutation Y119A) or wild-type NPC2 can be used as controls for increased endosomal cholesterol and normal mitochondrial cholesterol, or restored cholesterol transport, respectively. However, endogenous NPC2 must be depleted first. Depletion of either NPC1 or NPC2 is considered to cause the same phenotype, as they act in the same cholesterol "hand-off" pathway to transport cholesterol out of the endosome (43).

5.2.1. Endosome to ER cholesterol transport

NPC1 and NPC2 were depleted from in SH-SY5Y cells by RNAi, a method previously showing robust depletion in CHO cells (62,145). SH-SY5Y cells are a heterogeneous population; therefore, the generation of monoclonal cells would have selected for individual subpopulations, complicating comparison between clones and thereby precluding the use of CRISPR or stable expression of RNAi constructs. Initial experiments to produce stable expression monoclonal cells, I observed high plasticity in their morphology after a few passages as well as loss target mRNA depletion. Therefore, acute expression was chosen over stable expression. SH-SY5Y cells showed strong depletion of NPC1 and NPC2 mRNA levels after transduction, down to 10 % residual NPC2 mRNA (**Figure 4.1**). Furthermore, NPC2 protein levels were not detectable by western blotting after RNAi. However, no cholesterol accumulation by filipin staining could be detected in NPC2-depleted SH-SY5Y cells even after loading the cells with LDL. Compared to control cells, NPC2-depleted cells showed slightly weaker filipin fluorescence, but this was not quantified due to photobleaching and sensitivity

limitations of filipin staining (235). In contrast to NPC2-depleted cell, NPC1 depletion led to the classic cholesterol accumulation in perinuclear endosomes. Fibroblasts are the cells most commonly used to study NPC1 and NPC2 in human cells, for their ease of use and the availability of NPC patient cells. To verify that the miRNA vectors sufficiently deplete NPC2 and cause cholesterol accumulation, the same vectors were used in fibroblasts. While NPC2 mRNA depletion was slightly less severe, fibroblasts consistently showed strong cholesterol accumulation for either NPC1 or NPC2 miRNA vectors. The observations in SH-SY5Y cells were in contrast to the previously reported findings that NPC2-depletion causes the same phenotype as NPC1-depletion. One might argue that miRNA mediated depletion in SH-SY5Y cells is not able to fully eliminate NPC2 protein. However, no residual NPC2 protein could be found and previous studies in mouse models showed strong accumulation of cholesterol even with residual NPC2 expression (236). Therefore, my results suggested that in SH-SY5Y cells, NPC2 has different functions or that NPC2-depletion can somehow be circumvented by an alternate transport pathway.

In NPC disease, cholesterol accumulates in endosomes because of diminished cholesterol transport by mutant NPC1 and NPC2. The impaired cholesterol transport leads to decreased flow of unesterified cholesterol to the ER and reduced esterification by SOAT1 (237). Therefore, cholesterol esterification is commonly used as a read-out for cholesterol transport defects. SH-SY5Y cells depleted of NPC2 exhibited a reduction of cholesterol esterification at the ER, indicating reduced unesterified cholesterol transport from the endosome (**Figure 4.2**). Similarly, NPC1-depletion led to reduced cholesterol esterification. Although not as strongly decreased as in NPC1-depleted cells, cholesterol esterification levels in NPC2-depleted cells were decreased to an extent comparable with results in CHO cells previously published by the Karten lab (62). Reported reductions of cholesterol esterification in NPC2 patient fibroblasts have been variable, from near complete inhibition to 40 % reduction (237,238). However, my data showed that NPC2-depletion clearly induced cholesterol transport defects from endosomes to SOAT1 in the ER. Cholesterol biosynthesis can be affected by impaired cholesterol

transport to the ER, where the SREBP/SCAP complex resides. Reported cholesterol biosynthesis levels during NPC1 deficiency vary from reduced to unchanged rates measured in murine glia cells (239–241). While the reduced levels were measured using extraction of denovo synthesised cholesterol with cyclodextrin, the unchanged rates were reported as a combination of secreted cholesterol and total cellular cholesterol, indicating that a significant pool of cholesterol is secreted during labelling experiments and has to be considered for total synthesis quantification. However, studies in mice have reported an increase in cholesterol synthesis rates in the liver, but decreased rates in the brain for NPC1-deficient tissues, implying different effects of NPC1-depletion in different cell types (242). Furthermore, in the same study, the authors reported similar cholesterol biosynthesis rates in NPC2-deficient cells as the wildtype control cells across most tissues. Similarly, NPC2-deficient fibroblast cholesterol synthesis rates were similar to wildtype, while synthesis in NPC1-deficient cells was decreased (238). These observations indicate that cholesterol synthesis regulation is different in NPC1- and NPC2-deficient cells, although they both show reduced cholesterol esterification levels. I investigated the responses to different levels of exogenous cholesterol in the form of LDL in SH-SY5Y cells and found that cholesterol biosynthesis was increased in NPC1-depleted cells during LP depletion and repletion, as shown in HMGCR levels as well as acetate incorporation, whereas NPC2-depleted cells responded similarly to control cells under both conditions (**Figure 4.2**). The results for NPC2-depleted cells show similar regulation of cholesterol synthesis as in the study by Frolov et al using fibroblasts during starvation, however, NPC1-depletion in SH-SY5Y cells (this thesis) did not lead to a decrease in cholesterol synthesis as reported for fibroblasts but rather an increase (238). Of note there are slight differences in the experimental design between this thesis (feeding with LDL prior to the LPDS treatment) and the study in fibroblasts by Frolov et al (starvation in LPDS only), which could have led to generally lower biosynthesis in SH-SY5Y cells than expected during starvation in control cells, while the NPC1-depleted cells showed higher levels as endosome-ER transport is defective. Indeed, cholesterol synthesis between conditions in control cells are not drastically different as seen previously in CHO cells and fibroblast, indicating either that the pre-treatment of LDL is

enough to keep synthesis low or that synthesis is in general low in SH-SY5Y cells, as reported in neuronal cells (145,238,243). Although cholesterol biosynthesis and esterification are both regulated at the ER, other groups have proposed the hypothesis that different cholesterol pools in the ER regulate cholesterol biosynthesis and esterification at spatially different locations (233,244). These studies also suggested that these two regulatory pools could be supplied by separate transport pathways. Although no concrete evidence for separate regulatory pools has been brought forth, my data is in line with separate regulatory mechanism for synthesis and esterification in NPC2-depleted SH-SY5Y cells. While cholesterol in NPC2-deficient SH-SY5Y cells can reach ER domains containing SREBP/SCAP, transport to SOAT1 domains in the ER is Impaired.

Differences between NPC1- and NPC2-depleted cells were also apparent when cells were given LDL following a starvation period. NPC1-depleted cells showed increased synthesis but normal HMGCR expression, while NPC2-depleted cells were similar to control cells. Cholesterol synthesis in response to LDL were in line with previous results in CHO cells, which showed a lagging response to available LDL-cholesterol in NPC1-depleted cells due to cholesterol sequestration in the endocytic system, delaying the downregulation of cholesterol biosynthesis (145). While HMGCR mRNA levels in cells given LDL were the same in NPC1-depleted and control cells, synthesis was still increased. This disconnect between mRNA and synthesis could indicate that transcriptional activation by SREBP had ceased even in NPC1-depleted cells, but HMGCR protein levels were still high enough to facilitate the increased synthesis. Furthermore, the similar synthesis and HMGCR mRNA levels during fed condition across all cells further emphasizes that even in NPC1-depleted cells, cholesterol can reach the SREBP/SCAP complex regulatory domains of the ER. To investigate this further, a more detailed time course of HMGCR mRNA and protein levels, SREBP processing, and cholesterol synthesis would be required. Although interesting, my focus in this thesis was on NPC2 and, therefore, this was not pursued.

5.2.2. Cholesterol phenotype in SH-SY5Y cells

After establishing that NPC2-depletion does not cause cholesterol accumulation but still produces a cholesterol transport defect to the ER, I investigated cholesterol storage and uptake in more detail to determine how NPC2 depletion affects cholesterol distribution. Total cellular cholesterol levels in NPC disease are dependent on cell type and developmental stage. Whereas Ramirez et al. reported generally increased levels of cholesterol in tissues of NPC1-deficient compared to wildtype mice, NPC2-deficient tissues varied more in their cholesterol content compared to wildtype. While NPC1- and NPC2-deficient mice showed a similar increase in liver cholesterol; spleen, lung, kidney, small intestine showed significantly lower cholesterol levels in NPC2-deficient mice compared to NPC1-deficient mice. However, both NPC1- and NPC2-deficient mice had lower levels of cholesterol in the brain, due to decreased myelination (242). In my work, NPC1-depleted SH-SY5Y cells exhibited higher than normal total cellular cholesterol during LDL loading, whereas NPC2-depleted cells had similar cholesterol levels compared to control (**Figure 4.3**). Although in the brain cholesterol uptake is facilitated by HDL-like particles containing ApoE, the lipoprotein receptors involved in this uptake (LDLR and LRP) can still take up LDL to facilitate increased cholesterol availability (245). Starving the cells of exogenous LDL ameliorated this increase in NPC1-depleted cells but led to a reduction of cellular cholesterol in NPC2-depleted cells, even though either NPC1 or NPC2 depletion led to endosome to ER cholesterol transport deficiency. Although NPC1 and NPC2 are part of the same cholesterol transport pathway, these results show clear differences in cholesterol homeostasis in SH-SY5Y cells upon miRNA-mediated depletion of NPC1 or NPC2. SH-SY5Y cells are cancer cells and LDL cholesterol access increases proliferation in some cancers (181). Theoretically, it would be possible that NPC2-depleted cells counteract cholesterol accumulation through increased proliferation. However, growth assays indicated that NPC2-depletion did not influence cell proliferation. On the other hand, NPC1-depletion did increase growth, potentially indicating that this increased cholesterol pool can be accessed in NPC1-depleted cells. These findings stand in contrast to reports in other cancer cell lines, namely HeLa, SiHa, and C33A cell, where growth was correlated to NPC1 expression (246). However, SH-

SY5Y cells are a steroidogenic cell line, potentially explaining these differences in growth based on steroid production due to increased cholesterol transport to mitochondria (247).

The absence of cholesterol accumulation in NPC2-depleted cells with the concurrence of an endosome to ER cholesterol transport defect raises the question of the fate of LDL-derived cholesterol in SH-SY5Y cells. Previous studies have indicated that cholesterol accumulation might be overcome by endosomal exocytosis (182). Strauss et al. found that NPC1-depleted CHO cells showed increased cholesterol content in exosomes and suggested that exosome release could serve to regulate cholesterol content when endosome to ER transport is defective (182). As SH-SY5Y cells have been shown to release secretory vesicles and exosomes, I speculated that this could serve as a way to prevent cholesterol accumulation in NPC2-depleted cells (248). However, NPC1- and NPC2-depleted SH-SY5Y cells showed decreased cholesterol secretion and reduced activity of lysosomal NAG in the medium (**Figure 4.4**). Although these findings do not indicate a potential circumvention of cholesterol accumulation through secretion, they are in line with decreased levels of cholesterol efflux seen in NPC1-deficient fibroblasts (180). For a more detailed analysis of endosomal exocytosis, measurement of LAMP localization to the PM might be useful in future (249). Centrifugal transport from the perinuclear area to the PM, a process needed for endosomal exocytosis, is defective in NPC1-depleted CHO cells (211). This is in part due to the cholesterol sensing abilities of OPR1L, which facilitates endosome transport to the perinuclear area along the microtubule network during high cholesterol conditions (191,198,91). While endosomal cholesterol levels are low, ORP1L binds to VAP at the ER and tethers the two organelles together, arresting the endosome. During high cholesterol levels and NPC1-depletion, ORP1L-VAP binding is diminished and endosome are transported to the perinuclear area. Although NPC1-depleted SH-SY5Y arrest cholesterol-rich endosomes in the perinuclear region, NPC2-depleted SH-SY5Y did not accumulate cholesterol and could have still shown normal exocytosis. However, NPC2 but not NPC1, has also been implicated in lysosomal reformation in fibroblasts as NPC2-deficiency diminished the

ability to split smaller compartments of the LE/L hybrid organelle (106). Inhibition of lysosome reformation out of the LE/L hybrid organelle could prevent lysosomal exocytosis. Although it is not entirely clear, why cholesterol secretion is reduced in NPC2-depleted cells without cholesterol accumulation, my findings showed that endosomal exocytosis could not circumvent cholesterol accumulation in NPC2-depleted cells.

Alternatively, the absence of cholesterol accumulation could be due to decreased endocytosis of LDL. The DiI-LDL uptake and distribution pattern in NPC1-depleted cells revealed the classic perinuclear clustering of endocytic vesicles similar to filipin staining. NPC2-depleted cells on the other hand, showed a distinct pattern in between control and NPC1-depleted cells, with both, smaller and spread-out vesicles, and larger ones closer to the perinuclear area. Quantification of the internal fluorescence signal showed no difference in total DiI-LDL uptake by NPC1- or NPC2-depleted SH-SY5Y cells (**Figure 4.5**). Although DiI intensity was normalized to cell area, the high variability among individual cells could potentially mask subtle differences. To achieve high LDL uptake for this experiment, cells were deprived of exogenous cholesterol overnight before incubation. Therefore, these results represent LDL uptake following upregulation of LDLR expression, indicating that all cells (NPC1-depleted, NPC2-depleted or control) have equal LDL uptake during LDLR induction. Frolov et al. reported that in human fibroblasts, LDLR activity, measured as DiI-LDL uptake over 1 h, was decreased in NPC1-deficient cells but unchanged in NPC2-deficient cells (238). In that study, NPC1-depleted cells showed a reduction in LDL uptake of ~25% compared to control, a difference that would have been masked in my experiments due to the high variability, further emphasizing the drawbacks of SH-SY5Y heterogeneity. LDLR mRNA levels increased similarly in NPC1- and NPC2-depleted cells upon starvation, and decreased upon refeeding with LDL for 6 h, as one would expect. This starved condition is comparable with the DiI-LDL experiment results, underlining that there is no difference in LDL uptake in NPC2-depleted cells. Interestingly, LDLR expression seemed to be most sensitive to exogenous cholesterol in NPC2-depleted cells, showing the biggest difference between

starved and refed condition. A strong response to starvation and otherwise low levels during fed state could indicate sensitive regulation and low cholesterol buffer, leading to big differences between fed states.

For a comprehensive characterisation of the cholesterol phenotype of SH-SY5Y cells deficient in NPC1 or NPC2, the PM represents a very important pool of cellular cholesterol, containing the highest amount of cholesterol of all organelles. The PM also represents an organelle for excess cholesterol removal mediated by ABC-family proteins (250). Although my work showed that cholesterol secretion is reduced in SH-SY5Y cells, the cholesterol content of the PM and PM-associated vesicles could deliver hints on the fate of cholesterol in NPC2-depleted cells, potentially showing a rerouting of endocytosed cholesterol. Measuring PM cholesterol content has proven challenging, as cholesterol content is not uniform across the membrane and arbitrary measurement of PM regions can introduce bias (251). For this reason, I developed an unbiased workflow for quantification of PM cholesterol, using the expression of the cholesterol sensor D4H developed by Maekawa and Fairn et al. (188). The major advantage of this sensor over filipin is its resilience against photobleaching (depending on fluorophore used). The D4H sensor is also specific for chemically active accessible cholesterol, rather than the sphingomyelin sequestered pool, which can be transported between PM and ER for cholesterol homeostasis regulation (252,253). The D4H sensor should also be less sensitive to the phospholipid surrounding of cholesterol, compared to other probes like the wild type D4-domain (188,252). A recent study showed that D4H binding to the PM is dependent on protein concentration in the surrounding milieu, which could influence cholesterol binding especially in the protein rich cytosol (254). However, the D4H sensor in this study was not used to investigate absolute cholesterol concentration and rather for comparison between cells expressing different RNAi vectors. Furthermore, expression of D4H sensor is still being used for comparative cholesterol measurements (198,255).

Using this approach, no significant change in PM cholesterol was observed in NPC1- or NPC2-depleted SH-SY5Y cells (**Figure 4.7**). However, comparing NPC1- and NPC2-depleted cells, NPC1-depleted cells showed significantly higher PM-associated cholesterol. As the D4H sensor cannot permeate cellular membranes, only cholesterol accessible from the cytosol is stained using expression vectors, indicating increased D4H binding at the inner leaflet of the PM or closely associated to the PM. Early studies of PM cholesterol relied on PM isolation through differential centrifugation and showed no difference for NPC1-deficient fibroblasts, mirroring my results, whereas other studies using an enzymatic approach in CHO cells showed increased accessible PM cholesterol (256,257). The discrepancies among reports in the literature may also stem in part from differences in the culture conditions, in particular whether serum was present in the medium prior to analysis. However, recent studies using the D4H sensor, reported lower PM cholesterol levels in NPC1-deficient fibroblasts, indicated by less PM D4H signal but increased endosomal signal (59). One major drawback of the D4H sensor is its sensitivity to the lipid environment of cholesterol in the membrane, as well a threshold effect inducing co-operative binding of sensor (258). Higher endosomal cholesterol levels could induce endosomal staining more easily than PM, indicating an increase in endosomal cholesterol rather than a change in PM cholesterol. Furthermore, an increase in D4H signal at the PM could also indicate the association of cholesterol-rich vesicles with the PM rather than PM cholesterol itself, as the spatial signal resolution of my images is not able to differentiate between these two possibilities. The punctate D4H signal along the PM in SH-SY5Y could potentially indicate that the increased signal at the PM was a combination of PM and vesicles associated with the PM. However, these results further indicate the differences between NPC1- and NPC2-depletion on the cholesterol phenotype of SH-SY5Y cells. Whereas NPC1-depletion leads to a trend of higher PM cholesterol, NPC2-depletion leads to a tendency to lower PM cholesterol.

5.2.3. Compensatory pathways and difference to fibroblasts

Although the model of cholesterol transport from NPC2 to NPC1 seems to be the most important way for cholesterol to leave the endocytic system, alternative pathways

might exist that can partially compensate for the role of NPC2 and prevent endosomal cholesterol accumulation in the absence of NPC2. Different cholesterol transport proteins that contribute to the cholesterol export from endosomes besides NPC1 have been shown, for example STARD3 or LIMP2 (145,189). Therefore, similar redundant pathways could exist for NPC2, and these could be more important in SH-SY5Y cells compared to other cells. A list of potential candidates that could contribute to cholesterol transport in SH-SY5Y was prepared based on evidence in the literature. Candidates were chosen that could potentially directly take over cholesterol transport or interfere and alter cholesterol mobility through the endocytic system. To screen these targets for a potential role in cholesterol transport as a compensatory pathway, I investigated the effects of depleting these candidates alone or in conjunction with NPC2-depletion on endosomal cholesterol accumulation in SH-SY5Y cells and fibroblasts. Depletion of candidates could have effects on cholesterol distribution outside of lysosomal cholesterol; however, I only judged the candidates to the presence or absence of endosomal filipin staining. Doing so makes the analysis process more straightforward, but other effects on cholesterol transport might be missed. A list of over 20 candidate genes was prepared; however, in this thesis, only the candidates with verified depletion efficiency and sufficient experimental repetition will be discussed, namely ARL8, IGF2R, ORP1L, PSAP, RAB3, and VPS41 (**Table 5**, **Figure 4.9**.). Arl8 and VPS41 are both part of the HOPS complex that mediates LE fusion with lysosomes by facilitating tethering of both organelles. Both are also implicated in lysosomal or secretory vesicle release (192,201). I speculated that LE/L formation or secretory vesicle release could be overactive in SH-SY5Y cells, especially as a neuronal cell line capable of synaptic vesicle release, leading to cholesterol transport out of the cell (248). Similarly, RAB3 was chosen for its involvement in secretory vesicle release, potentially ameliorating cholesterol accumulation (200). However, although strong depletion of mRNA levels was observed in SH-SY5Y cells (**Figure 4.8**), neither candidate was able to induce cholesterol accumulation, with or without NPC2 co-depletion, indicating that secretory vesicle release is not preventing cholesterol accumulation in NPC2-depleted cells. As expected, fibroblasts showed endosomal cholesterol accumulation only when

NPC2 was depleted in addition to ARL8, RAB3 or VPS41. The mannose-6-phosphate receptor IGF2R is the receptor responsible for retention of NPC2 and delivery to the endocytic system. Previous reports showed that depletion of IGF2R led to endosomal cholesterol accumulation, due to NPC2 not reaching the endocytic system (60). In fibroblasts, depletion of IGF2R caused strong accumulation of cholesterol around the perinuclear area. However, SH-SY5Y cells did not show accumulation, indicating that if a compensatory pathway exists in SH-SH5Y cells, they do not rely on glycoprotein transport to the endocytic system over IGF2R, including transport of NPC2. ORP1L is important for endosomal positioning during maturation and also leads to cholesterol accumulation if depleted, by disruption of ER-endosome contact site formation (91,191). As OPR1L has cholesterol-binding and sensing motives, I speculated that altered endosomal perimeter cholesterol during NPC2-depletion might interfere with endosomal maturation, leading to mistrafficking of the endocytic compartment preventing perinuclear accumulation (92). Although depletion of OPR1L alone induced cholesterol accumulation in fibroblasts as expected, no accumulation was seen in SH-SY5Y cells, with or without NPC2 co-depletion. This finding indicates that endocytic transport in SH-SY5Y cells does not rely on ORP1L for maturation of endosomes and transport of cholesterol is not dependent on ORP1L function. The last candidate to be discussed is PSAP, the precursor for saposins, which are small proteins localized to the lysosomal lumen that have been indicated in lipid transport to LIMP2 (189,199). I speculated that saposins, through their similar function and localization, might be able to fill the role of NPC2 to some degree. However, depletion of PSAP did not lead to cholesterol accumulation in either SH-SY5Y cells or fibroblasts, indicating that saposins are not compensating for the absence of NPC2 in SH-SY5Y cells. However, SH-SY5Y cells depleted of PSAP showed consistent decrease in viability. These observations concur with another study that showed neuronal loss in a rare lipid storage disease diagnosed as prosaposin deficiency. The disease was identified to be caused by mutations in PSAP leading to pronounced neurolysosomal storage and insufficient myelination, similar to NPC disease (197). Although SH-SY5Y cells did not show cholesterol accumulation in PSAP-depleted cells, the decreased viability could have masked endosomal cholesterol

accumulation but also indicates that saposins might be vital for these neuroblastoma cells. These observations, together with the implicated role in another lipid storage disease, make PSAP an interesting target for further studies with the potential of filling the role of NPC2 in neuronal cells to some extent. In contrast to SH-SY5Y cells, all NPC2-deficient fibroblasts accumulated cholesterol in endosomes, regardless of co-depletion of other cholesterol transport candidates. These findings further emphasize the apparent difference in SH-SY5Y and fibroblast cholesterol transport and dependency on NPC2.

Through the DiI-LDL and compensatory pathway analysis, it became clear that endocytic trafficking might be involved in the differences seen between SH-SY5Y cells and fibroblast. To characterize this compartment further, I investigated lysosomal proteolysis activity and lysosomal biogenesis regulation. However, lysosomal proteolysis was not quantifiable in SH-SY5Y cells, whereas fibroblasts showed strong proteolytic activity (**Figure 4.11**). Although proteolytic activity has been shown to be reduced in lysosomal storage diseases, the assay failed to produce a measurable signal in any SH-SY5Y cells, regardless of NPC1 or NPC2 expression (259). Furthermore, analysis of the phosphorylation status of TFEB revealed that SH-SH5Y show a lower ratio of phosphorylated TFEB to total TFEB, indicating more active lysosomal biogenesis compared to fibroblasts (63,260). These apparent differences between SH-SY5Y led to a separate investigation into the expression profiles between the two cell lines, undertaken by colleagues in the lab. Data analysis of published fibroblast and SH-SY5Y RNAseq data revealed a generally lower activity of cholesterol homeostatic and endocytic system gene expression in SH-SY5Y cells. These differences could indicate a lower reliance on these pathways and potentially point to the existence of alternative pathways being used. Although it is unclear which pathway that could be, this comparison indicates that different gene expression levels between the cell lines could contribute to the differences observed after interference in cholesterol homeostasis and endocytic system.

Throughout this thesis research, it became abundantly clear that although NPC1 and NPC2 act in the same pathway and are responsible for NPC disease, NPC2 must have a separate role besides endosomal cholesterol "hand-off" to NPC1. While some effects caused by depletion of NPC1 or NPC2 are similar, for example the reduced sterol transport to the ER and deficient endosomal exocytosis, the effects on cholesterol homeostasis appear to be drastically different as seen in the lack of endosomal cholesterol accumulation, and reduced overall and PM cholesterol levels in NPC2- compared to NPC1-depleted cells. To further investigate these differences and potentially link them to a specific pathway, transcriptomics analysis of NPC1- and NPC2-depleted SH-SY5Y was performed. Performing pathway analysis of differentially expressed genes revealed no single significantly altered pathway. However, some variance between mRNA samples might have reduced the number of differentially expressed genes. Interestingly, despite the close functional relationship of the two proteins, only 35 hits could be identified through the microarray to be differentially expressed in both. Furthermore, of those 35 hits, only 19 were annotated targets. These results, although not providing further insight on why NPC2-depleted SH-SY5Y cells did not accumulate cholesterol, further emphasized the different outcomes of NPC1- and NPC2-depletion in SH-SY5Y cells.

Although many studies on NPC disease were done in fibroblasts, neurons are the most affected cell type, leading to loss of Purkinje neurons or synaptic dysfunction (234). For this reason, the neuroblastoma cell line SH-SY5Y was chosen. To further investigate the effects of NPC1- and NPC2-depletion on cholesterol transport in neuronal cells, I used rat primary neurons and the neuroblastoma cell line IMR32. Both cells types did not accumulate cholesterol after depletion of NPC2, indicating a general pattern where NPC2-depletion in neuronal cells does not induce cholesterol accumulation. Although studies of NPC2-deficient neurons are rare, NPC2 hypomorph mice did show neuronal cholesterol accumulation at 7 weeks (236). This accumulation was found within the neocortex, dentate gyrus, hippocampus, and cerebellum of mouse brain, which also showed loss of Purkinje neurons in the cerebellum. The absence of cholesterol

accumulation after miRNA induced depletion of NPC2 in neuronal cells in this study could potentially indicate some off-target effects of the RNAi. However, the lack of cholesterol accumulation was seen with two different sequences targeting human NPC2 as well as RNAi targeting rat NPC2 in the primary rat neurons, making off-target effects unlikely. To exclude the possibility that the minimal amounts of protein remaining is enough to retain cholesterol transport, CRISPR based knock down of NPC2 in primary neurons could help exclude this possibility (261). Moreover, in contrast to acute depletion by RNAi, germline knock down can affect the neurons even during development, prolonging the effects of NPC2 knock down.

5.3. NPC2 plays a role in the endocytic system

In neurons, cholesterol synthesis is low and cholesterol homeostasis depends in part on cholesterol import from glia through lipoproteins (108). This import is facilitated by the endocytic system, which takes up cholesterol in form of ApoE-containing lipoprotein particles (HDL-like particles) via LDLR and LRP and transports it to the perinuclear area where it is then mobilised for the rest of the cell by NPC1 and NPC2 (262). However, through the course of this study I showed that although NPC1-depletion leads to sequestration of cholesterol in the endocytic system due to defective mobilisation of cholesterol, NPC2-depletion did not have the same effect while still showing endosome to ER cholesterol transport deficiency. During further investigation of this phenotype, especially during DiI-LDL uptake experiments and filipin staining, I noticed alterations to endocytic particle density. In this part of my thesis, I will discuss the effects of NPC2-depletion on the endocytic system and the further implications for the role of NPC2 in it.

5.3.1. NPC2 depletion reduces endocytic vesicle density

In NPC1-deficient cells, LE- lysosomal fusion, endosomal exocytosis, and retromer function are impaired (184,185,106). Although most of these defects have been associated with the increased cholesterol accumulation, NPC2 has independently been associated to be important for lysosomal reformation through separation of the LE/L hybrid compartment (106). The findings described in this thesis of a lack of cholesterol accumulation, decreased cholesterol levels compared to NPC1-depleted cells, and

decreased cholesterol secretion could point to alterations in the endocytic systems caused by depletion of NPC2. Furthermore, DiI-LDL incubation experiments suggested a different endocytic vesicle distribution. Therefore, I investigated the effects of NPC1- and NPC2-depletion in SH-SY5Y cells on the endocytic system through an unbiased workflow to quantify density, size, and average distance to the nucleus of various endocytic vesicles, based on immunofluorescence staining with antibodies against markers for EE, LE/L, and proteins associated with lysosomal exocytosis and anterograde transport. NPC1-depleted cells showed a significant increase in the size of vesicles positive for LAMP1, LAMP2 and CD63, while Rab5-positive vesicles were unchanged (**Figure 4.16**). On the other hand, NPC2-depleted cells showed normal size of endocytic vesicles but their overall density was reduced compared to control cells and NPC1-depleted cells. LAMP1 and LAMP2 are glycoproteins that localize to the LE and lysosomal perimeter membrane. The increased size of these compartments is in line with the accumulation of cholesterol and inhibition of cargo proteolysis in LE/L that is classical for NPC1-depletion (263,264). CD63 is commonly used as a marker for exosomes and plays a role in lysosome to PM transport (265,266). The increased size of CD63-positive compartments further emphasizes the deficient anterograde transport and arrest at the perinuclear area in NPC1-depleted cells.

The absence of any LE or lysosomal vesicles size increase in NPC2-depleted cells suggest no cargo accumulation, although cholesterol transport to the ER is reduced. The reduction in vesicle density seen in NPC2-depleted SHSY5Y cells indicates a role for NPC2 in regulating the endocytic system. However, unchanged mRNA and protein levels of endocytic system markers indicate a role outside of transcriptional regulation (**Figure 4.19**). In-vitro studies in liposomes showed that NPC2 increases liposome fusion, a process important during EE processing (267,268). Together with the observation that NPC2 is also critical for lysosomal reformation, a role in endosomal compartment regulation seems likely (106). Furthermore, as NPC2-depleted cells show reduced numbers already in the EE, changes to the endosome maturation process and cholesterol transport through this compartment could change cholesterol availability for

the whole cell. Phosphorylation of TFEB seems to be lower in SH-SY5Y cells compared to fibroblasts, with most TFEB being in the unphosphorylated transcriptional active state (63). High TFEB activation even during fed states could indicate low ability to further activate transcription to regulate endosome homeostasis during starvation. If NPC2-depletion negatively influences endocytic vesicle density, this could be masked in a more regulatory active cell line like fibroblasts by just increasing endosomal biogenesis. Repeating these experiments in fibroblast measuring TFEB activation could shine a light on these speculations. The EE is also the main compartment regulating endocytosed cargo sorting and receptor recycling (70). Reduction in EE density caused by NPC2-depletion could affect LDL sorting and LDLR recycling as well. Although no differences in LDL uptake were measured, misguided LDL and LDLR sorting could lead to fast recycling out of the cell and retro-endocytosis. Although speculative, LDL uptake would stay the same, but overall available cholesterol would be reduced, a phenotype seen here in NPC2-depleted SH-SY5Y cells. To investigate this hypothesis, interference with the recycling machinery by depletion of Rab4 or Rab11 could reveal valuable insight. If NPC2-depletion leads to fast retro-exocytosis of internalized LDL particles, blocking the recycling compartment could lead to cholesterol accumulation. A very important factor for the release of LDL particles from LDLR is the acidification of the endosomal medium, and dysfunctional acidification could cause loss of the LDL particle along the recycling pathway (269). Investigating the endocytic system maturation process in the context of endosomal acidification could deliver valuably insight into this potential retro-endocytosis step.

Although the arrest of LE/L vesicles around the perinuclear area in NPC1-depleted cells can be clearly seen in these experiments, quantification of average distance of vesicles to the nucleus center failed to represent this observation (**Figure 4.18**). This could be in part due to the increased size of NPC1-depleted LE/L, which still cluster around the nucleus but would distribute them over a larger area as they physically need more space. SH-SY5Y heterogeneity could also influence this read-out. A potential way to overcome the cell variability might be to normalize the distance measurements to the

size of the cell. However, due to the spread-out and elliptical morphology of SH-SY5Y cells, the average area might be misleading compared to the actual length of the cell in one axis.

5.3.2. NPC2 variants protect endosomal vesicle number

To investigate if the potential regulatory effect of NPC2 on the endocytic system is dependent on a known functional domain, I employed NPC2 variants, which were expressed in addition to the miRNA-mediated depletion of endogenous NPC2. Wildtype NPC2 and NPC2 variants that are either unable to bind cholesterol (Y119A), or unable to bind to NPC1 (V81D), showed correct localization to the endocytic system, while the glycosylation mutant (N58A) was not retained in the cell, as expected (**Figure 4.22**) (60). The repetition of the endocytic vesicle analysis for LAMP2 and CD63 showed that wild type NPC2 and all variants were able to prevent the reduction of LAMP2- and CD63-positive vesicles caused by NPC2 depletion (**Figure 4.23**). Furthermore, expression of all variants led to an increase in proliferation rates of the cells (**Figure 4.24**). The fact that the sterol binding- and NPC1 binding-deficient mutant showed the same protective effect against the reduction of CD63 and LAMP2 positive vesicles indicates that the canonical function NPC2 in the cholesterol “hand-off” with NPC1 is not needed for the endocytic system regulation. This could mean that NPC2 is able to interact with the endocytic system through a completely unknown site. Recently, the lab of Judith Storch discovered another binding site in the form of a hydrophobic node at the position 75 to 83 which allows for direct interaction with LBPA (58). Although LBPA itself is more associated with multivesicular LE and therefore NPC2 binding to LBPA is probably not responsible for the changes in the EE, this hydrophobic node could also facilitate interaction with other partners (270). Furthermore, the fact that the glycosylation variant was also able prevent the reduction of endocytic vesicles shows that the regulation of this compartment is independent of interaction with the retaining receptor IGF2R. This means that NPC2 is either regulating and protecting the endocytic system as it travels through the secretory system or that bulk phase endocytic uptake of NPC2 after secretion, without specific retention through IFG2R, is sufficient. It has been shown

previously that NPC2 uptake can rescue NPC2-depletion induced cholesterol accumulation, therefore, secreted NPC2 could probably do the same for the endocytic system (58,271). Although these results show that NPC2 can regulate the endocytic system independent of its ability to bind cholesterol or NPC1, how it would interact or influence the endocytic system without these functions is still unclear. NPC2 proximity-biotinylation could provide valuable insight into this regulation, potentially revealing unknown binding partners that could affect endocytic system homeostasis. Interactome analysis could also provide clues on how NPC2 variant expression can increase cell proliferation. NPC2 overexpression in glioblastoma cells was previously shown to inhibit proliferation and migration (272). On the same line, depletion of NPC2 in HSC-T6 and LX2 cells caused increased cell proliferation based on BrdU incorporation (273). Although NPC2 depletion did not alter proliferation in SH-SY5Y cells, overexpression in addition to depletion of endogenous NPC2 did increase proliferation, in contrast to previous studies (272). Speculatively, depletion of endogenous NPC2 would probably affect abundance of intronic sequences and miRNA, which could alter cellular proliferation and explain these differences, as NPC2 is know to have intronic miRNA expression (274).

5.4. Overall conclusion and future perspectives

NPC1 and NPC2 are two very important proteins, facilitating the egress of cholesterol from the LE/L to the rest of the cell. Although NPC1 has received most of the attention during NPC research, NPC2 is equally important in this process. NPC2 is also involved in cholesterol transport independent of NPC1, namely in cholesterol transport to the mitochondria over STARD3.

In this study, I have shown that although NPC1-depletion leads to the classic cholesterol accumulation in the neuroblastoma cell line SH-SY5Y as well as increased lactate production, this could not be prevented through STARD3-co-depletion as seen before. Furthermore, it was shown that NPC1-depletion does not affect mitochondria morphology or mitochondrial to ER contact site formation. Work in this thesis revealed that although NPC2-depletion induced cholesterol accumulation in fibroblasts, this was

not true for SH-SY5Y cells, despite inducing a cholesterol transport defect. Furthermore, I showed that depletion of NPC2, but not NPC1 lowered cellular cholesterol levels. My work also revealed a role for NPC2 in endocytic system regulation outside the late endosomal cholesterol transport, inducing reduction of endocytic vesicles upon depletion. Furthermore, this reduction phenotype is preventable by expression of NPC2 variants, even if domains required for known functions are dysfunctional.

Although this work delivers a basis for further investigation into NPC2 and its differences to previously published work, it did not reveal a mechanistic explanation on how these alterations could be caused. Therefore, more research is needed, potentially by investigating the endocytic recycling complex further, to reveal whether NPC2 can affect this process. Furthermore, interactome analysis of NPC2 could reveal valuable insight into potential partners that could facilitate these changes. Lastly, expansion of the compensatory pathway analysis to investigate potential candidates for altered cholesterol transport could reveal not yet identified alternate pathways. Lots of questions still need to be answered to comprehensively reveal the role of NPC2. However, to conclude this thesis in one sentence: NPC2 is not merely a cholesterol delivery tool for NPC1.

6. BIBLIOGRAPHY

1. Yang ST, Kreutzberger AJB, Lee J, Kiessling V, Tamm LK. The Role of Cholesterol in Membrane Fusion. Chem Phys Lipids. 2016 Sep;199:136–43.

2. Horvath SE, Daum G. Lipids of mitochondria. Prog Lipid Res. 2013 Oct;52(4):590–614.

3. Chen Z, Rand RP. The influence of cholesterol on phospholipid membrane curvature and bending elasticity. Biophys J. 1997 Jul;73(1):267–76.

4. Mukherjee S, Maxfield FR. Membrane domains. Annu Rev Cell Dev Biol. 2004;20:839–66.

5. Simons K, Vaz WLC. Model systems, lipid rafts, and cell membranes. Annu Rev Biophys Biomol Struct. 2004;33:269–95.

6. Radhakrishnan A, Rohatgi R, Siebold C. Cholesterol access in cellular membranes controls Hedgehog signaling. Nat Chem Biol. 2020 Dec;16(12):1303–13.

7. Rone MB, Fan J, Papadopoulos V. Cholesterol transport in steroid biosynthesis: Role of protein-protein interactions and implications in disease states. Biochim Biophys Acta. 2009 Jul;1791(7):646–58.

8. Holst JP, Soldin OP, Guo T, Soldin SJ. Steroid hormones: relevance and measurement in the clinical laboratory. Clin Lab Med. 2004 Mar;24(1):105–18.

9. Staels B, Fonseca VA. Bile Acids and Metabolic Regulation. Diabetes Care. 2009 Nov;32(Suppl 2):S237–45.

10. Luo J, Yang H, Song BL. Mechanisms and regulation of cholesterol homeostasis. Nat Rev Mol Cell Biol. 2020 Apr;21(4):225–45.

11. Sitaula S, Burris TP. Cholesterol and Other Steroids. In: Bradshaw RA, Stahl PD, editors. Encyclopedia of Cell Biology [Internet]. Waltham: Academic Press; 2016 [cited

2022 Feb 9]. p. 173–9. Available from: https://www.sciencedirect.com/science/article/pii/B9780123944474100215

12. Burg JS, Espenshade PJ. Regulation of HMG-CoA reductase in mammals and yeast. Prog Lipid Res. 2011 Oct;50(4):403–10.

13. Yang T, Espenshade PJ, Wright ME, Yabe D, Gong Y, Aebersold R, et al. Crucial step in cholesterol homeostasis: sterols promote binding of SCAP to INSIG-1, a membrane protein that facilitates retention of SREBPs in ER. Cell. 2002 Aug 23;110(4):489–500.

14. Eberlé D, Hegarty B, Bossard P, Ferré P, Foufelle F. SREBP transcription factors: master regulators of lipid homeostasis. Biochimie. 2004 Nov;86(11):839–48.

15. Dorotea D, Koya D, Ha H. Recent Insights Into SREBP as a Direct Mediator of Kidney Fibrosis via Lipid-Independent Pathways. Front Pharmacol. 2020 Mar 17;11:265.

16. DeBose-Boyd RA. Feedback regulation of cholesterol synthesis: sterol-accelerated ubiquitination and degradation of HMG CoA reductase. Cell Res. 2008 Jun;18(6):609–21.

17. Goldstein JL, Brown MS. History of Discovery: The LDL Receptor. Arterioscler Thromb Vasc Biol. 2009 Apr;29(4):431–8.

18. Rudenko G, Henry L, Henderson K, Ichtchenko K, Brown MS, Goldstein JL, et al. Structure of the LDL Receptor Extracellular Domain at Endosomal pH. Science. 2002 Dec 20;298(5602):2353–8.

19. Vos D, Kuivenhoven JA, van de Sluis B. Recycling the LDL receptor to combat atherosclerosis. Aging (Albany NY). 2018 Nov 27;10(12):3638–40.

20. Kwon HJ, Abi-Mosleh L, Wang ML, Deisenhofer J, Goldstein JL, Brown MS, et al. Structure of N-terminal domain of NPC1 reveals distinct subdomains for binding and transfer of cholesterol. Cell. 2009 Jun 26;137(7):1213–24.

21. Zerenturk EJ, Sharpe LJ, Brown AJ. Sterols regulate 3β-hydroxysterol Δ24-reductase (DHCR24) via dual sterol regulatory elements: Cooperative induction of key enzymes in lipid synthesis by Sterol Regulatory Element Binding Proteins. Biochimica et Biophysica Acta (BBA) - Molecular and Cell Biology of Lipids. 2012 Oct 1;1821(10):1350–60.

22. Prabhu AV, Sharpe LJ, Brown AJ. The sterol-based transcriptional control of human 7-dehydrocholesterol reductase (DHCR7): Evidence of a cooperative regulatory program in cholesterol synthesis. Biochim Biophys Acta. 2014 Oct;1842(10):1431–9.

23. Brown AJ, Sharpe LJ. Chapter 11 - Cholesterol Synthesis. In: Ridgway ND, McLeod RS, editors. Biochemistry of Lipids, Lipoproteins and Membranes (Sixth Edition) [Internet]. Boston: Elsevier; 2016 [cited 2022 Feb 9]. p. 327–58. Available from: https://www.sciencedirect.com/science/article/pii/B9780444634382000110

24. Tabas I. Free Cholesterol-Induced Cytotoxicity: A Possible Contributing Factor to Macrophage Foam Cell Necrosis in Advanced Atherosclerotic Lesions. Trends in Cardiovascular Medicine. 1997 Oct 1;7(7):256–63.

25. Tabas I. Consequences of cellular cholesterol accumulation: basic concepts and physiological implications. J Clin Invest. 2002 Oct 1;110(7):905–11.

26. Goldstein JL, Dana SE, Brown MS. Esterification of Low Density Lipoprotein Cholesterol in Human Fibroblasts and Its Absence in Homozygous Familial Hypercholesterolemia. Proc Natl Acad Sci U S A. 1974 Nov;71(11):4288–92.

27. Chang TY, Chang CC, Cheng D. Acyl-coenzyme A:cholesterol acyltransferase. Annu Rev Biochem. 1997;66:613–38.

28. Maxfield FR, Tabas I. Role of cholesterol and lipid organization in disease. Nature. 2005 Dec;438(7068):612–21.

29. Cohen DE. Hepatocellular transport and secretion of biliary lipids. Curr Opin Lipidol. 1999 Aug;10(4):295–302.

30. Oram JF, Vaughan AM. ATP-Binding Cassette Cholesterol Transporters and Cardiovascular Disease. Circulation Research. 2006 Nov 10;99(10):1031–43.

31. ATP-binding cassette transporter A1: a cell cholesterol exporter that protects against cardiovascular disease - PubMed [Internet]. [cited 2022 Feb 9]. Available from: https://pubmed.ncbi.nlm.nih.gov/16183915/

32. Vanier MT, Millat G. Niemann-Pick disease type C. Clin Genet. 2003 Oct;64(4):269–81.

33. Crocker AC. The Cerebral Defect in Tay-Sachs Disease and Niemann-Pick Disease*. Journal of Neurochemistry. 1961;7(1):69–80.

34. Greer WL, Riddell DC, Gillan TL, Girouard GS, Sparrow SM, Byers DM, et al. The Nova Scotia (type D) form of Niemann-Pick disease is caused by a G3097-->T transversion in NPC1. Am J Hum Genet. 1998 Jul;63(1):52–4.

35. von Ranke FM, Pereira Freitas HM, Mançano AD, Rodrigues RS, Hochhegger B, Escuissato D, et al. Pulmonary Involvement in Niemann–Pick Disease: A State-of-the-Art Review. Lung. 2016 Aug 1;194(4):511–8.

36. Bi X, Liao G. Cholesterol in Niemann–Pick Type C disease. Subcell Biochem. 2010;51:319–35.

37. Higashi Y, Murayama S, Pentchev PG, Suzuki K. Cerebellar degeneration in the Niemann-Pick type C mouse. Acta Neuropathol. 1993;85(2):175–84.

38. Xie C, Burns DK, Turley SD, Dietschy JM. Cholesterol is sequestered in the brains of mice with Niemann-Pick type C disease but turnover is increased. J Neuropathol Exp Neurol. 2000 Dec;59(12):1106–17.

39. Imrie J, Dasgupta S, Besley GTN, Harris C, Heptinstall L, Knight S, et al. The natural history of Niemann-Pick disease type C in the UK. J Inherit Metab Dis. 2007 Feb;30(1):51–9.

40. Vanier MT, Latour P. Laboratory diagnosis of Niemann-Pick disease type C: the filipin staining test. Methods Cell Biol. 2015;126:357–75.

41. Carstea ED, Morris JA, Coleman KG, Loftus SK, Zhang D, Cummings C, et al. Niemann-Pick C1 disease gene: homology to mediators of cholesterol homeostasis. Science. 1997 Jul 11;277(5323):228–31.

42. Naureckiene S, Sleat DE, Lackland H, Fensom A, Vanier MT, Wattiaux R, et al. Identification of HE1 as the second gene of Niemann-Pick C disease. Science. 2000 Dec 22;290(5500):2298–301.

43. Vanier MT, Duthel S, Rodriguez-Lafrasse C, Pentchev P, Carstea ED. Genetic heterogeneity in Niemann-Pick C disease: a study using somatic cell hybridization and linkage analysis. Am J Hum Genet. 1996 Jan;58(1):118–25.

44. Pentchev PG. Niemann-Pick C research from mouse to gene. Biochim Biophys Acta. 2004 Oct 11;1685(1–3):3–7.

45. Davies JP, Ioannou YA. Topological Analysis of Niemann-Pick C1 Protein Reveals That the Membrane Orientation of the Putative Sterol-sensing Domain Is Identical to Those of 3-Hydroxy-3-methylglutaryl-CoA Reductase and Sterol Regulatory Element Binding Protein Cleavage-activating Protein*. Journal of Biological Chemistry. 2000 Aug 11;275(32):24367–74.

46. Radhakrishnan A, Sun LP, Kwon HJ, Brown MS, Goldstein JL. Direct binding of cholesterol to the purified membrane region of SCAP: mechanism for a sterol-sensing domain. Mol Cell. 2004 Jul 23;15(2):259–68.

47. Li X, Wang J, Coutavas E, Shi H, Hao Q, Blobel G. Structure of human Niemann–Pick C1 protein. PNAS. 2016 Jul 19;113(29):8212–7.

48. Watari H, Blanchette-Mackie EJ, Dwyer NK, Glick JM, Patel S, Neufeld EB, et al. Niemann-Pick C1 protein: Obligatory roles for N-terminal domains and lysosomal targeting in cholesterol mobilization. Proc Natl Acad Sci U S A. 1999 Feb 2;96(3):805–10.

49. Pfeffer SR. NPC intracellular cholesterol transporter 1 (NPC1)-mediated cholesterol export from lysosomes. J Biol Chem. 2019 Feb 1;294(5):1706–9.

50. Li X, Lu F, Trinh MN, Schmiege P, Seemann J, Wang J, et al. 3.3 Å structure of Niemann-Pick C1 protein reveals insights into the function of the C-terminal luminal domain in cholesterol transport. Proc Natl Acad Sci U S A. 2017 Aug 22;114(34):9116–21.

51. Li X, Saha P, Li J, Blobel G, Pfeffer SR. Clues to the mechanism of cholesterol transfer from the structure of NPC1 middle lumenal domain bound to NPC2. PNAS. 2016 Sep 6;113(36):10079–84.

52. Carette JE, Raaben M, Wong AC, Herbert AS, Obernosterer G, Mulherkar N, et al. Ebola virus entry requires the cholesterol transporter Niemann-Pick C1. Nature. 2011 Aug 24;477(7364):340–3.

53. García-Dorival I, Cuesta-Geijo MÁ, Barrado-Gil L, Galindo I, Garaigorta U, Urquiza J, et al. Identification of Niemann-Pick C1 protein as a potential novel SARS-CoV-2 intracellular target. Antiviral Res. 2021 Oct;194:105167.

54. Vial C, Calderón JF, Klein AD. NPC1 as a Modulator of Disease Severity and Viral Entry of SARSCoV- 2. Curr Mol Med. 2021;21(1):2–4.

55. Xu S, Benoff B, Liou HL, Lobel P, Stock AM. STRUCTURAL BASIS OF STEROL BINDING BY NPC2, A LYSOSOMAL PROTEIN DEFICIENT IN NIEMANN-PICK TYPE C2 DISEASE. J Biol Chem. 2007 Aug 10;282(32):23525–31.

56. Infante RE, Wang ML, Radhakrishnan A, Kwon HJ, Brown MS, Goldstein JL. NPC2 facilitates bidirectional transfer of cholesterol between NPC1 and lipid bilayers, a step in cholesterol egress from lysosomes. PNAS. 2008 Oct 7;105(40):15287–92.

57. Cheruku SR, Xu Z, Dutia R, Lobel P, Storch J. Mechanism of cholesterol transfer from the Niemann-Pick type C2 protein to model membranes supports a role in lysosomal cholesterol transport. J Biol Chem. 2006 Oct 20;281(42):31594–604.

58. McCauliff LA, Langan A, Li R, Ilnytska O, Bose D, Waghalter M, et al. Intracellular cholesterol trafficking is dependent upon NPC2 interaction with lysobisphosphatidic acid. Elife. 2019 03;8.

59. Ilnytska O, Lai K, Gorshkov K, Schultz ML, Tran BN, Jeziorek M, et al. Enrichment of NPC1-deficient cells with the lipid LBPA stimulates autophagy, improves lysosomal function, and reduces cholesterol storage. Journal of Biological Chemistry. 2021 Jul 1;297(1):100813.

60. Willenborg M, Schmidt CK, Braun P, Landgrebe J, Figura K von, Saftig P, et al. Mannose 6-phosphate receptors, Niemann-Pick C2 protein, and lysosomal cholesterol accumulation. J Lipid Res. 2005 Jan 12;46(12):2559–69.

61. Li J, Pfeffer SR. Lysosomal membrane glycoproteins bind cholesterol and contribute to lysosomal cholesterol export. Burd CG, editor. eLife. 2016 Sep 24;5:e21635.

62. Kennedy BE, Charman M, Karten B. Niemann-Pick Type C2 protein contributes to the transport of endosomal cholesterol to mitochondria without interacting with NPC1. J Lipid Res. 2012 Dec;53(12):2632–42.

63. Napolitano G, Ballabio A. TFEB at a glance. J Cell Sci. 2016 Jul 1;129(13):2475–81.

64. Prichard KL, O'Brien NS, Murcia SR, Baker JR, McCluskey A. Role of Clathrin and Dynamin in Clathrin Mediated Endocytosis/Synaptic Vesicle Recycling and Implications in Neurological Diseases. Front Cell Neurosci. 2022 Jan 18;15:754110.

65. Ehrlich M, Boll W, Oijen A van, Hariharan R, Chandran K, Nibert ML, et al. Endocytosis by Random Initiation and Stabilization of Clathrin-Coated Pits. Cell. 2004 Sep 3;118(5):591–605.

66. Kaksonen M, Roux A. Mechanisms of clathrin-mediated endocytosis. Nat Rev Mol Cell Biol. 2018 May;19(5):313–26.

67. Traer CJ, Rutherford AC, Palmer KJ, Wassmer T, Oakley J, Attar N, et al. SNX4 coordinates endosomal sorting of TfnR with dynein-mediated transport into the endocytic recycling compartment. Nat Cell Biol. 2007 Dec;9(12):1370–80.

68. Naslavsky N, Caplan S. The enigmatic endosome – sorting the ins and outs of endocytic trafficking. Journal of Cell Science. 2018 Jul 6;131(13):jcs216499.

69. Jovic M, Sharma M, Rahajeng J, Caplan S. The early endosome: a busy sorting station for proteins at the crossroads. Histol Histopathol. 2010 Jan;25(1):99–112.

70. Maxfield FR, McGraw TE. Endocytic recycling. Nat Rev Mol Cell Biol. 2004 Feb;5(2):121–32.

71. Mayor S, Presley JF, Maxfield FR. Sorting of membrane components from endosomes and subsequent recycling to the cell surface occurs by a bulk flow process. J Cell Biol. 1993 Jun;121(6):1257–69.

72. Huotari J, Helenius A. Endosome maturation. EMBO J. 2011 Aug 31;30(17):3481–500.

73. Rink J, Ghigo E, Kalaidzidis Y, Zerial M. Rab conversion as a mechanism of progression from early to late endosomes. Cell. 2005 Sep 9;122(5):735–49.

74. Horiuchi H, Lippé R, McBride HM, Rubino M, Woodman P, Stenmark H, et al. A novel Rab5 GDP/GTP exchange factor complexed to Rabaptin-5 links nucleotide exchange to effector recruitment and function. Cell. 1997 Sep 19;90(6):1149–59.

75. Del Conte-Zerial P, Brusch L, Rink JC, Collinet C, Kalaidzidis Y, Zerial M, et al. Membrane identity and GTPase cascades regulated by toggle and cut-out switches. Mol Syst Biol. 2008;4:206.

76. Langemeyer L, Borchers AC, Herrmann E, Füllbrunn N, Han Y, Perz A, et al. A conserved and regulated mechanism drives endosomal Rab transition. Pfeffer SR, Zerial M, editors. eLife. 2020 May 11;9:e56090.

77. Solinger JA, Spang A. Tethering complexes in the endocytic pathway: CORVET and HOPS. The FEBS Journal. 2013;280(12):2743–57.

78. Möbius W, van Donselaar E, Ohno-Iwashita Y, Shimada Y, Heijnen HFG, Slot JW, et al. Recycling compartments and the internal vesicles of multivesicular bodies harbor most of the cholesterol found in the endocytic pathway. Traffic. 2003 Apr;4(4):222–31.

79. Karten B, Peake KB, Vance JE. Mechanisms and consequences of impaired lipid trafficking in Niemann–Pick type C1-deficient mammalian cells. Biochimica et Biophysica Acta (BBA) - Molecular and Cell Biology of Lipids. 2009 Jul 1;1791(7):659–70.

80. Schmidt O, Teis D. The ESCRT machinery. Curr Biol. 2012 Feb 21;22(4):R116–20.

81. Adell MAY, Migliano SM, Upadhyayula S, Bykov YS, Sprenger S, Pakdel M, et al. Recruitment dynamics of ESCRT-III and Vps4 to endosomes and implications for reverse membrane budding. Burd CG, editor. eLife. 2017 Oct 11;6:e31652.

82. Maxfield FR, Yamashiro DJ. Endosome acidification and the pathways of receptor-mediated endocytosis. Adv Exp Med Biol. 1987;225:189–98.

83. Kundra R, Kornfeld S. Asparagine-linked Oligosaccharides Protect Lamp-1 and Lamp-2 from Intracellular Proteolysis. Journal of Biological Chemistry. 1999 Oct;274(43):31039–46.

84. Marshansky V, Futai M. The V-type H+-ATPase in vesicular trafficking: targeting, regulation and function. Curr Opin Cell Biol. 2008 Aug;20(4):415–26.

85. Costa GA, de Souza SB, da Silva Teixeira LR, Okorokov LA, Arnholdt ACV, Okorokova-Façanha AL, et al. Tumor cell cholesterol depletion and V-ATPase inhibition as an inhibitory mechanism to prevent cell migration and invasiveness in melanoma. Biochimica et Biophysica Acta (BBA) - General Subjects. 2018 Mar 1;1862(3):684–91.

86. Granger E, McNee G, Allan V, Woodman P. The role of the cytoskeleton and molecular motors in endosomal dynamics. Semin Cell Dev Biol. 2014 Jul;31(100):20–9.

87. Collinet C, Stöter M, Bradshaw CR, Samusik N, Rink JC, Kenski D, et al. Systems survey of endocytosis by multiparametric image analysis. Nature. 2010 Mar 11;464(7286):243–9.

88. Driskell OJ, Mironov A, Allan VJ, Woodman PG. Dynein is required for receptor sorting and the morphogenesis of early endosomes. Nat Cell Biol. 2007 Jan;9(1):113–20.

89. Bananis E, Murray JW, Stockert RJ, Satir P, Wolkoff AW. Microtubule and motor-dependent endocytic vesicle sorting in vitro. J Cell Biol. 2000 Oct 2;151(1):179–86.

90. Jordens I, Fernandez-Borja M, Marsman M, Dusseljee S, Janssen L, Calafat J, et al. The Rab7 effector protein RILP controls lysosomal transport by inducing the recruitment of dynein-dynactin motors. Curr Biol. 2001 Oct 30;11(21):1680–5.

91. Rocha N, Kuijl C, van der Kant R, Janssen L, Houben D, Janssen H, et al. Cholesterol sensor ORP1L contacts the ER protein VAP to control Rab7-RILP-p150 Glued and late endosome positioning. J Cell Biol. 2009 Jun 29;185(7):1209–25.

92. Ridgway ND, Zhao K. Cholesterol transfer at endosomal-organelle membrane contact sites. Current Opinion in Lipidology. 2018 Jun;29(3):212–7.

93. Luzio JP, Pryor PR, Bright NA. Lysosomes: fusion and function. Nat Rev Mol Cell Biol. 2007 Aug;8(8):622–32.

94. Ward DM, Pevsner J, Scullion MA, Vaughn M, Kaplan J. Syntaxin 7 and VAMP-7 are SolubleN-Ethylmaleimide–sensitive Factor Attachment Protein Receptors Required for Late Endosome–Lysosome and Homotypic Lysosome Fusion in Alveolar Macrophages. MBoC. 2000 Jul;11(7):2327–33.

95. Vanlandingham PA, Ceresa BP. Rab7 Regulates Late Endocytic Trafficking Downstream of Multivesicular Body Biogenesis and Cargo Sequestration. J Biol Chem. 2009 May 1;284(18):12110–24.

96. Pols MS, ten Brink C, Gosavi P, Oorschot V, Klumperman J. The HOPS Proteins hVps41 and hVps39 Are Required for Homotypic and Heterotypic Late Endosome Fusion. Traffic. 2013;14(2):219–32.

97. Luzio JP, Hackmann Y, Dieckmann NMG, Griffiths GM. The Biogenesis of Lysosomes and Lysosome-Related Organelles. Cold Spring Harb Perspect Biol. 2014 Jan 9;6(9):a016840.

98. Pryor PR, Mullock BM, Bright NA, Gray SR, Luzio JP. The Role of Intraorganellar Ca2+In Late Endosome–Lysosome Heterotypic Fusion and in the Reformation of Lysosomes from Hybrid Organelles. Journal of Cell Biology. 2000 May 29;149(5):1053–62.

99. Cao Q, Zhong XZ, Zou Y, Murrell-Lagnado R, Zhu MX, Dong XP. Calcium release through P2X4 activates calmodulin to promote endolysosomal membrane fusion. J Cell Biol. 2015 Jun 22;209(6):879–94.

100. Feng X, Yang J. Lysosomal Calcium in Neurodegeneration. Messenger (Los Angel). 2016 Jun;5(1–2):56–66.

101. Lloyd-Evans E, Morgan AJ, He X, Smith DA, Elliot-Smith E, Sillence DJ, et al. Niemann-Pick disease type C1 is a sphingosine storage disease that causes deregulation of lysosomal calcium. Nat Med. 2008 Nov;14(11):1247–55.

102. Shen D, Wang X, Li X, Zhang X, Yao Z, Dibble S, et al. Lipid storage disorders block lysosomal trafficking by inhibiting a TRP channel and lysosomal calcium release. Nat Commun. 2012 Mar 13;3:731.

103. Du W, Su QP, Chen Y, Zhu Y, Jiang D, Rong Y, et al. Kinesin 1 Drives Autolysosome Tubulation. Dev Cell. 2016 May 23;37(4):326–36.

104. Chen Y, Yu L. Development of Research into Autophagic Lysosome Reformation. Mol Cells. 2018 Jan 31;41(1):45–9.

105. Chen Y, Yu L. Recent progress in autophagic lysosome reformation. Traffic. 2017;18(6):358–61.

106. Goldman SDB, Krise JP. Niemann-Pick C1 Functions Independently of Niemann-Pick C2 in the Initial Stage of Retrograde Transport of Membrane-impermeable Lysosomal Cargo 2. Journal of Biological Chemistry. 2010 Feb 12;285(7):4983–94.

107. Buratta S, Tancini B, Sagini K, Delo F, Chiaradia E, Urbanelli L, et al. Lysosomal Exocytosis, Exosome Release and Secretory Autophagy: The Autophagic- and Endo-Lysosomal Systems Go Extracellular. Int J Mol Sci. 2020 Apr 8;21(7):2576.

108. Reddy A, Caler EV, Andrews NW. Plasma membrane repair is mediated by Ca(2+)-regulated exocytosis of lysosomes. Cell. 2001 Jul 27;106(2):157–69.

109. Gómez NM, Lu W, Lim JC, Kiselyov K, Campagno KE, Grishchuk Y, et al. Robust lysosomal calcium signaling through channel TRPML1 is impaired by lysosomal lipid accumulation. FASEB J. 2018 Feb;32(2):782–94.

110. MacDougall DD, Lin Z, Chon NL, Jackman SL, Lin H, Knight JD, et al. The high-affinity calcium sensor synaptotagmin-7 serves multiple roles in regulated exocytosis. Journal of General Physiology. 2018 Mai;150(6):783–807.

111. Tucker WC, Weber T, Chapman ER. Reconstitution of Ca2+-regulated membrane fusion by synaptotagmin and SNAREs. Science. 2004 Apr 16;304(5669):435–8.

112. Vieira OV. Rab3a and Rab10 are regulators of lysosome exocytosis and plasma membrane repair. Small GTPases. 2016 Nov 1;9(4):349–51.

113. Vella LJ, Hill AF, Cheng L. Focus on Extracellular Vesicles: Exosomes and Their Role in Protein Trafficking and Biomarker Potential in Alzheimer's and Parkinson's Disease. Int J Mol Sci. 2016 Feb 6;17(2):173.

114. Kim A. A Panoramic Overview of Mitochondria and Mitochondrial Redox Biology. Toxicol Res. 2014 Dec;30(4):221–34.

115. Elustondo P, Martin LA, Karten B. Mitochondrial cholesterol import. Biochim Biophys Acta Mol Cell Biol Lipids. 2017 Jan;1862(1):90–101.

116. Clark BJ, Wells J, King SR, Stocco DM. The purification, cloning, and expression of a novel luteinizing hormone-induced mitochondrial protein in MA-10 mouse Leydig tumor cells. Characterization of the steroidogenic acute regulatory protein (StAR). J Biol Chem. 1994 Nov 11;269(45):28314–22.

117. Larsen MC, Lee J, Jorgensen JS, Jefcoate CR. STARD1 Functions in Mitochondrial Cholesterol Metabolism and Nascent HDL Formation. Gene Expression and Molecular mRNA Imaging Show Novel Splicing and a 1:1 Mitochondrial Association. Front Endocrinol (Lausanne). 2020 Oct 20;11:559674.

118. Tsujishita Y, Hurley JH. Structure and lipid transport mechanism of a StAR-related domain. Nat Struct Biol. 2000 May;7(5):408–14.

119. Granot Z, Silverman E, Friedlander R, Melamed-Book N, Eimerl S, Timberg R, et al. The life cycle of the steroidogenic acute regulatory (StAR) protein: from transcription through proteolysis. Endocr Res. 2002 Nov;28(4):375–86.

120. Yamazaki T, Matsuoka C, Gendou M, Izumi S, Zhao D, Artemenko I, et al. Mitochondrial processing of bovine adrenal steroidogenic acute regulatory protein. Biochim Biophys Acta. 2006 Oct;1764(10):1561–7.

121. Bose HS, Lingappa VR, Miller WL. The steroidogenic acute regulatory protein, StAR, works only at the outer mitochondrial membrane. Endocr Res. 2002 Nov;28(4):295–308.

122. Artemenko IP, Zhao D, Hales DB, Hales KH, Jefcoate CR. Mitochondrial processing of newly synthesized steroidogenic acute regulatory protein (StAR), but not total StAR, mediates cholesterol transfer to cytochrome P450 side chain cleavage enzyme in adrenal cells. J Biol Chem. 2001 Dec 7;276(49):46583–96.

123. Tuckey RC, Headlam MJ, Bose HS, Miller WL. Transfer of cholesterol between phospholipid vesicles mediated by the steroidogenic acute regulatory protein (StAR). J Biol Chem. 2002 Dec 6;277(49):47123–8.

124. Bose M, Whittal RM, Miller WL, Bose HS. Steroidogenic Activity of StAR Requires Contact with Mitochondrial VDAC1 and Phosphate Carrier Protein. J Biol Chem. 2008 Apr 4;283(14):8837–45.

125. Blachly-Dyson E, Forte M. VDAC channels. IUBMB Life. 2001 Nov;52(3–5):113–8.

126. Prasad M, Kaur J, Pawlak KJ, Bose M, Whittal RM, Bose HS. Mitochondria-associated endoplasmic reticulum membrane (MAM) regulates steroidogenic activity via steroidogenic acute regulatory protein (StAR)-voltage-dependent anion channel 2 (VDAC2) interaction. J Biol Chem. 2015 Jan 30;290(5):2604–16.

127. Vance JE. Phospholipid synthesis in a membrane fraction associated with mitochondria. J Biol Chem. 1990 May 5;265(13):7248–56.

128. Wang PTC, Garcin PO, Fu M, Masoudi M, St-Pierre P, Panté N, et al. Distinct mechanisms controlling rough and smooth endoplasmic reticulum contacts with mitochondria. J Cell Sci. 2015 Aug 1;128(15):2759–65.

129. Zhang P, Konja D, Zhang Y, Wang Y. Communications between Mitochondria and Endoplasmic Reticulum in the Regulation of Metabolic Homeostasis. Cells. 2021 Aug 25;10(9):2195.

130. Szabadkai G, Bianchi K, Várnai P, De Stefani D, Wieckowski MR, Cavagna D, et al. Chaperone-mediated coupling of endoplasmic reticulum and mitochondrial Ca2+ channels. J Cell Biol. 2006 Dec 18;175(6):901–11.

131. Cárdenas C, Miller RA, Smith I, Bui T, Molgó J, Müller M, et al. Essential regulation of cell bioenergetics by constitutive InsP3 receptor Ca2+ transfer to mitochondria. Cell. 2010 Jul 23;142(2):270–83.

132. Giorgi C, Baldassari F, Bononi A, Bonora M, De Marchi E, Marchi S, et al. Mitochondrial Ca2+ and apoptosis. Cell Calcium. 2012 Jul;52(1):36–43.

133. Losón OC, Song Z, Chen H, Chan DC. Fis1, Mff, MiD49, and MiD51 mediate Drp1 recruitment in mitochondrial fission. Mol Biol Cell. 2013 Mar;24(5):659–67.

134. Santel A, Fuller MT. Control of mitochondrial morphology by a human mitofusin. J Cell Sci. 2001 Mar;114(Pt 5):867–74.

135. Kornmann B, Currie E, Collins SR, Schuldiner M, Nunnari J, Weissman JS, et al. An ER-Mitochondria Tethering Complex Revealed by a Synthetic Biology Screen. Science. 2009 Jul 24;325(5939):477–81.

136. Petrungaro C, Kornmann B. Lipid exchange at ER-mitochondria contact sites: a puzzle falling into place with quite a few pieces missing. Curr Opin Cell Biol. 2019 Apr;57:71–6.

137. Cui Z, Vance JE, Chen MH, Voelker DR, Vance DE. Cloning and expression of a novel phosphatidylethanolamine N-methyltransferase. A specific biochemical and cytological marker for a unique membrane fraction in rat liver. J Biol Chem. 1993 Aug 5;268(22):16655–63.

138. Area-Gomez E, del Carmen Lara Castillo M, Tambini MD, Guardia-Laguarta C, de Groof AJC, Madra M, et al. Upregulated function of mitochondria-associated ER membranes in Alzheimer disease. EMBO J. 2012 Nov 5;31(21):4106–23.

139. Lee ZY, Prouteau M, Gotta M, Barral Y. Compartmentalization of the endoplasmic reticulum in the early C. elegans embryos. J Cell Biol. 2016 Sep 12;214(6):665–76.

140. Peretti D, Kim S, Tufi R, Lev S. Lipid Transfer Proteins and Membrane Contact Sites in Human Cancer. Frontiers in Cell and Developmental Biology [Internet]. 2020 [cited 2022 Feb 15];7. Available from: https://www.frontiersin.org/article/10.3389/fcell.2019.00371

141. Duarte A, Castillo AF, Podestá EJ, Poderoso C. Mitochondrial fusion and ERK activity regulate steroidogenic acute regulatory protein localization in mitochondria. PLoS One. 2014;9(6):e100387.

142. Lang A, John Peter AT, Kornmann B. ER–mitochondria contact sites in yeast: beyond the myths of ERMES. Current Opinion in Cell Biology. 2015 Aug 1;35:7–12.

143. Hönscher C, Mari M, Auffarth K, Bohnert M, Griffith J, Geerts W, et al. Cellular metabolism regulates contact sites between vacuoles and mitochondria. Dev Cell. 2014 Jul 14;30(1):86–94.

144. Elbaz-Alon Y, Rosenfeld-Gur E, Shinder V, Futerman AH, Geiger T, Schuldiner M. A dynamic interface between vacuoles and mitochondria in yeast. Dev Cell. 2014 Jul 14;30(1):95–102.

145. Charman M, Kennedy BE, Osborne N, Karten B. MLN64 mediates egress of cholesterol from endosomes to mitochondria in the absence of functional Niemann-Pick Type C1 protein. Journal of Lipid Research. 2010 May 1;51(5):1023–34.

146. Zhang M, Liu P, Dwyer NK, Christenson LK, Fujimoto T, Martinez F, et al. MLN64 mediates mobilization of lysosomal cholesterol to steroidogenic mitochondria. J Biol Chem. 2002 Sep 6;277(36):33300–10.

147. Martello A, Platt FM, Eden ER. Staying in touch with the endocytic network: The importance of contacts for cholesterol transport. Traffic. 2020 May;21(5):354–63.

148. Watari H, Arakane F, Moog-Lutz C, Kallen CB, Tomasetto C, Gerton GL, et al. MLN64 contains a domain with homology to the steroidogenic acute regulatory protein (StAR) that stimulates steroidogenesis. Proc Natl Acad Sci U S A. 1997 Aug 5;94(16):8462–7.

149. Han Y, Li M, Qiu F, Zhang M, Zhang YH. Cell-permeable organic fluorescent probes for live-cell long-term super-resolution imaging reveal lysosome-mitochondrion interactions. Nat Commun. 2017 Nov 3;8(1):1307.

150. Wong YC, Ysselstein D, Krainc D. Mitochondria–lysosome contacts regulate mitochondrial fission via RAB7 GTP hydrolysis. Nature. 2018 Feb;554(7692):382–6.

151. Elbaz-Alon Y, Guo Y, Segev N, Harel M, Quinnell DE, Geiger T, et al. PDZD8 interacts with Protrudin and Rab7 at ER-late endosome membrane contact sites associated with mitochondria. Nat Commun. 2020 Jul 20;11(1):3645.

152. Myburgh R, Cherpin O, Schlaepfer E, Rehrauer H, Speck RF, Krause KH, et al. Optimization of Critical Hairpin Features Allows miRNA-based Gene Knockdown Upon Single-copy Transduction. Mol Ther Nucleic Acids. 2014 Oct 28;3:e207.

153. Ichihara M, Murakumo Y, Masuda A, Matsuura T, Asai N, Jijiwa M, et al. Thermodynamic instability of siRNA duplex is a prerequisite for dependable prediction of siRNA activities. Nucleic Acids Res. 2007 Sep;35(18):e123.

154. Huang L, Pike D, Sleat DE, Nanda V, Lobel P. Potential Pitfalls and Solutions for Use of Fluorescent Fusion Proteins to Study the Lysosome. PLOS ONE. 2014 Feb 21;9(2):e88893.

155. Kennedy BE, Madreiter CT, Vishnu N, Malli R, Graier WF, Karten B. Adaptations of energy metabolism associated with increased levels of mitochondrial cholesterol in Niemann-Pick type C1-deficient cells. J Biol Chem. 2014 Jun 6;289(23):16278–89.

156. Wang ML, Motamed M, Infante RE, Abi-Mosleh L, Kwon HJ, Brown MS, et al. Identification of surface residues on Niemann-Pick C2 essential for hydrophobic handoff of cholesterol to NPC1 in lysosomes. Cell Metab. 2010 Aug 4;12(2):166–73.

157. Chikh K, Vey S, Simonot C, Vanier MT, Millat G. Niemann-Pick type C disease: importance of N-glycosylation sites for function and cellular location of the NPC2 protein. Mol Genet Metab. 2004 Nov;83(3):220–30.

158. Okamura N, Kiuchi S, Tamba M, Kashima T, Hiramoto S, Baba T, et al. A porcine homolog of the major secretory protein of human epididymis, HE1, specifically binds cholesterol. Biochim Biophys Acta. 1999 Jun 10;1438(3):377–87.

159. Schindelin J, Arganda-Carreras I, Frise E, Kaynig V, Longair M, Pietzsch T, et al. Fiji: an open-source platform for biological-image analysis. Nat Methods. 2012 Jul;9(7):676–82.

160. Shapiro F, Silanikove N. Rapid and accurate determination of d- and l-lactate, lactose and galactose by enzymatic reactions coupled to formation of a fluorochromophore: Applications in food quality control. Food Chemistry. 2010 Mar 15;119(2):829–33.

161. Rodríguez A, Webster P, Ortego J, Andrews NW. Lysosomes Behave as Ca2+-regulated Exocytic Vesicles in Fibroblasts and Epithelial Cells. J Cell Biol. 1997 Apr 7;137(1):93–104.

162. Fan Y, He JJ. HIV-1 Tat Promotes Lysosomal Exocytosis in Astrocytes and Contributes to Astrocyte-mediated Tat Neurotoxicity. Journal of Biological Chemistry. 2016 Oct;291(43):22830–40.

163. Nugues C, Helassa N, Rajamanoharan D, Burgoyne RD, Haynes LP. Lysosome exocytosis is required for mitosis [Internet]. 2018 Oct [cited 2022 Jan 12] p. 375816. Available from: https://www.biorxiv.org/content/10.1101/375816v3

164. Ouellet M, Guillebaud G, Gervais V, St-Pierre DL, Germain M. A novel algorithm identifies stress-induced alterations in mitochondrial connectivity and inner membrane structure from confocal images. PLOS Computational Biology. 2017 Jun 22;13(6):e1005612.

165. Edelstein AD, Tsuchida MA, Amodaj N, Pinkard H, Vale RD, Stuurman N. Advanced methods of microscope control using μManager software. Journal of Biological Methods. 2014 Nov 7;1(2):e10–e10.

166. Edelstein A, Amodaj N, Hoover K, Vale R, Stuurman N. Computer Control of Microscopes Using μManager. Current Protocols in Molecular Biology. 2010;92(1):14.20.1-14.20.17.

167. Torres S, García-Ruiz CM, Fernandez-Checa JC. Mitochondrial Cholesterol in Alzheimer's Disease and Niemann-Pick Type C Disease. Front Neurol. 2019;10:1168.

168. Kovalevich J, Langford D. Considerations for the use of SH-SY5Y neuroblastoma cells in neurobiology. Methods Mol Biol. 2013;1078:9–21.

169. Kennedy BE, LeBlanc VG, Mailman TM, Fice D, Burton I, Karakach TK, et al. Pre-Symptomatic Activation of Antioxidant Responses and Alterations in Glucose and Pyruvate Metabolism in Niemann-Pick Type C1-Deficient Murine Brain. PLoS One. 2013 Dec 18;8(12):e82685.

170. Woś M, Szczepanowska J, Pikuła S, Tylki-Szymańska A, Zabłocki K, Bandorowicz-Pikuła J. Mitochondrial dysfunction in fibroblasts derived from patients with Niemann-Pick type C disease. Arch Biochem Biophys. 2016 Mar 1;593:50–9.

171. Jezek P, Plecitá-Hlavatá L. Mitochondrial reticulum network dynamics in relation to oxidative stress, redox regulation, and hypoxia. Int J Biochem Cell Biol. 2009 Oct;41(10):1790–804.

172. McCarron JG, Wilson C, Sandison ME, Olson ML, Girkin JM, Saunter C, et al. From Structure to Function: Mitochondrial Morphology, Motion and Shaping in Vascular Smooth Muscle. JVR. 2013;50(5):357–71.

173. Aoyama-Ishiwatari S, Hirabayashi Y. Endoplasmic Reticulum–Mitochondria Contact Sites—Emerging Intracellular Signaling Hubs. Frontiers in Cell and Developmental Biology [Internet]. 2021 [cited 2022 Feb 7];9. Available from: https://www.frontiersin.org/article/10.3389/fcell.2021.653828

174. Xu L, Wang X, Tong C. Endoplasmic Reticulum–Mitochondria Contact Sites and Neurodegeneration. Front Cell Dev Biol. 2020 Jun 18;8:428.

175. Fujimoto M, Hayashi T, Su TP. The role of cholesterol in the association of endoplasmic reticulum membranes with mitochondria. Biochem Biophys Res Commun. 2012 Jan 6;417(1):635–9.

176. Patterson MC, Vanier MT, Suzuki K, Morris JA, Carstea E, Neufeld EB, et al. Niemann-Pick Disease Type C: A Lipid Trafficking Disorder. In: Valle DL, Antonarakis S, Ballabio A, Beaudet AL, Mitchell GA, editors. The Online Metabolic and Molecular Bases of Inherited Disease [Internet]. New York, NY: McGraw-Hill Education; 2019 [cited 2022 Jan 6]. Available from: ommbid.mhmedical.com/content.aspx?aid=1181465066

177. Pentchev PG, Comly ME, Kruth HS, Vanier MT, Wenger DA, Patel S, et al. A defect in cholesterol esterification in Niemann-Pick disease (type C) patients. Proc Natl Acad Sci U S A. 1985 Dec;82(23):8247–51.

178. Mbua NE, Flanagan-Steet H, Johnson S, Wolfert MA, Boons GJ, Steet R. Abnormal accumulation and recycling of glycoproteins visualized in Niemann-Pick type C cells using the chemical reporter strategy. Proc Natl Acad Sci U S A. 2013 Jun 18;110(25):10207–12.

179. Chikh K, Vey S, Simonot C, Vanier MT, Millat G. Niemann–Pick type C disease: importance of N-glycosylation sites for function and cellular location of the NPC2 protein. Molecular Genetics and Metabolism. 2004 Nov 1;83(3):220–30.

180. Boadu E, Nelson RC, Francis GA. ABCA1-dependent mobilization of lysosomal cholesterol requires functional Niemann–Pick C2 but not Niemann–Pick C1 protein. Biochimica et Biophysica Acta (BBA) - Molecular and Cell Biology of Lipids. 2012 Mar 1;1821(3):396–404.

181. Raftopulos NL, Washaya TC, Niederprüm A, Egert A, Hakeem-Sanni MF, Varney B, et al. Prostate cancer cell proliferation is influenced by LDL-cholesterol availability and cholesteryl ester turnover. Cancer & Metabolism. 2022 Jan 15;10(1):1.

182. Strauss K, Goebel C, Runz H, Möbius W, Weiss S, Feussner I, et al. Exosome secretion ameliorates lysosomal storage of cholesterol in Niemann-Pick type C disease. J Biol Chem. 2010 Aug 20;285(34):26279–88.

183. Neufeld EB, Wastney M, Patel S, Suresh S, Cooney AM, Dwyer NK, et al. The Niemann-Pick C1 protein resides in a vesicular compartment linked to retrograde transport of multiple lysosomal cargo. J Biol Chem. 1999 Apr 2;274(14):9627–35.

184. Kaufmann AM, Krise JP. Niemann-Pick C1 Functions in Regulating Lysosomal Amine Content. J Biol Chem. 2008 Sep 5;283(36):24584–93.

185. Dominko K, Rastija A, Sobocanec S, Vidatic L, Meglaj S, Lovincic Babic A, et al. Impaired Retromer Function in Niemann-Pick Type C Disease Is Dependent on Intracellular Cholesterol Accumulation. Int J Mol Sci. 2021 Dec 9;22(24):13256.

186. Cerny J, Feng Y, Yu A, Miyake K, Borgonovo B, Klumperman J, et al. The small chemical vacuolin-1 inhibits Ca(2+)-dependent lysosomal exocytosis but not cell resealing. EMBO Rep. 2004 Sep;5(9):883–8.

187. Lu Y, Dong S, Hao B, Li C, Zhu K, Guo W, et al. Vacuolin-1 potently and reversibly inhibits autophagosome-lysosome fusion by activating RAB5A. Autophagy. 2014 Oct 30;10(11):1895–905.

188. Maekawa M, Fairn GD. Complementary probes reveal that phosphatidylserine is required for the proper transbilayer distribution of cholesterol. J Cell Sci. 2015 Apr 1;128(7):1422–33.

189. Heybrock S, Kanerva K, Meng Y, Ing C, Liang A, Xiong ZJ, et al. Lysosomal integral membrane protein-2 (LIMP-2/SCARB2) is involved in lysosomal cholesterol export. Nature Communications. 2019 Aug 6;10(1):1–12.

190. Conrad KS, Cheng TW, Ysselstein D, Heybrock S, Hoth LR, Chrunyk BA, et al. Lysosomal integral membrane protein-2 as a phospholipid receptor revealed by biophysical and cellular studies. Nature Communications. 2017 Dec 4;8(1):1–13.

191. Wijdeven RH, Janssen H, Nahidiazar L, Janssen L, Jalink K, Berlin I, et al. Cholesterol and ORP1L-mediated ER contact sites control autophagosome transport and fusion with the endocytic pathway. Nat Commun. 2016 10;7:11808.

192. Khatter D, Sindhwani A, Sharma M. Arf-like GTPase Arl8: Moving from the periphery to the center of lysosomal biology. Cell Logist. 2015 Sep 21;5(3):e1086501.

193. Belmonte SA, López CI, Roggero CM, De Blas GA, Tomes CN, Mayorga LS. Cholesterol content regulates acrosomal exocytosis by enhancing Rab3A plasma membrane association. Dev Biol. 2005 Sep 15;285(2):393–408.

194. Hunter MR, Scourfield EJ, Emmott E, Graham SC. VPS18 recruits VPS41 to the human HOPS complex via a RING–RING interaction. Biochem J. 2017 Nov 1;474(21):3615–26.

195. Cabrera M, Ostrowicz CW, Mari M, LaGrassa TJ, Reggiori F, Ungermann C. Vps41 Phosphorylation and the Rab Ypt7 Control the Targeting of the HOPS Complex to Endosome–Vacuole Fusion Sites. MBoC. 2009 Apr 1;20(7):1937–48.

196. Remmel N, Locatelli-Hoops S, Breiden B, Schwarzmann G, Sandhoff K. Saposin B mobilizes lipids from cholesterol-poor and bis(monoacylglycero)phosphate-rich membranes at acidic pH. The FEBS Journal. 2007;274(13):3405–20.

197. Elleder M, Jerábková M, Befekadu A, Hrebícek M, Berná L, Ledvinová J, et al. Prosaposin deficiency -- a rarely diagnosed, rapidly progressing, neonatal neurovisceral lipid storage disease. Report of a further patient. Neuropediatrics. 2005 Jun;36(3):171–80.

198. Zhao K, Foster J, Ridgway ND. Oxysterol-binding protein-related protein 1 variants have opposing cholesterol transport activities from the endolysosomes. Mol Biol Cell. 2020 Apr 1;31(8):793–802.

199. Meng Y, Heybrock S, Neculai D, Saftig P. Cholesterol Handling in Lysosomes and Beyond. Trends in Cell Biology. 2020 Jun 1;30(6):452–66.

200. Fukuda M. Regulation of secretory vesicle traffic by Rab small GTPases. Cell Mol Life Sci. 2008 Sep;65(18):2801–13.

201. Neurodegenerative VPS41 variants inhibit HOPS function and mTORC1-dependent TFEB/TFE3 regulation. EMBO Molecular Medicine. 2021 May 7;13(5):e13258.

202. Puertollano R, Ferguson SM, Brugarolas J, Ballabio A. The complex relationship between TFEB transcription factor phosphorylation and subcellular localization. EMBO J. 2018 Jun 1;37(11):e98804.

203. Nabar NR, Kehrl JH. The Transcription Factor EB Links Cellular Stress to the Immune Response. Yale J Biol Med. 2017 Jun;90(2):301–15.

204. Huang DW, Sherman BT, Lempicki RA. Systematic and integrative analysis of large gene lists using DAVID bioinformatics resources. Nat Protoc. 2009;4(1):44–57.

205. Thomas PD, Kejariwal A, Guo N, Mi H, Campbell MJ, Muruganujan A, et al. Applications for protein sequence–function evolution data: mRNA/protein expression analysis and coding SNP scoring tools. Nucleic Acids Research. 2006 Jul 1;34(suppl_2):W645–50.

206. Thomas PD, Campbell MJ, Kejariwal A, Mi H, Karlak B, Daverman R, et al. PANTHER: A Library of Protein Families and Subfamilies Indexed by Function. Genome Res. 2003 Jan 9;13(9):2129–41.

207. Szklarczyk D, Franceschini A, Wyder S, Forslund K, Heller D, Huerta-Cepas J, et al. STRING v10: protein-protein interaction networks, integrated over the tree of life. Nucleic Acids Res. 2015 Jan;43(Database issue):D447-452.

208. Hulsen T, de Vlieg J, Alkema W. BioVenn – a web application for the comparison and visualization of biological lists using area-proportional Venn diagrams. BMC Genomics. 2008 Oct 16;9(1):488.

209. Nielsen GK, Dagnaes-Hansen F, Holm IE, Meaney S, Symula D, Andersen NT, et al. Protein replacement therapy partially corrects the cholesterol-storage phenotype in a mouse model of Niemann-Pick type C2 disease. PLoS One. 2011;6(11):e27287.

210. Platt FM, Lachmann RH. Treating lysosomal storage disorders: current practice and future prospects. Biochim Biophys Acta. 2009 Apr;1793(4):737–45.

211. Ko DC, Gordon MD, Jin JY, Scott MP. Dynamic Movements of Organelles Containing Niemann-Pick C1 Protein: NPC1 Involvement in Late Endocytic Events. Mol Biol Cell. 2001 Mar;12(3):601–14.

212. Yambire KF, Fernandez-Mosquera L, Steinfeld R, Mühle C, Ikonen E, Milosevic I, et al. Mitochondrial biogenesis is transcriptionally repressed in lysosomal lipid storage diseases. Chacinska A, Dikic I, Sellin J, editors. eLife. 2019 Feb 18;8:e39598.

213. Norat P, Soldozy S, Sokolowski JD, Gorick CM, Kumar JS, Chae Y, et al. Mitochondrial dysfunction in neurological disorders: Exploring mitochondrial transplantation. npj Regen Med. 2020 Nov 23;5(1):1–9.

214. Balboa E, Castro J, Pinochet MJ, Cancino GI, Matías N, Sáez PJ, et al. MLN64 induces mitochondrial dysfunction associated with increased mitochondrial cholesterol content. Redox Biol. 2017 Aug;12:274–84.

215. Garcia-Ruiz C, Mari M, Colell A, Morales A, Caballero F, Montero J, et al. Mitochondrial cholesterol in health and disease. Histol Histopathol. 2009 Jan;24(1):117–32.

216. Desai R, Campanella M. Exploring mitochondrial cholesterol signalling for therapeutic intervention in neurological conditions. British Journal of Pharmacology. 2019;176(22):4284–92.

217. Rodríguez-Pascau L, Coll MJ, Casas J, Vilageliu L, Grinberg D. Generation of a human neuronal stable cell model for niemann-pick C disease by RNA interference. JIMD Rep. 2012;4:29–37.

218. Glancy B, Kane DA, Kavazis AN, Goodwin ML, Willis WT, Gladden LB. Mitochondrial lactate metabolism: history and implications for exercise and disease. The Journal of Physiology. 2021;599(3):863–88.

219. Jang M, Kim SS, Lee J. Cancer cell metabolism: implications for therapeutic targets. Exp Mol Med. 2013 Oct;45(10):e45–e45.

220. Sung EA, Yu KR, Shin JH, Seo Y, Kim HS, Koog MG, et al. Generation of patient specific human neural stem cells from Niemann-Pick disease type C patient-derived fibroblasts. Oncotarget. 2017 Aug 7;8(49):85428–41.

221. Vassilev B, Sihto H, Li S, Hölttä-Vuori M, Ilola J, Lundin J, et al. Elevated levels of StAR-related lipid transfer protein 3 alter cholesterol balance and adhesiveness of breast cancer cells: potential mechanisms contributing to progression of HER2-positive breast cancers. Am J Pathol. 2015 Apr;185(4):987–1000.

222. Asif K, Memeo L, Palazzolo S, Frión-Herrera Y, Parisi S, Caligiuri I, et al. STARD3: A Prospective Target for Cancer Therapy. Cancers. 2021 Jan;13(18):4693.

223. Westermann B. Bioenergetic role of mitochondrial fusion and fission. Biochim Biophys Acta. 2012 Oct;1817(10):1833–8.

224. Wu S, Zhou F, Zhang Z, Xing D. Mitochondrial oxidative stress causes mitochondrial fragmentation via differential modulation of mitochondrial fission–fusion proteins. The FEBS Journal. 2011;278(6):941–54.

225. Ferlemann FC, Menon V, Condurat AL, Rößler J, Pruszak J. Surface marker profiling of SH-SY5Y cells enables small molecule screens identifying BMP4 as a modulator of neuroblastoma differentiation. Sci Rep. 2017 Oct 19;7(1):13612.

226. Ordonez MP, Roberts EA, Kidwell CU, Yuan SH, Plaisted WC, Goldstein LSB. Disruption and therapeutic rescue of autophagy in a human neuronal model of Niemann Pick type C1. Hum Mol Genet. 2012 Jun 15;21(12):2651–62.

227. Yang S, Zhou R, Zhang C, He S, Su Z. Mitochondria-Associated Endoplasmic Reticulum Membranes in the Pathogenesis of Type 2 Diabetes Mellitus. Frontiers in Cell and Developmental Biology [Internet]. 2020 [cited 2022 Feb 22];8. Available from: https://www.frontiersin.org/article/10.3389/fcell.2020.571554

228. Issop L, Fan J, Lee S, Rone MB, Basu K, Mui J, et al. Mitochondria-associated membrane formation in hormone-stimulated Leydig cell steroidogenesis: role of ATAD3. Endocrinology. 2015 Jan;156(1):334–45.

229. Zhunina OA, Yabbarov NG, Grechko AV, Starodubova AV, Ivanova E, Nikiforov NG, et al. The Role of Mitochondrial Dysfunction in Vascular Disease, Tumorigenesis, and Diabetes. Frontiers in Molecular Biosciences [Internet]. 2021 [cited 2022 Feb 22];8. Available from: https://www.frontiersin.org/article/10.3389/fmolb.2021.671908

230. Gerhold JM, Cansiz-Arda Ş, Lõhmus M, Engberg O, Reyes A, van Rennes H, et al. Human Mitochondrial DNA-Protein Complexes Attach to a Cholesterol-Rich Membrane Structure. Sci Rep. 2015 Oct 19;5(1):15292.

231. Rusiñol AE, Cui Z, Chen MH, Vance JE. A unique mitochondria-associated membrane fraction from rat liver has a high capacity for lipid synthesis and contains pre-Golgi secretory proteins including nascent lipoproteins. J Biol Chem. 1994 Nov 4;269(44):27494–502.

232. Annunziata I, Sano R, d'Azzo A. Mitochondria-associated ER membranes (MAMs) and lysosomal storage diseases. Cell Death Dis. 2018 Feb 28;9(3):1–16.

233. Kristiana I, Yang H, Brown AJ. Different kinetics of cholesterol delivery to components of the cholesterol homeostatic machinery: implications for cholesterol trafficking to the endoplasmic reticulum. Biochim Biophys Acta. 2008 Dec;1781(11–12):724–30.

234. Vance JE, Karten B. Niemann-Pick C disease and mobilization of lysosomal cholesterol by cyclodextrin. Journal of Lipid Research. 2014 Aug 1;55(8):1609–21.

235. Wilhelm LP, Voilquin L, Kobayashi T, Tomasetto C, Alpy F. Intracellular and Plasma Membrane Cholesterol Labeling and Quantification Using Filipin and GFP-D4. Methods Mol Biol. 2019;1949:137–52.

236. Sleat DE, Wiseman JA, El-Banna M, Price SM, Verot L, Shen MM, et al. Genetic evidence for nonredundant functional cooperativity between NPC1 and NPC2 in lipid transport. PNAS. 2004 Apr 20;101(16):5886–91.

237. Byers DM, Morgan MW, Cook HW, St. C. Palmer FB, Spence MW. Niemann-Pick Type II fibroblasts exhibit impaired cholesterol esterification in response to shingomyelin hydrolysis. Biochimica et Biophysica Acta (BBA) - Molecular Basis of Disease. 1992 Jan 16;1138(1):20–6.

238. Frolov A, Zielinski SE, Crowley JR, Dudley-Rucker N, Schaffer JE, Ory DS. NPC1 and NPC2 Regulate Cellular Cholesterol Homeostasis through Generation of Low Density Lipoprotein Cholesterol-derived Oxysterols *. Journal of Biological Chemistry. 2003 Jul 11;278(28):25517–25.

239. Reid PC, Sugii S, Chang TY. Trafficking defects in endogenously synthesized cholesterol in fibroblasts, macrophages, hepatocytes, and glial cells from Niemann-Pick type C1 mice. J Lipid Res. 2003 May;44(5):1010–9.

240. Xie C, Lund EG, Turley SD, Russell DW, Dietschy JM. Quantitation of two pathways for cholesterol excretion from the brain in normal mice and mice with neurodegeneration. J Lipid Res. 2003 Sep;44(9):1780–9.

241. Karten B, Hayashi H, Francis GA, Campenot RB, Vance DE, Vance JE. Generation and function of astroglial lipoproteins from Niemann–Pick type C1-deficient mice. Biochem J. 2005 May 1;387(Pt 3):779–88.

242. Ramirez CM, Liu B, Aqul A, Taylor AM, Repa JJ, Turley SD, et al. Quantitative role of LAL, NPC2, and NPC1 in lysosomal cholesterol processing defined by genetic and pharmacological manipulations. J Lipid Res. 2011 Apr;52(4):688–98.

243. Zhang J, Liu Q. Cholesterol metabolism and homeostasis in the brain. Protein Cell. 2015 Apr;6(4):254–64.

244. Dahl NK, Gutheil WG, Liscum L. Abnormal regulation of low density lipoprotein-sensitive events in a cholesterol transport mutant. J Biol Chem. 1993 Aug 15;268(23):16979–86.

245. Pohlkamp T, Wasser CR, Herz J. Functional Roles of the Interaction of APP and Lipoprotein Receptors. Frontiers in Molecular Neuroscience [Internet]. 2017 [cited 2022 Apr 26];10. Available from: https://www.frontiersin.org/article/10.3389/fnmol.2017.00054

246. Du X, Zhang Y, Jo SR, Liu X, Qi Y, Osborne B, et al. Akt activation increases cellular cholesterol by promoting the proteasomal degradation of Niemann-Pick C1. Biochem J. 2015 Oct 15;471(2):243–53.

247. Guarneri P, Cascio C, Piccoli T, Piccoli F, Guarneri R. Human neuroblastoma SH-SY5Y cell line: neurosteroid-producing cell line relying on cytoskeletal organization. J Neurosci Res. 2000 Jun 1;60(5):656–65.

248. Goodall AR, Danks K, Walker JH, Ball SG, Vaughan PFT. Occurrence of Two Types of Secretory Vesicles in the Human Neuroblastoma SH-SY5Y. Journal of Neurochemistry. 1997;68(4):1542–52.

249. Andrews NW. Detection of Lysosomal Exocytosis by Surface Exposure of Lamp1 Luminal Epitopes. In: Öllinger K, Appelqvist H, editors. Lysosomes: Methods and Protocols [Internet]. New York, NY: Springer; 2017 [cited 2022 Feb 26]. p. 205–11. (Methods in Molecular Biology). Available from: https://doi.org/10.1007/978-1-4939-6934-0_13

250. Chang TY, Chang CCY, Ohgami N, Yamauchi Y. Cholesterol sensing, trafficking, and esterification. Annu Rev Cell Dev Biol. 2006;22:129–57.

251. Goluszko P, Nowicki B. Membrane Cholesterol: a Crucial Molecule Affecting Interactions of Microbial Pathogens with Mammalian Cells. Infect Immun. 2005 Dec;73(12):7791–6.

252. Maekawa M. Domain 4 (D4) of Perfringolysin O to Visualize Cholesterol in Cellular Membranes—The Update. Sensors (Basel). 2017 Mar 3;17(3):504.

253. Litvinov DY, Savushkin EV, Dergunov AD. Intracellular and Plasma Membrane Events in Cholesterol Transport and Homeostasis. Journal of Lipids. 2018 Aug 6;2018:e3965054.

254. Courtney KC, Fung KY, Maxfield FR, Fairn GD, Zha X. Comment on 'Orthogonal lipid sensors identify transbilayer asymmetry of plasma membrane cholesterol'. eLife. 7:e38493.

255. Lu SM, Volchuk A, Fairn GD. Focal cholesterol depletion during Fcγ receptor-mediated phagocytosis contributes to Lyn kinase regulation [Internet]. bioRxiv; 2018 [cited 2022 Apr 22]. p. 388637. Available from: https://www.biorxiv.org/content/10.1101/388637v1

256. Garver WS, Krishnan K, Gallagos JR, Michikawa M, Francis GA, Heidenreich RA. Niemann-Pick C1 protein regulates cholesterol transport to the trans-Golgi network and plasma membrane caveolae. Journal of Lipid Research. 2002 Apr 1;43(4):579–89.

257. Millard EE, Srivastava K, Traub LM, Schaffer JE, Ory DS. Niemann-Pick Type C1 (NPC1) Overexpression Alters Cellular Cholesterol Homeostasis *. Journal of Biological Chemistry. 2000 Dec 8;275(49):38445–51.

258. Buwaneka P, Ralko A, Liu SL, Cho W. Evaluation of the available cholesterol concentration in the inner leaflet of the plasma membrane of mammalian cells. Journal of Lipid Research [Internet]. 2021 Jan 1 [cited 2022 Feb 24];62. Available from: https://www.jlr.org/article/S0022-2275(21)00066-3/abstract

259. Kopitz J, Arnold A, Meissner T, Cantz M. Protein catabolism in fibroblasts cultured from patients with mucolipidosis II and other lysosomal disorders. Biochem J. 1993 Oct 15;295 (Pt 2):577–80.

260. Bala S, Szabo G. TFEB, a master regulator of lysosome biogenesis and autophagy, is a new player in alcoholic liver disease. Dig Med Res. 2018 Sep;1:16.

261. Fang H, Bygrave AM, Roth RH, Johnson RC, Huganir RL. An optimized CRISPR/Cas9 approach for precise genome editing in neurons. Day JJ, Chen L, Choquet D, editors. eLife. 2021 März;10:e65202.

262. Williams KR, Saunders AM, Roses AD, Armati PJ. Uptake and internalization of exogenous apolipoprotein E3 by cultured human central nervous system neurons. Neurobiol Dis. 1998 Oct;5(4):271–9.

263. Elrick MJ, Yu T, Chung C, Lieberman AP. Impaired proteolysis underlies autophagic dysfunction in Niemann–Pick type C disease. Hum Mol Genet. 2012 Nov 15;21(22):4876–87.

264. Yu D, Swaroop M, Wang M, Baxa U, Yang R, Yan Y, et al. Niemann-Pick disease type C: induced pluripotent stem cell-derived neuronal cells for modeling neural disease and evaluating drug efficacy. J Biomol Screen. 2014 Sep;19(8):1164–73.

265. Andreu Z, Yáñez-Mó M. Tetraspanins in extracellular vesicle formation and function. Front Immunol. 2014;5:442.

266. Hurwitz SN, Cheerathodi MR, Nkosi D, York SB, Meckes DG. Tetraspanin CD63 Bridges Autophagic and Endosomal Processes To Regulate Exosomal Secretion and Intracellular Signaling of Epstein-Barr Virus LMP1. Journal of Virology [Internet]. 2018 Mar 1 [cited 2020 Apr 27];92(5). Available from: https://jvi.asm.org/content/92/5/e01969-17

267. Abdul-Hammed M, Breiden B, Adebayo MA, Babalola JO, Schwarzmann G, Sandhoff K. Role of endosomal membrane lipids and NPC2 in cholesterol transfer and membrane fusion. J Lipid Res. 2010 Jul 1;51(7):1747–60.

268. Huotari J, Helenius A. Endosome maturation. EMBO J. 2011 Aug 31;30(17):3481–500.

269. Aulinskas TH, Oram JF, Bierman EL, Coetzee GA, Gevers W, van der Westhuyzen DR. Retro-endocytosis of low density lipoprotein by cultured human skin fibroblasts. Arteriosclerosis. 1985 Feb;5(1):45–54.

270. Besson N, Hullin-Matsuda F, Makino A, Murate M, Lagarde M, Pageaux JF, et al. Selective incorporation of docosahexaenoic acid into lysobisphosphatidic acid in cultured THP-1 macrophages. Lipids. 2006 Feb;41(2):189–96.

271. Liou HL, Dixit SS, Xu S, Tint GS, Stock AM, Lobel P. NPC2, the protein deficient in Niemann-Pick C2 disease, consists of multiple glycoforms that bind a variety of sterols. J Biol Chem. 2006 Dec 1;281(48):36710–23.

272. Wei D, Shen S, Lin K, Lu F, Zheng P, Wu S, et al. NPC2 as a Prognostic Biomarker for Glioblastoma Based on Integrated Bioinformatics Analysis and Cytological Experiments. Frontiers in Genetics [Internet]. 2021 [cited 2022 Mar 7];12. Available from: https://www.frontiersin.org/article/10.3389/fgene.2021.611442

273. Wang YH, Twu YC, Wang CK, Lin FZ, Lee CY, Liao YJ. Niemann-Pick Type C2 Protein Regulates Free Cholesterol Accumulation and Influences Hepatic Stellate Cell Proliferation and Mitochondrial Respiration Function. Int J Mol Sci. 2018 Jun 5;19(6):1678.

274. Mahlab-Aviv S, Boulos A, Peretz AR, Eliyahu T, Carmel L, Sperling R, et al. Small RNA sequences derived from pre-microRNAs in the supraspliceosome. Nucleic Acids Research. 2018 Nov 16;46(20):11014–29.